REVUE ROUMAINE DE CHIMIE (ROUMANIAN JOURNAL OF CHEMISTRY)

Tome 53, N° 11 **Novembre 2008**

PAPERS

Ligia-Maria OMOTA, Olga IULIAN, Oana CIOCÎRLAN and Irina NIȚĂ

Viscosity of water, 1,4-dioxane and dimethyl sulfoxide binary and ternary systems at temperatures from 293.15 K to 313.15 K

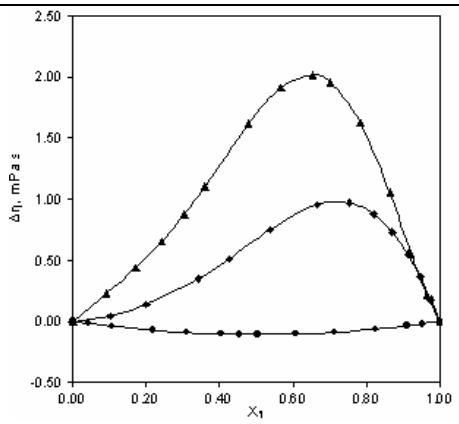

Rev. Roum. Chim., **2008**, *53*(11), 977-988

Key words: viscosity deviations, 1,4-dioxane, dimethyl sulfoxide**,** water.

Mihaela PETRE

Solubility of propylene and propane gases in *N*-methylpyrrolidone and dimethylformamide solvents

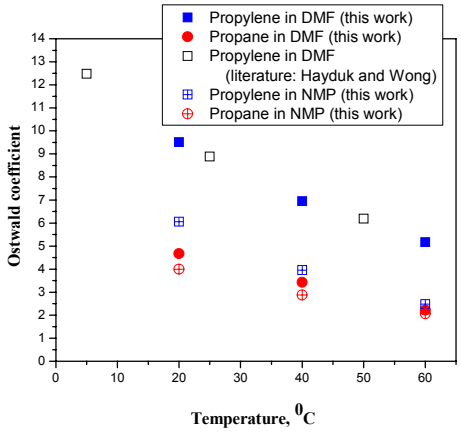

Rev. Roum. Chim., **2008**, *53*(11), 989-993

Key words: propylene, propane, *N*-methylpyrrolidone, dimethylformamide, Ostwald coefficients.

Viorel BRÂNZOI, Florina BRÂNZOI and Florentina GOLGOVICI

The electrochemical behaviour of some composite coatings obtained by electrosynthesis on metallic substrate

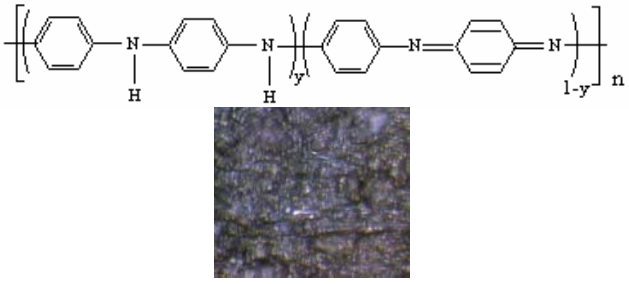

Rev. Roum. Chim., **2008**, *53*(11), 995-1005

Key words: composite coating, conductive polymers, electrochemical oxidation, cyclic voltammetry and electrochemical impedance spectroscopy method.

Cristian PIRVU, Alexandra BANU, Octavian RADOVICI and Maria MARCU

Aplication of electrochemical impedance spectroscopy (EIS) to study of phenolic films

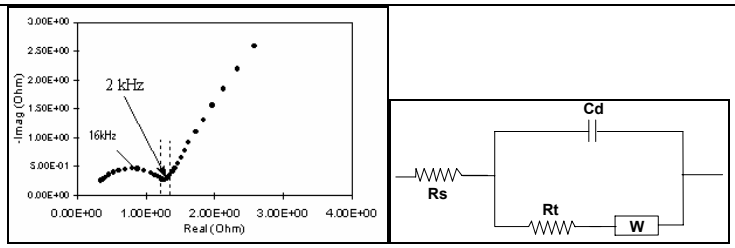

Rev. Roum. Chim., **2008**, *53*(11), 1007-1015

Key words: electrochemical impedance, phenol, electrooxidation, pseudocapacitance, equivalent circuit.

Doina DIMONIE , Constantin RADOVICI , Ramona Marina COSEREA, Sorina GÂREA and Mircea TEODORESCU

The polymer molecular weight and silicate treatment influence upon the morphology of nanocomposites for food packaging

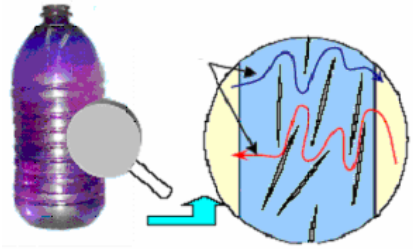

Rev. Roum. Chim., **2008**, *53*(11), 1017-1026

Key words: nanocomposites, poly (ethylene–co–vinyl acetate), layered silicates, barrier properties, melt processing.

Dan DRAGU and Mihai BUDA

Practical aspects associated with the use of Jacobi polynomials in the simulation of quasi-reversible electrode processes with linear potential scan and diffusional control in one dimension

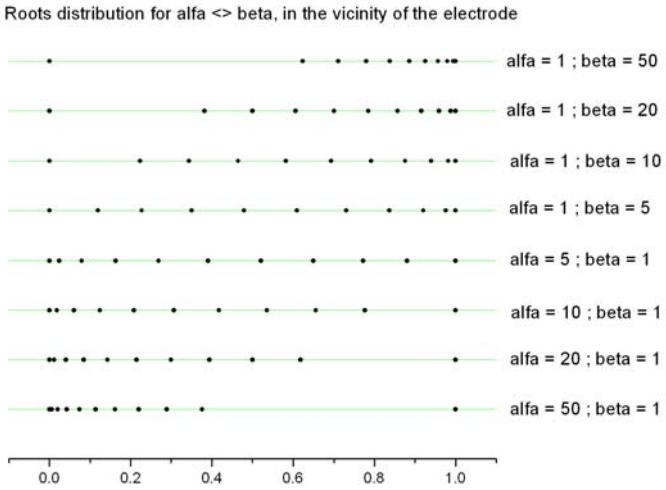

Rev. Roum. Chim., **2008**, *53*(11), 1027-1039

Key words: cyclic voltammetry, simulation, general Jacobi polynomials, orthogonal collocation.

Gabriela Geanina VASILE and Ion Gh. TĂNASE

Comparative study of different extraction methods for evaluation of biovailability of terrestrial sediment – bound metallic elements

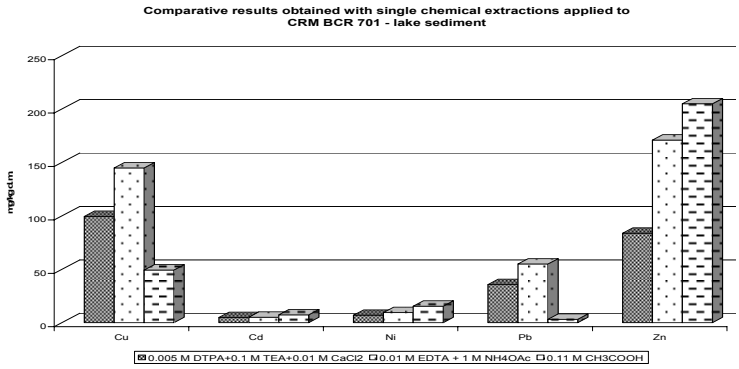

Rev. Roum. Chim., **2008**, *53*(11), 1041-1049

Key words: BCR 701, sediment, mobile elements, EDTA

Zenovia MOLDOVAN, Florica IONESCU, Ioana VASILESCU, Simona LIȚESCU and Laurenția ALEXANDRESCU

HDPE-EPDM thermoplastic vulcanizates. Mechanical and IR spectrometric properties

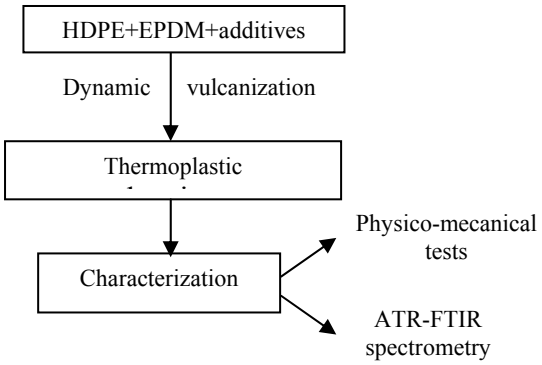

Rev. Roum. Chim., **2008**, *53*(11), 1051-1057

Key words: HDPE/EPDM thermoplastic vulcanizates.

Ruxanda BODÎRLĂU and Carmen-Alice TEACĂ

Softwood chemical modification by reaction with organic anhydrides

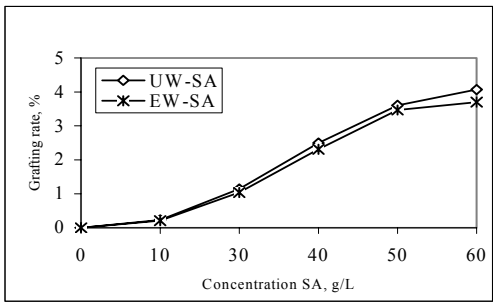

Rev. Roum. Chim., **2008**, *53*(11), 1059-1064

Key words: softwood, chemical modification; FT-IR; weight percent gain; water absorption.

Zaki AJJI

Radiation-induced preparation of gypsum/ poly(methyl acrylate) composites

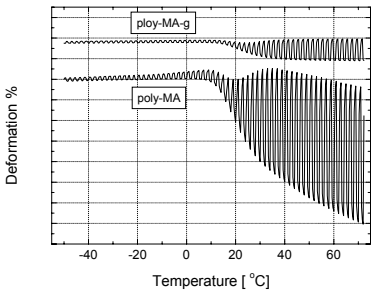

Rev. Roum. Chim., **2008**, *53*(11), 1065-1068

Key words: gypsum, polymer composites, methyl acrylate, radiation polymerization.

Annemarie PURI, Alina BĂDĂNOIU and Georgeta VOICU

Eco-friendly binders based on fly ash

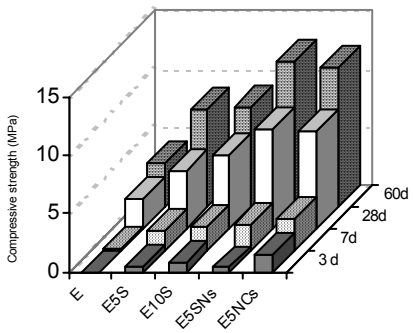

Rev. Roum. Chim., **2008**, *53*(11), 1069-1075

Key words: fly ash, lime, alkali-activated binders, sodium silicate.

Revue Roumaine de Chimie, **2008**, *53*(11), 977–988

VISCOSITY OF WATER, 1,4-DIOXANE AND DIMETHYL SULFOXIDE BINARY AND TERNARY SYSTEMS AT TEMPERATURES FROM 293.15 K TO 313.15 K

Ligia-Maria OMOTA[a], Olga IULIAN[a], Oana CIOCÎRLAN[a*] and Irina NIȚĂ[b]

[a] Department of Applied Physical Chemistry & Electrochemistry, University "Politehnica" of Bucharest, 313 Splaiul Independentei, Bucharest 060042, Roumania
[b] Department of Technology and Chemical Engineering, University "Ovidius" of Constanta, 124 bd. Mamaia, Constanta 900527, Roumania

Received January 23, 2008

The viscosity of the binary water+1,4-dioxane, water+dimethyl sulfoxide and 1,4-dioxane+ dimethyl sulfoxide systems and the corresponding ternary system was measured as function of composition and temperature. The experimental measurements were made at 293.15 K, 303.15 K and 313.15 K for the binary mixtures and at 303.15 K and 313.15 K, for the ternary system. The viscosity data were used to test the applicability of some correlative and predictive equations in literature: Kendall and Monroe, Grunberg-Nissan, Katty-Chaudhri, Tamura-Kurata, McAllister and Soliman. From experimental data the viscosity deviations ($\Delta\eta$) and excess Gibbs energy of activation of viscous flow (G^{*E}) were calculated and correlated by the Redlich-Kister's equations. The results are discussed in terms of the interactions between components.

INTRODUCTION

Many chemical engineering applications require knowledge of thermodynamic and transport properties of the multicomponent systems. In addition, these properties are useful to understand the behavior of the liquid mixtures. Generally, the correlation and prediction of the properties for the multicomponent systems from their constituent binary mixtures is widely used in the study of the liquid state. Estimation of the viscosity could be made by predictive and/or correlative equations. There are developed many empirical and semi-empirical equations to describe the binary mixture viscosity.[1]

Correlation of the viscosity with these equations requires several adjusting parameters. In the last years, the equations for the binary systems have been extended to the ternary mixtures by introducing a ternary adjustable parameter.[2] Many efforts are made to develop the predictive equations of the viscosity for the ternary and multicomponent systems. Some of them are based on a molecular approach,[3,4] while others are based on a group contribution concept.[5,6] However, a general theory for predicting the viscosity of the ternary systems from those of the pure components and constituent binary systems is not yet available.[7,8] In these circumstances, the experimental measurements, even if these are expensive and time-consuming, remain an important way to obtain realistic information concerning the dependence of the viscosity on composition in systems with many components.

This paper is an extension of our studies on physico-chemical properties of the solvent mixtures. In earlier papers [9-13] we have reported the vapour-liquid equilibrium (VLE) and density data for the binary and ternary systems containing water, 1,4-dioxane and dimethyl sulfoxide (DMSO). For the same systems, in this work we present the viscosity data. Most of the experimental viscosities available in the literature for these systems were reported at few temperatures for binary aqueous systems,[14,15] the ternary water+1,4-dioxane+DMSO system has been partially presented in our previous published work.[16]

* Corresponding author: ciocirlan_o@yahoo.com

The present work reports dynamic viscosities (η) for the binary water+1,4-dioxane , water+dimethyl sulfoxide (DMSO) and 1,4-dioxane+dimethyl sulfoxide systems and for the ternary water+1,4-dioxane+dimethyl sulfoxide system. The experimental measurements were carried out at 293.15 K, 303.15 and 313.15 K, for the binary systems, and at 303.15 and 313.15, for the ternary mixtures, covering the whole composition range. The kinematic and dynamic viscosity data of the binary and ternary systems were used to test the applicability of some correlative and predictive equations in literature. From the experimental values of viscosity, the viscosity deviations ($\Delta\eta$) and excess Gibbs energies of activation of viscous flow (G^{*E}) for the binary and ternary systems were calculated and correlated by the Redlich-Kister's equation. The variation of these thermodynamic properties with composition and temperature of the mixtures were found to be useful in understanding the nature the interactions between the component molecules.

EXPERIMENTAL

Materials. The chemicals used in this study were purified by distillation. DMSO was distilled under vacuum of 0.8-0.9 kPa at 338.65 K. The analytical reagent grade 1,4-dioxane from Merck was distilled at 374.35 K. The water was doubly distilled. The purity of the compounds was checked not only by comparing the measured densities and viscosities with those reported in the literature but also by gas chromatography. The purity found by gas chromatography was better than 99.8 mass %. The properties of the purified solvents, measured at 298.15, 303.15 and 313.15 along with literature values at the same temperatures are gathered in Table 1.

Table 1

Comparison of experimental values of densities and viscosities of pure liquids with corresponding literature values at different temperatures

Component	T, K	ρ, g cm^{-3}		η, mPa s	
		experimental	literature	experimental	literature
Water	293.15	0.9982	0.9982[17,18], 0.99821[19] 0.98820[20]	1.0050	0.999[17], 1.0032[18] 1.00219[21], 1.0021[20]
	303.15	0.9956	0.9957[18,22], 0.99607[23] 0.99565[24], 0.99564[20]	0.8007	0.797[22], 0.8005[18] 0.7931[23], 0.8075[20]
	313.15	0.9922	0.9922[18], 0.99283[23], 0.99221[24], 0.99222[20]	0.6560	0.6568[18], 0.6382[23] 0.65277[21], 0.6660[20]
1,4-Dioxane	293.15	1.0339	1.0334[25], 1.0317[26]	1.3125	
	303.15	1.0225	1.0222[27], 1.02244[28], 1.0225[29], 1.02221[30]	1.1127	1.0937[27], 1.1000[28] 1.086[29], 1.101[30]
	313.15	1.0121	1.0110[30]	0.9603	0.9425[30]
DMSO	293.15	1.1012	1.10041[17], 1.10040[31] 1.10145[32]	2.2255	2.194[17], 2.216[31]
	303.15	1.0901	1.0907[29], 1.09054[33] 1.09038[23]	1.8180	1.662[29], 1.8034[33] 1.8102[23]
	313.15	1.0804	1.08064[23], 1.0804[34] 1.0806[35]	1.5553	1.5152[23]

Apparatus and procedure. Kinematic viscosity measurements of pure solvents and their binary and ternary mixtures were carried out using an Ubbelohde viscometer for which the accuracy of the flow time was ±0.1 seconds and the corresponding uncertainty in the kinematic viscosity was ± 0.001 10^{-6} m^2 s^{-1}. The time of fall always exceeded 60 seconds. The viscometer was calibrated with double distilled water and pure solvents. At least five time flow measurements were performed for each composition and temperature and the results were averaged. A thermostatically controlled bath was used to keep the temperature within ±0.05 K.

All mixtures were prepared by weighing the appropriate volumes of liquids in airtight stoppered glass bottle. The reproductibility in mole fraction was within ±0.0002. The weightings were done on a HR-120 (A&D Japan) balance with a precision of $\pm 0.1 \cdot 10^{-3}$ g. All mixtures were completely miscible over the whole composition range.

RESULTS AND DISCUSSION

Viscosities and their correlation

The experimental data of viscosities for binary and ternary systems containing water, 1,4-dioxane and dimethyl sulfoxide (DMSO) was utilised to test various correlative and predictive viscosity methods in literature. The feasibility of several specific equations to correlate composition-viscosity data for binary and ternary systems was tested. For ternary system the equations incorporate parameters from the binary systems and one or more ternary parameters.

Thus, the equation proposed by Kendall and Monroe[36] is a predictive relation that takes into account only the viscosity of pure components:

$$\eta = \left(\sum_{i=1}^{n} X_i \eta_i^{1/3} \right)^3 \tag{1}$$

The correlative equations of Grunberg-Nissan[37]and Katti- Chaudhri[38] were initially developed only for the binary systems, having one adjustable parameter. Canosa[2] has proposed in 1998 an extension of these equations to the ternary mixtures by introducing of a ternary adjustable parameter. The general form of these equations is done by relations (2) and (3), respectively:

$$\ln \eta = \sum_{i}^{n} X_i \ln \eta_i + \sum_{i}^{n} \sum_{j>i}^{n} X_i X_j A_{ij} + \sum_{i}^{n} \sum_{j>i}^{n} \sum_{k>j}^{n} X_i X_j X_k A_{ijk} \tag{2}$$

$$\ln(\eta V) = \sum_{i}^{n} X_i \ln(\eta_i V_i) + \sum_{i}^{n} \sum_{j>i}^{n} X_i X_j A_{ij} + \sum_{i}^{n} \sum_{j>i}^{n} \sum_{k>j}^{n} X_i X_j X_k A_{ijk} \tag{3}$$

where η is the dynamic viscosity of the mixture, η_i is the viscosity of pure component i, X_i are the mole fractions, A_{ij} and A_{ijk} are the interaction parameters; V_i is molar volume of pure component i.

In this paper we have taken in consideration the Canosa's contribution and applied it to the Tamura and Kurata equation, [39] also initially developed only for the binary systems. The new mathematical relation of the Tamura and Kurata equation for n-component mixtures is:

$$\eta = \sum_{i}^{n} X_i \phi_i \eta_i + 2 \sum_{i}^{n} \sum_{j>i}^{n} \left(X_i X_j \phi_i \phi_j \right)^{0.5} A_{ij} + 2 \sum_{i}^{n} \sum_{j>i}^{n} \sum_{k>j}^{n} \left(X_i X_j X_k \phi_i \phi_j \phi_k \right)^{0.5} A_{ijk} \tag{4}$$

where ϕ_i is the volume fraction.

McAllister's two-parameters equation,[40] based on Eyring's theory of absolute reaction rates, takes into account interactions both of like and unlike molecules by a two-dimensional three-body interaction. This equation has extended to ternary mixtures by Kalidas and Laddha.[41]

$$\begin{aligned} \ln \nu = & \sum_{i=1}^{n} X_i^3 \ln(\nu_i M_i) - \ln M_{av} + 3 \sum_{i=1}^{n} \sum_{\substack{j=1 \\ j \neq i}}^{n} X_i^2 X_j \ln\left(\nu_{ij} \frac{2M_i + M_j}{3} \right) \\ & + 6 \sum_{i}^{n} \sum_{j>i}^{n} \sum_{k>j}^{n} X_i X_j X_k \ln\left(\nu_{ijk} \frac{M_i + M_j + M_k}{3} \right) \end{aligned} \tag{5}$$

ν is the kinematic viscosity of the mixture, ν_i is the viscosity of pure component i, ν_{ij} and ν_{ijk} are binary and ternary interaction parameters, respectively, M_i is the pure components molecular mass, M_{av} is the molecular mass of mixture.

The McAllister equation of the four-body interactions[40] is more complex and may be used more favorable for mixtures with strong interactions. This equation has three adjustable parameters and for ternary systems is expressed as:[42]

$$\begin{aligned} \ln \nu = & \sum_{i}^{3} X_i^4 \ln(\nu_i M_i) - \ln\left(\sum_{i}^{3} X_i M_i \right) + 4 \sum_{i}^{3} \sum_{\substack{j \\ j \neq i}}^{3} X_i^3 X_j \ln\left(A_{iiij} \frac{3M_i + M_j}{4} \right) \\ & + 6 \sum_{i}^{3} \sum_{\substack{j \\ i<j}}^{3} X_i^2 X_j^2 \ln\left(A_{iijj} \frac{M_i + M_j}{2} \right) \\ & + 12 \sum_{i}^{3} \sum_{\substack{j \\ j \neq i}}^{3} \sum_{\substack{k \\ k \neq j, j<k}}^{3} X_i^2 X_j X_k \ln\left(A_{iijk} \frac{2M_i + M_j + M_k}{4} \right) \end{aligned} \tag{6}$$

The data were also correlated with a modified form of the McAllister equation proposed by Soliman.[43] The general form of the equation is as follows:

$$\ln \nu = \sum_{i=1}^{n} X_i^3 \ln \nu_i + 3\sum_{i=1}^{n}\sum_{\substack{j=1 \\ i\neq j}}^{n} X_i^2 X_j \ln A_{ij} + \sum_{i=1}^{n}\sum_{\substack{j=1 \\ j\neq i}}^{n} \frac{\left(X_i + X_j\right)^3 B_{ij} X_i X_j}{\left(\frac{M_i}{M_j}\right)^2 X_i + X_j} + 6\sum_{i}^{n}\sum_{j>i}^{n}\sum_{k>j}^{n} X_i X_j X_k \ln A_{ijk} \quad (7)$$

The values of coefficients were evaluated by method of least-squares, with the corresponding standard deviation, (σ), calculated by using the relation:

$$\sigma = \left[\frac{\sum\left(Y_{\exp} - Y_{calc}\right)^2}{N_{\exp} - N_{par}}\right]^{0.5} \quad (8)$$

where Y is the experimental and calculated viscosity, respectively. N_{exp} is the number of experimental data and N_{par} is the number of parameters.

Binary systems

The experimental values of viscosity at different temperatures for the water + 1,4-dioxane, water + DMSO and 1,4-dioxane DMSO systems over the whole composition range expressed by mole fraction are given in Table 2.

The tabulated data show that the values of viscosity of the both aqueous systems present a maximum at low concentration of 1,4-dioxane and DMSO, respectively. In the 1,4-dioxane+DMSO mixture, the viscosity decreases with the increase of the mole fraction of 1,4-dioxane.

The experimental mixture viscosities were correlated/predicted through the eqs. (1-7). In order to determine the kinematic viscosity in eqs. (5-7), the densities presented in a previous paper[13] were used. The values of the adjustable parameters and the standard deviations are reported in Table 3. The analysis of standard deviations reveals that the capability of these equations to estimate the viscosity of the binary systems depends on the complexity of the mixtures. For a binary system without strong interactions, like 1,4-dioxane+DMSO, any equation can be used to correlate adequately the viscosity data. For the aqueous systems only the three parameters equations of McAllister and Soliman give the best results for these non-ideal systems. The correlating ability significantly improves as the number of the adjustable parameters is increased.

Table 2

Experimental viscosities (η), viscosity deviations ($\Delta\eta$) and excess Gibbs energy of activation of viscous flow (G^{*E}) for the binary systems at different temperatures

T, K	293.15			303.15			313.15		
X_1	η, *mPa s*	$\Delta\eta$, *mPa s*	G^{*E}, *J mol^{-1}*	η, *mPa s*	$\Delta\eta$, *mPa s*	G^{*E}, *J mol^{-1}*	η, *mPa s*	$\Delta\eta$, *mPa s*	G^{*E}, *J mol^{-1}*
water(1)+1,4-dioxane(2)									
0.0000	1.3125	0	0	1.1127	0	0	0.9603	0	0
0.1007	1.3481	0.067	304.2	1.1263	0.045	295.7	0.9753	0.046	329.6
0.1995	1.4469	0.196	693.5	1.1895	0.139	674.4	1.0059	0.106	674.7
0.3422	1.6630	0.426	1262.4	1.3551	0.349	1311.2	1.1020	0.246	1252.3
0.4256	1.7645	0.583	1584.9	1.4920	0.512	1706.4	1.1990	0.368	1641.5
0.5379	1.9793	0.832	2004.9	1.6949	0.750	2191.9	1.3553	0.559	2146.3
0.6640	2.2300	1.122	2381.5	1.8578	0.952	2533.4	1.4830	0.725	2513.2
0.7530	2.2948	1.214	2451.7	1.8470	0.969	2533.3	1.4753	0.744	2528.1
0.8197	2.2032	1.143	2309.2	1.7334	0.876	2338.9	1.3829	0.672	2332.9
0.8710	2.0130	0.968	2024.2	1.5702	0.729	2030.0	1.2495	0.554	2013.1
0.9130	1.7655	0.734	1626.6	1.3795	0.552	1628.2	1.1000	0.418	1606.4
0.9470	1.5044	0.483	1153.8	1.1843	0.367	1161.9	0.9450	0.273	1128.7
0.9760	1.2240	0.232	603.9	0.9868	0.179	614.1	0.7960	0.133	593.1
1.0000	1.0050	0	0	0.8007	0	0	0.6560	0	0

Table 2 (continued)

water(1)+DMSO(2)									
0.0000	2.2255	0	0	1.8180	0	0	1.5553	0	0
0.0915	2.4515	0.338	538.8	1.9550	0.230	499.7	1.6545	0.182	495.6
0.1713	2.6765	0.660	1005.3	2.0820	0.438	922.8	1.7480	0.347	919.4
0.2415	2.8714	0.941	1388.7	2.2237	0.651	1311.7	1.8400	0.502	1290.3
0.3038	3.0658	1.211	1728.0	2.3833	0.874	1675.7	1.9388	0.657	1628.6
0.3594	3.2743	1.487	2041.0	2.5523	1.100	2009.6	2.0457	0.814	1941.0
0.4795	3.8322	2.192	2726.3	2.9441	1.614	2689.2	2.3048	1.181	2594.8
0.5669	4.2124	2.679	3148.3	3.1509	1.910	3064.1	2.4516	1.406	2975.3
0.6541	4.3588	2.932	3394.2	3.1679	2.015	3251.8	2.4679	1.501	3181.2
0.7021	4.2602	2.892	3413.8	3.0584	1.955	3244.4	2.3885	1.465	3184.8
0.7842	3.7056	2.437	3174.9	2.6427	1.623	2986.5	2.0738	1.224	2939.5
0.8637	2.7242	1.553	2481.2	1.9906	1.051	2336.3	1.5702	0.792	2290.9
0.9218	1.8706	0.770	1571.6	1.4343	0.554	1521.6	1.1383	0.412	1473.9
0.9649	1.3067	0.259	677.0	1.0476	0.211	712.6	0.8404	0.153	674.0
1.0000	1.0050	0	0	0.8007	0	0	0.6560	0	0
1,4-dioxane(1)+DMSO(2)									
0.0000	2.2255	0	0	1.8180	0	0.	1.5553	0	0
0.0419	2.1660	-0.021	-11.4	1.7718	-0.017	-14.1	1.5151	-0.015	-17.8
0.1062	2.0800	-0.049	-26.5	1.7035	-0.040	-34.9	1.4560	-0.036	-43.8
0.2171	1.9424	-0.085	-49.5	1.5930	-0.072	-68.2	1.3615	-0.065	-83.1
0.3094	1.8384	-.0105	-64.0	1.5093	-0.091	-90.6	1.2895	-0.082	-110.3
0.4050	1.7402	-0.116	-74.6	1.4295	-0.103	-109.3	1.2227	-0.092	-129.6
0.4541	1.6934	-0.118	-77.7	1.3915	-0.106	-116.3	1.1909	-0.094	-136.4
0.5041	1.6481	-0.117	-79.4	1.3550	-0.108	-121.2	1.1603	-0.095	-141.3
0.6071	1.5621	-0.109	-77.7	1.2864	-0.103	-124.0	1.1034	-0.091	-141.5
0.7139	1.4826	-0.091	-68.0	1.2252	-0.089	-113.7	1.0529	-0.078	-127.5
0.8250	1.4096	-0.063	-49.0	1.1729	-0.063	-85.1	1.0095	-0.055	-94.7
0.9112	1.3592	-0.034	-27.9	1.1394	-0.036	-50.7	0.9824	-0.031	-54.9
0.9530	1.3365	-0.019	-15.6	1.1259	-0.020	-28.7	0.9712	-0.017	-31.1
1.0000	1.3125	0	0	1.1127	0	0	0.9603	0	0

Table 3

Adjustable parameters and standard deviations of the equation (1) to (7) for the binary systems at different temperatures

Equation	Parameters/Standard deviation	Temperature, K			Temperature, K			Temperature, K		
		293.15	303.15	313.15	293.15	303.15	313.15	293.15	303.15	313.15
		Water +1,4-dioxane			Water +DMSO			1,4-dioxane +DMSO		
Kendall-Monroe	σ	0.7136	0.5769	0.4383	1.7448	1.2257	0.9194	0.0522	0.0529	0.0479
Grunberg-Nissan	A_{12}	2.4886	2.5017	2.2948	3.9269	3.5993	3.3366	-0.1347	-0.1807	-0.1950
	σ	0.4242	0.3303	0.2577	0.8287	0.5600	0.4248	0.0017	0.0057	0.0042
Tamura-Kurata	A_{12}	3.7517	3.0457	2.3869	6.9445	4.9781	3.7935	1.5741	1.2728	1.0799
	σ	0.1566	0.1131	0.0913	0.3069	0.2025	0.1466	0.0009	0.0026	0.0013
Katti-Chaudhri	A_{12}	3.5237	3.5479	3.3516	4.6813	4.3448	4.0703	-0.1283	-0.1877	-0.2129
	σ	0.4771	0.3757	0.2956	0.8871	0.6050	0.4597	0.0018	0.0053	0.0038
McAllister (Eq.5)	A_{12}	9.9103	7.9118	6.0287	20.3498	12.7855	9.1909	1.4093	1.1504	0.9952
	A_{21}	0.7127	0.6449	0.5455	1.6789	1.4219	1.1837	1.6642	1.3828	1.1837
	σ	0.1473	0.0939	0.0756	0.1609	0.0835	0.0731	0.0002	0.0003	0.0001
McAllister (Eq.6)	A_{1112}	8.9669	6.6501	5.1729	14.0599	8.2681	6.3167	1.3738	1.1327	0.9826
	A_{1122}	0.7769	0.7800	0.6299	2.7186	2.4914	1.8507	1.5292	1.2639	1.0862
	A_{2221}	1.8919	1.4742	1.2459	2.7591	1.9964	1.7052	1.7479	1.4470	1.2422
	σ	0.0509	0.0463	0.0309	0.0305	0.0083	0.0109	0.0001	0.0001	0.0001
Soliman	A_{12}	2.8715	2.8249	2.2499	9.5711	6.9508	4.9734	1.3346	1.1188	0.9684
	A_{21}	0.9212	0.7844	0.6528	1.7521	1.4599	1.2109	1.5525	1.3345	1.1432
	B_{12}	0.5004	0.3943	0.3719	0.3474	0.2532	0.2577	0.2080	0.1048	0.1026
	σ	0.0459	0.0192	0.0241	0.1135	0.0492	0.0481	0.0001	0.0003	0.0002

From the measured viscosities, the viscosity deviations and excess Gibbs energies of activation of viscous flow were calculated and presented in Table 2. The viscosity deviations ($\Delta\eta$) were computed through the equation (9) and the excess Gibbs energies of activation of viscous flow (G^{*E}) were calculated on the basis of the theory of absolute reaction rate with the relation (10).

$$\Delta\eta = \eta - \sum_{i=1}^{n} X_i \eta_i \qquad (9)$$

$$G^{*E} = RT\left[\ln(V\eta) - \sum_{i=1}^{N} X_i \ln(V_i \eta_i)\right] \qquad (10)$$

η and η_i are the dynamic viscosity of the mixture, and of the pure component i, respectively; V and V_i are the molar volume of the mixture, and of the pure component i, respectively. X_i are the mole fractions, R and T have their usual meaning. Both excess properties (Y^E) were fitted to Redlich-Kister's equation: [44]

$$Y^E = X_i X_j \sum_{k=0}^{p} A_k \left(X_j - X_i\right)^k \qquad (11)$$

where A_i are the adjustable parameters and p is the degree of polynomial expansion. The choice of the number of parameters was based on the standard deviation (σ) calculated using type (8) equation. The obtained coefficients and the standard deviations at three temperatures are given in Table 4. The experimental and calculated excess properties at 303.15 K are plotted in Figures 1 and 2.

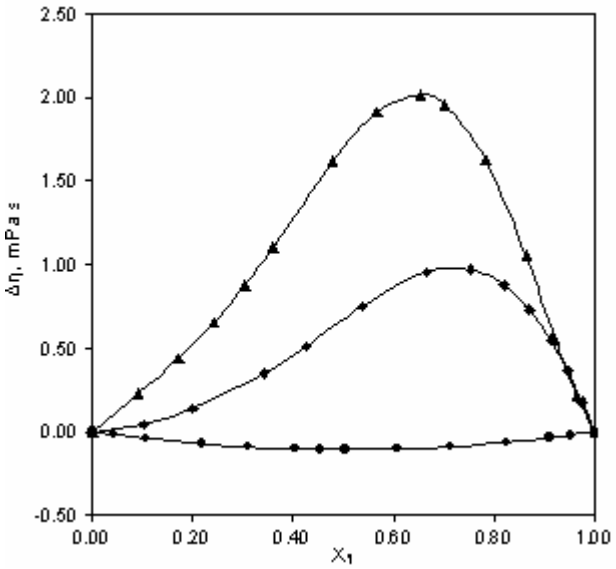

Fig. 1 – Viscosity deviations of the binary systems at T=303.15 K for: ♦ water(1) +1,4-dioxane(2), ▲ water(1) +DMSO(2), ● 1,4-dioxane(1) + DMSO(2), (——) Redlich-Kister's correlation.

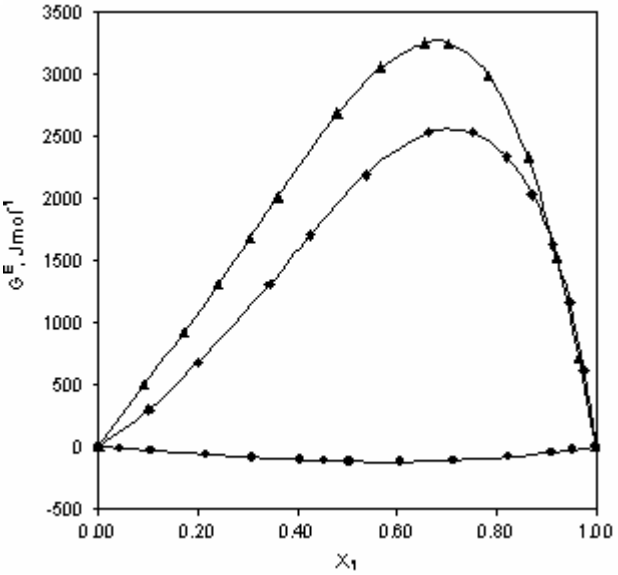

Fig. 2 – Excess molar Gibbs of activation of viscous flow of the binary systems at T=303.15 K for: ♦ water(1) +1,4-dioxane(2), ▲ water(1) +DMSO(2), ● 1,4-dioxane(1) + DMSO(2), (——) Redlich-Kister's correlation.

The viscosity deviations and excess Gibbs energies of activation of viscous flow for the binary water +DMSO and water+1,4-dioxane systems are positive over the entire composition range as shown in Table 2 and figures 1-2. An increase of temperature considerably modifies the viscosity deviations of these binary mixtures; however, G^{*E} scarcely changes. The water +DMSO system presents the viscosity maxima between 2.9–1.5 mPa s at X_{water}=0.6541 and water+1,4-dioxane system, between 2.29-0.74 mPa s at X_1=0.7530 at studied temperatures. The aqueous systems present asymmetrical curves with the maximum values in the water-rich region. The 1,4-dioxane+DMSO mixture shows small negative deviations for both $\Delta\eta$ and G^{*E}, decreasing their algebraic values as temperature raised. Temperature has a strong influence on the excess Gibbs energies of activation of viscous flow. The viscosity minima lies between –0.117 and -0.095 mPa s at X_{water}=0.5041.

Table 4

Coefficients A_i of eq. (11) and standard deviations $\sigma(Y^E)$ for the binary systems at different temperatures

T, K	293.15		303.15		313.15	
	$\Delta\eta$, mPa s	G^{*E}, J mol^{-1}	$\Delta\eta$, mPa s	G^{*E}, J mol^{-1}	$\Delta\eta$, mPa s	G^{*E}, J mol^{-1}
Water + 1,4-dioxane						
A_0	2.9757	7495.7	2.6859	8185.4	1.9753	7953.3
A_1	-4.6205	-7611.7	-4.2819	-8613.4	-3.4384	-8942.6
A_2	4.5891	5345.2	1.9576	2838.9	1.7866	3560.5
A_3	-2.0360	-1585.0	0.8783	938.3	1.0617	1563.4
A_4	-2.4882	1463.3	-0.7122	3636.1	-0.7129	3228.6
A_5	1.7579	-3989.1	-0.5498	-5694.1	-0.3516	-4844.4
σ	0.0008	7.722	0.0006	8.741	0.0008	6.054
Water + DMSO						
A_0	9.2637	11374.3	6.7769	11173.9	4.9629	10796.6
A_1	-11.9166	-10139.0	-7.5905	-9373.7	-5.6851	-9369.3
A_2	4.6181	3926.5	0.1196	2274.3	0.9978	3124.4
A_3	11.1256	-918.2	6.5416	-1179.6	5.0220	-647.4
A_4	-10.3609	8959.2	-3.2653	5702.3	-3.4444	5460.8
A_5		3334.1		2480.5		2420.0
A_6		-13400.3		-6203.6		-7575.0
σ	0.0003	13.756	0.0001	6.080	0.0004	7.189
1,4-dioxane +DMSO						
A_0	-0.4691	-316.1	-0.4299	-483.9	-0.3804	-565.0
A_1	-0.0541	40.4	0.0152	158.8		135.7
A_2	-	-		-15.3		
σ	0.0001	0.301	0.0001	0.2919	0.0001	0.326

The viscosity deviations are functions of size and shape of molecules as well as molecular interactions between the components. Fort and Moore[45] state that a positive viscosity deviation is characteristic of systems with strong interaction between components whereas mixtures where dispersion forces are predominant present negative viscosity deviations. Similarly to the case of viscosity deviation, the excess molar volume and deviations from Raoult's law are related to the molecular interactions between components of the mixture.

The binary systems with water show important negative values V^E over the whole composition range at temperatures between 293.15 and 313.15 K and asymmetrical curves V^E - composition.[11,13] Thus, the binary water + DMSO system presents the V^E minima between –0.85 and –1.25 cm^3 mol^{-1} at X_{water}≈0.6 at mentioned temperatures; the binary system water+1,4-dioxane presents V^E minima between -0.65 and –0.75 cm^3 mol^{-1}at X_{water} ≈0.7, in the same domain of temperatures.[13] Binary mixture of 1,4-dioxane+DMSO presents lower V^E than aqueous systems with symmetrical minima between –0.2 and –0.7 cm^3 mol^{-1} in the range 293.15 - 313.15 K temperatures.[13]

Binary systems of water and organic solvents are systems with strong deviations from Raoult's law; the binary water+DMSO mixtures are characterized by strong negative deviations from Raoult's law; [9-10] the water+1,4-dioxane mixtures have an azeotropic point and show strong positive deviations from ideality. Binary mixture of 1,4-dioxane+DMSO presents positive deviations from Raoult's law.[10]

The system behavior is the result of the pure components structure and interactions between them upon mixing. The structural information shows that water is an interesting solvent with small size, quadruple moment which is able to support extensive hydrogen-bonding network.[46.] At ambient pressure, DMSO exists in the liquid state over a wide temperature range (T_f=291 K and T_b=462 K) and is completely miscible with water. The high boiling temperature has been attributed to the large dipole moment of DMSO molecule (μ=3.96 D at 298.15 K). In the strongly polar S=O bond, oxygen is the most electronegative site of DMSO. Dipole or ionic interactions are responsible for self-association DMSO molecules. Acting as a proton acceptor, it can alter the structure of water. From thermodynamic consideration, Lindberg[47] has argued that the water-

DMSO hydrogen bond is stronger than the water-water hydrogen bond. The studies indicate a strong interaction between water and DMSO, and the general conclusion is that in the mole fraction range $0.7 < X_{water} < 0.6$ the interactions due to hydrogen bonds are at maximum, suggesting the existence of stoichiometrically well-defined $1DMSO:2H_2O$ aggregates.[17,45-48] The water+DMSO mixtures are interesting because of their microheterogeneity indicating cluster formation.[49] Infrared spectroscopy shows that small quantities of DMSO have little effect on the water structure.[50] Other methods[51,52] even lead to the conclusion that small amounts of DMSO act as a "structure breaker" in water.

1,4-Dioxane ($\mu = 0.4$ D) and water are miscible at all solvent compositions and some of their physical properties, such as boiling points, vapor pressures and densities, are approximately identical, but their dielectric constants and dipole moments are very different. Dioxane is an aprotic solvent, whereas water is both an electron donor and acceptor. The X-ray diffraction, mass spectrometry and NMR relaxation were used to investigate the structure of the mixtures containing water and 1,4-dioxane.[53] The investigation results show that in the water-rich region ($X_{water} > \sim 0.9$) the water-water hydrogen bonded network is predominantly formed in the mixtures. When $X_{water} <\sim 0.6$, the clusters characteristic of pure 1,4 dioxane are gradually formed. In this domain the structure of pure 1,4-dioxane is dominant; the water molecules forms hydrogen bonds with pure 1,4-dioxane clusters without altering its bulk structure. Between the mentioned molar fractions, because of unlike interactions, both opened ice-like structure of water and inherent structure of 1,4-dioxane are broken down, and the hydrogen-bonded clusters of 1,4- dioxane and water molecules are the main species in the binary solutions.

The positive $\Delta\eta$ and negative V^E, with accentuated maxima or minima and the structural informations characterise the aqueous binary systems as complex systems, with strong interactions of hydrogen bond and dipole –dipole type. This behaviour is in accordance to Fort and Moore idea[45] and corresponds to systems containing associated components. In the case of DMSO + 1,4-dioxane system, the poor unlike dipole-dipole interactions between SO groups of the DMSO and the O group of 1,4-dioxane, and the capability of 1,4-dioxane molecules to break the polymer chains of DMSO molecules[54], are responsible of small negative $\Delta\eta$ and moderate negative V^E.

Vogel and Weiss[55] affirm that, generally, the mixtures with strong interactions between different molecules present positive viscosity deviations and negative deviations from Raoult's law; whereas, for mixtures without strong specific interactions, the viscosity deviations are negative and deviations of Raoult's law are positive. From the investigated systems, only those containing DMSO present this type of behaviour.

Ternary systems

The experimental viscosities as well as the computed properties: viscosity deviation and excess Gibbs energies of activation of viscous flow for the ternary water+1,4-dioxane+DMSO at 303.15 K and 313.15 K are listed in Table 5. The viscosity deviations and the excess Gibbs energies of activation were computed with eqs. (9) and (10) and fitted to the Redlich-Kister equation:

$$Y^E = Y^E_{bin} + X_1X_2X_3\left(A + B_{12}\left(X_2 - X_1\right) + B_{13}\left(X_3 - X_1\right) + B_{23}\left(X_3 - X_2\right) + C_{12}\left(X_2 - X_1\right)^2 + C_{13}\left(X_3 - X_1\right)^2 + C_{23}\left(X_3 - X_2\right)^2 + \ldots\right) \quad (12)$$

where $Y^E_{bin} = Y^E_{12} + Y^E_{13} + Y^E_{23}$; Y^E_{ij} are given by eq. (11).

Table 5

Values of viscosities (η), viscosity deviation ($\Delta\eta$) and excess Gibbs energies of activation of viscous flow (G^{*E}) as function of composition for the ternary system at different temperatures

T, K		303.15			313.15		
X_1	X_2	η^*, *mPa s*	$\Delta\eta$, *mPa s*	G^{*E}, *J mol^{-1}*	η^*, *mPa s*	$\Delta\eta$, *mPa s*	G^{*E}, *J mol^{-1}*
0.0999	0.8001	1.1898	0.038	301.7	1.0098	0.021	279.8
0.1000	0.5998	1.3323	0.039	329.4	1.1248	0.017	294.2
0.0998	0.4010	1.4929	0.059	358.8	1.2624	0.036	334.6

Table 5 (continued)

0.1000	0.1999	1.7147	0.140	458.4	1.4425	0.097	418.8
0.1997	0.6000	1.3734	0.182	766.8	1.1562	0.138	753.3
0.1998	0.4020	1.5594	0.228	825.6	1.3070	0.171	798.8
0.2000	0.2001	1.8276	0.354	958.4	1.5280	0.272	931.7
0.1998	0.1000	2.0070	0.463	1059.6	1.6727	0.357	1028.5
0.3002	0.5999	1.3707	0.281	1109.8	1.1450	0.217	1098.8
0.3000	0.4000	1.6407	0.410	1288.1	1.3521	0.305	1246.0
0.3000	0.2000	1.9866	0.615	1489.0	1.6072	0.441	1410.7
0.2999	0.1002	2.1884	0.746	1595.4	1.7822	0.557	1536.0
0.3997	0.5001	1.5287	0.470	1571.5	1.2496	0.351	1531.5
0.4000	0.4002	1.6858	0.557	1672.6	1.3794	0.422	1640.1
0.4002	0.1998	2.1482	0.878	1987.1	1.7417	0.666	1941.7
0.3998	0.1002	2.3846	1.044	2104.3	1.9165	0.781	2041.3
0.5000	0.4001	1.6947	0.668	1980.9	1.4011	0.534	1999.3
0.5001	0.3000	1.9655	0.868	2197.9	1.5599	0.633	2117.4
0.5002	0.1998	2.1389	0.971	2253.9	1.7757	0.789	2291.8
0.4998	0.1002	1.5017	1.348	2576.5	2.0477	1.002	2501.5
0.5997	0.3002	1.9354	0.939	2417.5	1.5260	0.689	2342.5
0.6001	0.1997	2.2278	1.161	2603.4	1.7683	0.872	2546.6
0.6000	0.1000	2.6597	1.523	2880.8	2.0747	1.119	2793.9
0.7000	0.2001	2.0698	1.105	2628.5	1.6438	0.837	2590.9
0.6998	0.1000	2.6479	1.612	3064.9	1.9612	1.095	2860.4
0.8001	0.1500	1.9214	1.023	2504.2	1.4854	0.739	2406.8
0.7990	0.0500	2.3545	1.385	2816.4	1.7634	0.957	2645.1
0.9000	0.0500	1.5247	0.658	1786.5	1.2107	0.495	1745.2
0.9000	0.0250	1.5640	0.679	1795.2	1.2463	0.515	1762.9

[*] Iulian et al.[9]

The eqs. (1)-(7), extended for the ternary system, were used to predict/correlate the experimental viscosity data. For the ternary systems, three procedures were used in the fitting of these equations. In the first, we predicted the viscosity of the ternary mixtures using only the binary parameters, without any ternary parameters. In the second procedure we fixed the binary parameters and fitted only the ternary parameters. Finally, in the third procedure, we fitted all parameters. Table 6 shows the complete results of the prediction and correlation with these equations, at 303.15 and 313.15 K.

Table 6

Adjustable parameters and standard deviations of the equation (1) to (7) for the ternary system at different temperatures

Eq.	T, K	A_{12}	A_{13}	A_{23}	A_{21}	A_{31}	A_{32}	B_{12}	B_{13}	B_{23}	A_{123}	σ
(1)	303.15											0.8692[a]
	313.15											0.6461[a]
(2)	303.15											0.4189[a]
											-5.1695	0.3567[b]
		3.8702	4.9454	-1.1898							-14.215	0.3080[c]
	313.15											0.3009[a]
											-4.7109	0.2539[b]
		3.4647	4.4445	-1.1559							-11.733	0.2193[c]
(3)	303.15											0.4603[a]
											-5.5386	0.3955[b]
		5.0468	5.8129	-1.4400							-14.881	0.3409[c]
	313.15											0.3349[a]
											-5.0827	0.2860[b]
		4.6423	5.3064	-1.4056							-12.408	0.2463[c]
(4)	303.15											0.1666[a]
											-2.7764	0.1294[b]
		2.7477	5.0399	0.6909							0.7707	0.1106[a]
	313.15											0.1146[a]
											-2.0699	0.0829[b]
		2.0802	3.6889	0.6523							1.4704	0.0678[c]

Table 6 (continued)

(5)	303.15												0.2638[a]
										0.7644			0.1314[b]
		6.5361	14.871	1.7975	0.7700	1.4929	2.1842			0.4323			0.0902[c]
	313.15												0.1273[a]
										0.5649			0.1001[b]
		4.8479	9.2734	1.4736	0.6479	1.3135	1.6575			0.4618			0.0579[c]
(7)	303.15												0.0932[a]
										0.9741			0.0946[b]
		1.6691	8.9739	1.4037	0.8531	1.6076	1.8937	0.6447	-0.0342	-0.3185	0.9512		0.0529[c]
	313.15												0.0865[a]
											0.8310		0.0806[b]
		1.7197	5.8165	3.9964	0.6892	1.3449	6.5603	0.4706	0.0224	-4.9986	0.5721		0.0207[c]
(6)		A_{1112}	A_{1113}	A_{2221}	A_{2223}	A_{3331}	A_{3332}	A_{1122}	A_{1133}	A_{2233}	A_{1123}	A_{2213}	A_{3312}	
	303.15													0.1739[a]
											1.1015	1.4885	2.0693	0.0385[b]
		5.8683	9.6320	1.3372	0.9242	2.1571	1.3835	0.8431	2.4386	1.1297	0.8701	2.4456	1.9325	0.0368[c]
	313.15													0.0849[a]
											0.8130	1.3632	1.7842	0.0302[b]
		4.2828	6.0177	1.1578	0.8051	1.7543	1.1517	0.7262	2.0109	1.0461	0.8759	1.7288	1.5973	0.0135[c]

[a] prediction from binary parameters; [b] optimization of the ternary parameters; [c] optimization of all model parameters

The prediction results obtained with McAllister and Soliman equations are better than those obtained with the other equations, because, probably of great parameter number and their advanced theoretical support. The viscosity prediction using only binary parameters gives inferior results. Generally, a rise of number of parameters leads to a smaller standard deviation and, especially, the increase of number of ternary parameters improves the viscosity predictions. The optimization of all parameters leads to an improvement of the computational results.

The computed properties: viscosity deviation and excess Gibbs energies of activation of viscous flow at two temperatures for the ternary system, presented in Table 5, show that they are positive over the whole composition range, as we expected from binary values. Also, it can be observed that an increase of the temperature affects considerably the viscosity deviation, while the excess Gibbs energy hardly modifies. The isolines at constant values of $\Delta\eta$ and G^{*E} at 303.15 K have been drawn in Figures 3 and 4, respectively. The results of correlation with Redlich-Kister equation (eq.12), the coefficients and the standard deviations are gathered in Table 7.

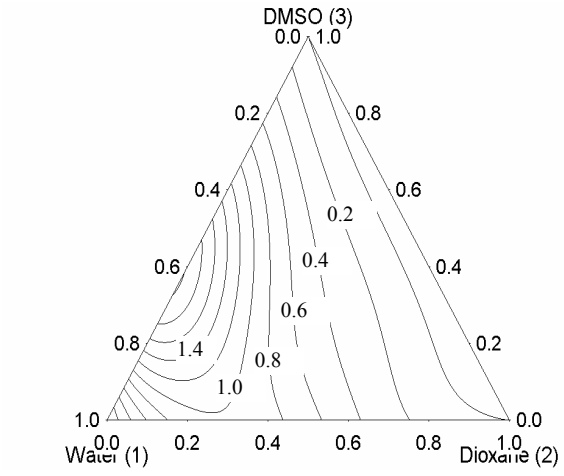

Fig. 3 – Isolines at constant $\Delta\eta$ for the ternary water(1)+1,4-dioxane (2)+DMSO(3) system at 303.15 K.

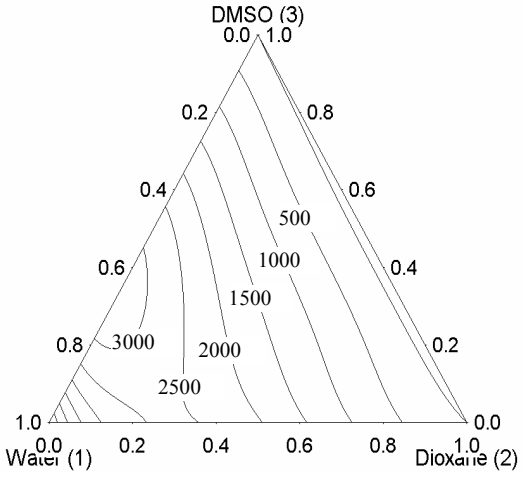

Fig. 4 – Isolines at constant G^{*E} for the ternary water(1)+1,4-dioxane (2)+DMSO(3) system at 303.15 K.

Table 7

Coefficients of Redlich-Kister's equation and standard deviation for excess properties of the water +1,4-dioxane +DMSO ternary system

T, K	303.15		313.15	
	$\Delta\eta$, *mPa s*	G^{*E}, *J mol*$^{-1}$	$\Delta\eta$, *mPa s*	G^{*E}, *J mol*$^{-1}$
A	-13.9193	-16954.5	-9.2993	-15218.0
B_{12}	15.3267	14975.0	10.1514	13817.9
B_{13}	14.9566	15337.5	10.1738	13894.3
B_{23}	-0.2701	363.5	0.1224	69.7
C_{12}	7.8328	9035.1	-0.6326	-1658.1
C_{13}	1.9931	-14057.4	-2.4038	-19984.9
C_{23}	7.4440	5301.5	5.8324	5810.2
D_{12}	-37.5280	-18526.7	-13.4328	-4430.8
D_{13}	-27.7109	3283.6	-18.6658	7790.7
D_{23}	7.8709	14597.1	6.2618	13234.1
σ	0.0431	42.755	0.0147	18.995

CONCLUSION

Viscosities of binary and ternary systems with water, 1,4-dioxane, and DMSO were experimentally measured at various temperatures and correlated by means of Kendall and Monroe, Grunberg-Nissan, Katti-Chaudhri, Tamura-Kurata, McAllister and Soliman equations. For the 1,4-dioxane+DMSO binary system without strong interactions, any equation can be used to correlate adequately the viscosity data; for the systems with water only the three parameters equations of McAllister and Soliman give better results. The viscosity prediction for the ternary system with the same models leads to the best results.

Excess functions have been calculated and fitted to the Redlich-Kister equations. For binary and ternary systems, the deviations in viscosity and the excess Gibbs energy of activation for viscous flow are positive over the whole composition range, except for the binary 1,4-dioxane + DMSO which show small negative deviations for both excess properties. The magnitude of viscosity deviations vary in order: water+DMSO > water+1,4-dioxane> 1,4-dioxane+ DMSO, corresponding with excess volumes behavior.[13]

The systems present important deviations, as a consequence of their structures and interactions. The aqueous binary systems are complex systems with strong interactions of hydrogen bond and dipole – dipole type. The DMSO+1,4-dioxane binary system present poor unlike dipole-dipole interactions.

REFERENCES

1. R.C. Reid, J. M. Prausnitz and B. E. Poling, "The properties of Gases and Liquids", McGraw-Hill, New York, 1987, p.473-483.
2. J.Canosa, A. Rodriguez and J. Tojo, *J. Chem. Eng. Data*, **1998**, *43***,** 961-966.
3. W. Cao, K. Knudsen, A. Fredeslund and P. Rasmussen, *Ind. Eng. Chem. Res.*, **1992**, *31,* 2603-2619.
4. W. Cao, K. Knudsen, A. Fredeslund and P. Rasmussen, *Ind. Eng. Chem. Res.*, **1993**, *32,* 2077-2087.
5. W. Cao, K. Knudsen, A. Fredeslund and P. Rasmussen, *Ind. Eng. Chem. Res.*, **1993**, *32*, 2088-2092.
6. D. T. Wu and R. Marshall, *Fluid Phase Equilib.*, **1986**, *30,* 149-156.
7. W. D. Monnery, W. Y. Svrcek and A. K. Mehrotra, *Can. J. Chem. Eng.*, **1995**, *73*, 3-40.
8. L. Tassi, "Multiphase Reactor and Polymerization System Hydrodynamics", Gulf Publishing Co, New Jersey, 1996, Chapt.5.
9. O. Iulian, L. M. Hamplea and G. Jinescu, *Hung. J. Ind. Chem*., **1997**, *25*, 249-255.
10. L. M. Hamplea, "Vapor-liquid equilibria in mixed systems of non-electrolytes", Ph.D. Thesis, University POLITEHNICA of Bucharest, 1997.
11. M.C.Iliuta, O. Iulian and L.M.Omota, *ELDATA: Int. Electron. J. Phys.-Chem. Data*, **1998**, *4*, 121-128.
12. L.M. Omota, O. Iulian, C.Mateescu, *Hung.J. of Ind. Chem*., **2001**, *29*, 1-5.
13. L. M. Omota, O. Iulian, F. Omota and O. Ciocirlan, *Rev. Roum. Chim*., in press.
14. T. M. Aminabhavi and B. Gopalakrishna, *J. Chem. Eng. Data*, **1995,** *40*, 856 – 861.
15. J. N. Nayak, M. I . Aralagupi, B. V. Kumar Naidu and T. M. Aminabhavi, **2004**, *49*, 468-474.
16. O. Iulian, G. Jinescu, M. Iliuta and L. M. Hamplea, *Hung. J. Ind. Chem*., **1994**, *22*, 95-100.
17. M. M. Palaiologou, I. E. Molinou and N. Tsierkezos, *J. Chem. Eng. Data,* **2002**, *47*, 1285-89.
18. M. Dizechi and E. Marschall, *J. Chem. Eng. Data,* **1982**, *27*, 358-363.
19. X. Esteve, K. R. Patil, J. Fernandez and A. Coronas, *J. Chem. Thermodynamics,* **1995**, *27*, 281-292.
20. N. Tsierkezov and I. Molinou, *J. Chem. Eng. Data,* **1998**, *43*, 989-993.
21. M. Cocchi, M. Manfredini, A. Marchetti, L. Pigani, R. Seeber, L. Tassi, A. Ulrici and C. Zanardi, *J. Chem. Thermodynamics,* **2002**, *34,* 593-611.
22. J. Kestin, M. Sokolov and W. A. Wakeham, *J. Phys. Chem. Ref. Data,* **1978**, *7*, 941-948.
23. U. R. Kapadi, S. K. Chavan and O. S. Yemul, *J. Chem. Eng. Data,* **1997**, *42*, 548-550.

24. P. Baraldi, G. C. Franchini, A. Marchetti, G. Sanna, L. Tassi, A. Ulrici and G. Vaccari, *J. Solution Chem.,* **2000**, *29,* 489-504.
25. C. M. Kinart, W. J. Kinart and A. Wiklinska, *J. Chem. Eng. Data,* **2002**, *47,* 23-25.
26. H. Czechowski, B. Kywucki, M. Stockhausen and J. Jadtyn, *J. Chem. Eng. Data,* **1995**, *40,* 214-215.
27. G. E. Papanatasiou and I. Ziogas, *J. Chem. Eng. Data,* **1992**, *37,* 167-172.
28. S. Ottani, D. Vitalini, F. Comelli and C. Castellari, *J. Chem. Eng. Data,* **2002**, *47,* 1197-1204.
29. T. M. Aminabhavi and V. B. Patil, *J. Chem. Eng. Data,* **1998**, *43,* 497-503.
30. M. Contreras, *J. Chem. Eng. Data,* **2001**, *46,* 1149-1152.
31. R. T. Bicknell, D. B. Davies and K. G. Lawrence, *J.Chem. Soc. Faraday Trans.1,* **1982**, *78,* 1595-1601.
32. T. M. Aminabhavi, R. C. Patel, E. S. Jaydevappa and B. R. Prasad, *J. Chem. Eng. Data,* **1982**, *27*, 50-53.
33. S. L. Osval and N. B. Patel, *J. Chem. Eng. Data,* **1995**, *40,* 845-849.
34. P. Pacak, *J. Solution Chem.,* **1987**, *16*, 71-79.
35. S. Aznarez, L. Mussari and M. A. Postigo, *J. Chem. Eng. Data,* **1993**, *38*, 270-273.
36. J. Kendall and K. P. Monroe, *J. Amer. Chem. Soc.*, **1917**, *39*, 1787-1790.
37. L. Grunberg and A. H. Nissan, *Nature,* **1949**, *164,* 799-800.
38. P. K. Katti and M. M. Chaudry, *J. Chem. Eng. Data*, **1964**, *9***,** 442-448.
39. M. Tamura and M. Kurata, *Bull. Chem. Soc. Jpn*., **1952**, *25*, 32-36.
40. R. A. McAllister, *AIChEJ*, **1960**, *6,* 427-431.
41. R. Kallidas and G. S. Laddha, *J. Chem. Eng. Data*, **1964**, *9,* 142-145.
42. M. Takahashi and Y. Kobayashi, *J. Chem. Eng. Data,* **1982**, *27,* 326-328.
43. K. Soliman and E. Marschall, *J. Chem. Eng. Data*, **1990**, *35,* 375-381.
44. O. Redlich and A. T. Kister, *Ind. Eng. Chem.*, **1948,** *40,* 345-348.
45. R. J. Fort and W. R. Moore, *Trans. Faraday Soc.,* **1966**, *62*, 112-119.
46. T. Aminabhavi and B. Gopalakrishna, *J. Chem. Eng. Data*, **1995**, *40*, 856-861.
47. J. J. Lindberg, *Suom. Kemistiseuran Tied.*, **1961**, *70,* 33-39.
48. M. S. Skaf, *J. Phys. Chem.*, **1999**, *103*, 10719-10725.
49. D. N. Shin, J. W. Wijnen, J. B. Engberts and A. Wakisaka, *J. Phys. Chem. B*, **2001**, *105*, 6759-6770.
50. G. Brink and M. Falk, *J. Mol. Struct.*, **1970**, *5*, 27-30.
51. C. de Visser, M. J. M. Heuvelsland, L. A. Dunn and G. Somsen, *J. Chem. Soc. Faraday Trans. 1,* **1978**, *74,* 1159-1169.
52. G. Petrella, M. Petrella, M. Gastagnolo, A. Dell'Atti and A. de Giglio, *J. Solution Chem.*, **1981**, *10***,** 129-138.
53. T. Takamuku, A. Yamaguchi, M. Tabata, N. Nishi, K. Yoshida, H. Wakita and T. Yamaguchi, *J. Mol. Liquids*, **1999**, 163-177.
54. K. Quitzsch, H. P. Prinz, K. Suehnel, V. S. Pham, G. Geisler, *Z. Phys. Chem*., **1969**, *241*, 273-278.
55. H. Vogel and A. Weiss, *Ber.Bunsen-Ges.*, **1982**, *86*, 193-198.

Revue Roumaine de Chimie, **2008**, *53*(11), 989–993

SOLUBILITY OF PROPYLENE AND PROPANE GASES IN *N*-METHYLPYRROLIDONE AND DIMETHYLFORMAMIDE SOLVENTS

Mihaela PETRE*

Department of Chemical and Petrochemical Engineering, Faculty of Petroleum Refining and Petrochemistry, "Petrol-Gaze" University Ploieşti, 39 Blvd. Bucuresti, 100520, Roumania

Received February 13, 2008

Propylene and propane gases solubilities in *N*-methylpyrrolidone and Dimethylformamide anhydrous solvents have been measured at 20, 40, 60 ºC and pressure range between 50.65 and 506.5 kPa. Reported mole fraction solubilities were used to determine the Ostwald coefficients for a gases partial pressure of 101.3 kPa.

INTRODUCTION

Separation technology of unsaturate hydrocarbons: ethylene, propylene and butenes from ethylene-ethane, propylene-propane, butene-butane fractions, obtained from refinery gases, are based on classical distillation at ordinary temperature or low temperature in case of ethylene and propylene or, in butene separation case from C_4 fraction, by extractive-distillation in presence of different selective solvents[1]. Theoretically, propylene separation from propane could be performed also by extractive-distillation but, practically this thing is difficult and not interesting economically because, the extractive-distillation needs propane reflux at the top of the column which leads at obtaining of a high pressure with undesirable effects on the bottom column temperature, in a sense of a strong increasing of this, with effects in propylene-propane separation. That's why, for propylene-propane separation, when after separation process, propylene must be obtained in vapor phase for its using in different processes and, it was proposed a physical absorption process[2] at low pressure in presence of two absorbents used like solvents in a the extractive-distillation process: N-methylpirrolidone *(NMP*) and dimethylformamide (*DMF*). As it is known, for modeling absorption process it is necessary to know the solubility date for propane-propylene system in presence of two absorbents, at different temperatures and pressures.

EXPERIMENTAL

Solubility measurements were performed using a proper construction equilibrium apparatus previously described[3]. The glass trap with 100 cm^3 absorbent is introduced in equilibrium cell at constant a experimental temperature ensured with a water bath. The cell is depressuring at absolute pressure below 1 mmHg by using the vacuum pump. The depressuring line is closed and the gas charged is slowly open from gas reservoir. The inlet pressure of the gas is read at digital manometer DPI 705 (Druck Limited England) with an accuracy of ±0,1 kPa. The charged gas is made in a way in which, at the impact of the gas with glass trap with absorbent, this remains intact. This operation (depressuring- filling with gas) is repeated two times for being sure that in the equilibrium cell is only gas, and not air. After the second operation, one can wait for half an hour so the glass trap- gas system approaches the desired temperature for experimental determination. The temperature (T) was controlled by Rotronic Thermotrol within ±0,01°C. In this moment it is read the pressure from the cell which is considered the initial pressure (P_i) of the gas before starting the absorption in the liquid. Then, the equilibrium cell is suddenly mixted so that the glass trap with absorbent can be broken and in this way the gas solubilization in the absorbent is done. Then we may stir for 1 hour until the pressure remains constant so that the equilibrium state can be reached. At the end of the determination the equilibrium pressure (the final pressure - P_f) is recorded with the same DPI 705, and after than the equilibrium cell is released from gas reservoir. All the experiments were performed at least three time to ensure good accuracy, replicate measurements gave results consistently within 1% of the mean value.

The propylene and propane gases were purchased from Linde Gas Bucharest at purity of 99.8 % weight. The *DMF* solvent was obtained from Merck-Schuchardt with 99.0 % weight purity and the *NMP* solvent was obtained from Carom-Oneşti with 98.0 % weight purity.

* Corresponding author: mihaelampetre@yahoo.com

During the performing of the experiments, special precautions were taken with the solvents, particulary with the *DMF* solvent. This solvent is considered dangerous if inhaled or contacted. The solvents were exposed to the air for a minimum duration of time only, and any fumes or vapors released were vented to the fume hood. The complete solubility apparatus was mounted in a fume hood.

From experimental data, is calculated the solubility of these two gases in absorbent (in molar fraction), based on the gases law, for the initial moment (for the gas from the cell before the glass is broken) and also, for the final moment (after the glass trap is broken and reaches the equilibrium). No *NMP* or *DMF* were considered in vapor phase because at the experimental temperatures vapor pressures of both solvents are unsignificant. So:

$$P_i V = z_i n_i RT \tag{1}$$

$$P_f V = z_f n_f RT \tag{2}$$

Considering that the gas volume is constant (cell volume), by decreasing the equation (2) from the equation (1), is obtained:

$$\Delta PV = \Delta nRT \tag{3}$$

From equation (3) it is calculated the number of moles solubilised gas, noted only with "*n*", in assumption that the compressibility factors z_i and z_f are practically equals:

$$n = \frac{\Delta PV}{RT} \tag{4}$$

In this case, molar fraction of solubilized gas is calculated with equation:

$$x = \frac{n}{n + n_{absorbant}} \tag{5}$$

RESULTS AND DISCUSSION

Data for the solubility of propylene and propane in *NMP* and *DMF* anhydrous were obtained at following temperatures: 20, 40, 60°C and pressures between 50.65 and 506.5 kPa. The results are presented in figures 1 and 2. The data were correlated using Soave-Redlich-Kwong (*SRK*) equation. The optimum interaction parameter, k_{ij}, in the mixing rule of the equation of state was obtained by minimizing the error in the predicted bubble point pressure.

$$f(k_{ij}) = \sum \left| \frac{P_{\exp} - P_{calc}}{P_{\exp}} \right| \cdot \frac{100}{N} \tag{6}$$

where $P_{\exp}$ is the experimental bubble point pressure, P_{calc} is the calculated bubble point pressure and N is the number of data points. The solubility data were well-correlated by Soave-Redlich-Kwong equation of state. The maximum mean absolute deviation was 1.31%.

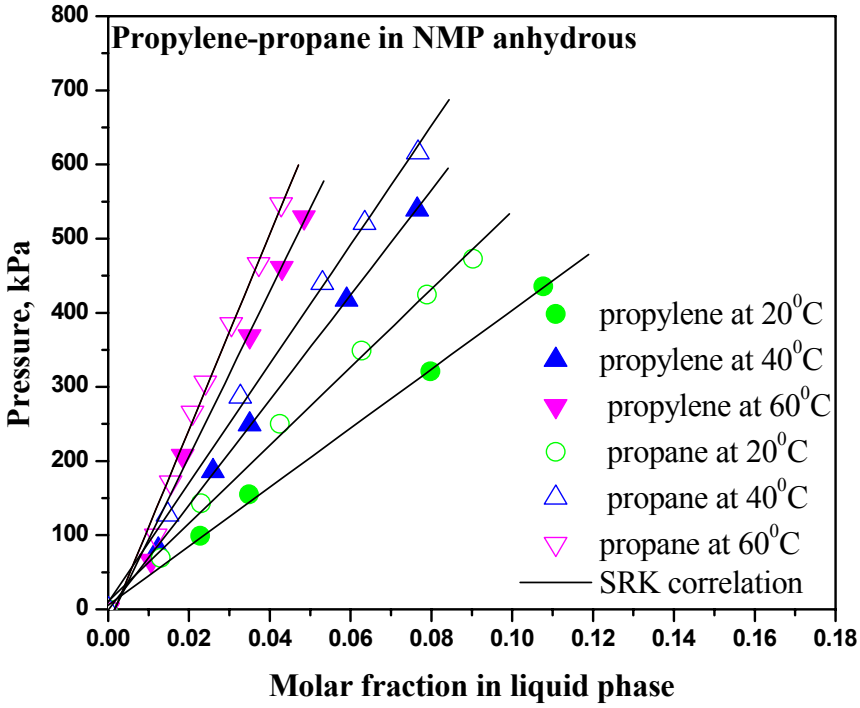

Fig. 1 – The solubility propylene and propane in *NMP* anhydrous.

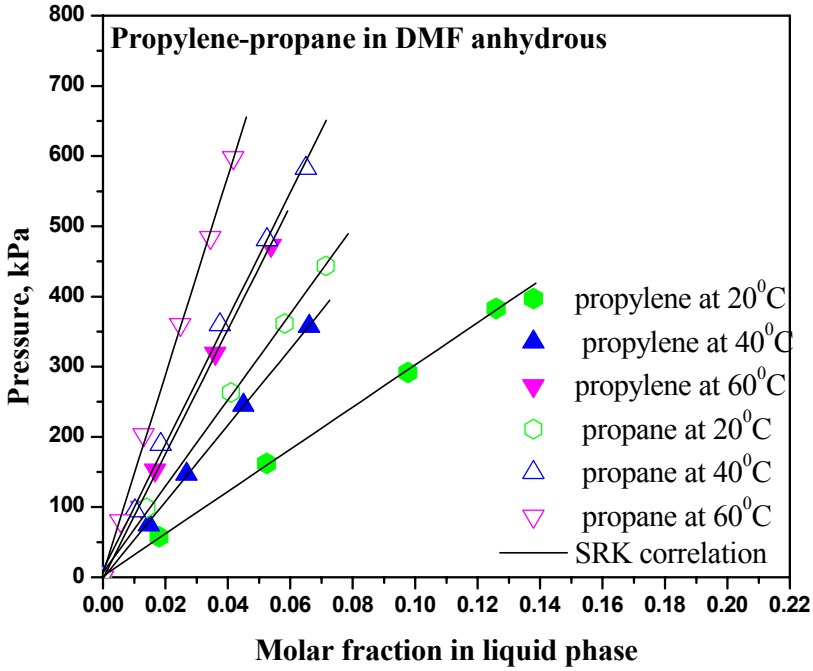

Fig. 2 – The solubility propylene and propane in *DMF* anhydrous.

The mole fraction solubilities were used in order to calculate the Ostwald coefficients for the propylene and propane gases in both solvents for a gas partial pressure of 101.3 kPa. The Ostwald coefficient, defined by the volume of pure gas and volume of solvent which, when we mix them together at experimental temperature and pressure, will produce a saturated solution. This coefficient is clearly defined and can be readily calculated from experimental data.

The Ostwald coefficient (L) as defined for a gas partial pressure (p) of 101.3 kPa can de determined from the mole fraction solubility (x_1):

$$L = \frac{101.3\, V_G\, x_1}{\left[P\, V_L (1 - x_1)\right]} \tag{7}$$

where P is total experimental pressure, V_G is molar volume of gas, V_L is molar volume of saturated solvent.

Because the *NMP* and *DMF* solvents are non-volatile at experimental temperatures ($p = P$), this means that Ostwald coefficient is independent of pressure.

The molar volumes of propylene and propane gas at experimental temperatures were calculated using Soave-Redlich-Kwong equation of state and *PRO-II* Simulator. The results are presented in Table 1.

The saturated molar volumes of solvents were calculated with an equation developed by Rackett and modified by Spencer and Danner[4].

$$V_L = \frac{R\, T_C}{P_C} Z_{RA}^{\left[1+(1-T_R)^{2/7}\right]} \tag{8}$$

where T_C (in K) and P_C (in bar) are critical properties of pure solvents, T_R is reduced temperature in K and Z_{RA} is a constant. If Z_{RA} values are not listed in literature, they may be estimated by equation[5]:

$$Z_{RA} = 0.29056 - 0.08775\omega \tag{9}$$

where ω is acentric factor of solvent.

The critical properties and the acentric factors for *NMP* and *DMF* were listed from *PRO-II* Simulator Database[6] and used in equations (9) and (8) for molar saturated volumes calculus. The results are presented in Table 2.

Propylene and propane solubilities in *NMP* and *DMF* solvents are reported both as the mole fraction solute and as the Ostwald coefficients for a gas partial pressure of 101.3 kPa. For temperatures from 20 ºC to 60 ºC these data are graphically represented in Figure 3. A comparison, with Hayduk data from the literature [7] is made only for propylene solubilities in *DMF*.

Table 1

The molar volumes of propylene and propane gas

Temperature, ºC	Propylene V_G, m^3/kmol	Propane V_G, m^3/kmol
20	23.71	23.66
40	25.39	25.35
60	27.07	27.04

Table 2

The molar saturated volumes of *NMP* and *DMF*

Temperature, ºC	*NMP* V_L, m^3/kmol	*DMF* V_L, m^3/kmol
20	0.09617	0.07707
40	0.09768	0.0784
60	0.09923	0.0798

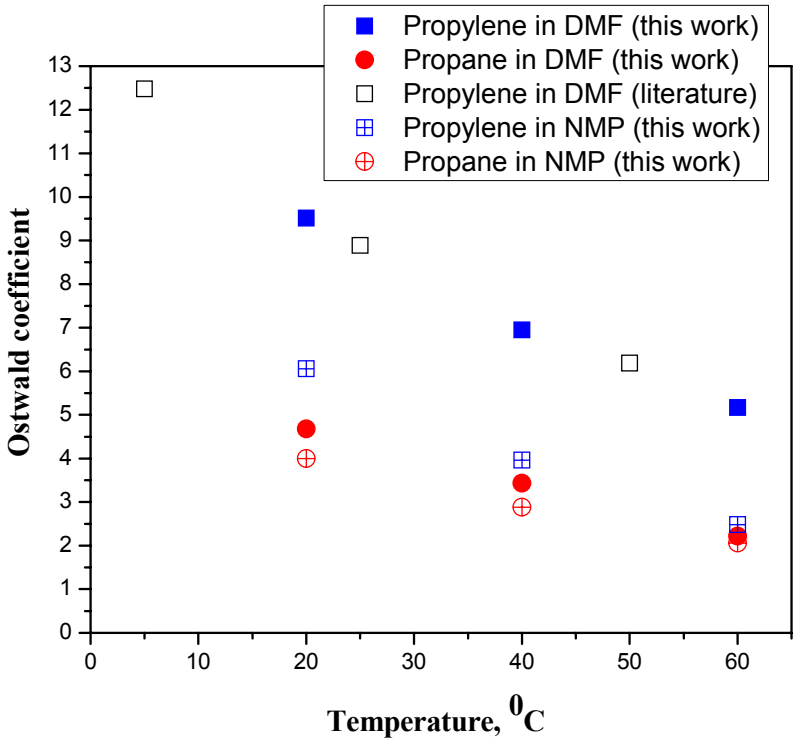

Fig. 3 – Propylene and propane Ostwald coefficients in *NMP* and *DMF*.

From figure 3 result that Ostwald coefficients of propylene and propane decreases with temperature increase. The Ostwald coefficients of propylene is higher than of propane. On the other hand, at the same temperature, the Ostwald coefficients of propylene and propane in *DMF* is higher than in *NMP*.

Ostwald coefficients of propylene in *DMF* from this work are in good agreement with the reported data in literature because, together, describe a good variation curve with temperature.

CONCLUSIONS

In this work were reported experimental solubility data for propane and propylene in the *NMP* and *DMF* anhydrous absorbents at different

temperatures and pressures. From the solubility data, Ostwald coefficients were calculated at 101.3 kPa. The graphically represented results indicated that the *DMF* absorbent is better then *NMP*.

REFERENCES

1. C. Strătulă, "Fracționarea, Principii și Metode de Calcul", Ed. Tehnică, București, 1986, p. 320-340;
2. Y. R. Mehra (Odessa, TX), *U.S. Pat*. 4743282, May 10, 1988.
3. M. Petre and C. Strătulă, *Rev. Chim.*, **2006,** *57*, 1269-1272.
4. C. F. Spencer and R. P. Danner, *J Chem. Eng. Data*, **1972**, *17*, 236-241.
5. T. Yamada and R.D. Gunn, *J. Chem. Eng. Data*, **1973**, *18*, 234-236.
6. PRO-II Simulator Database.
7. W. Hayduk and C.-F. Wong, *Can. J. Chem. Eng*., **1990**, *68*, 653-660.

Revue Roumaine de Chimie, **2008**, *53*(11), 995–1005

THE ELECTROCHEMICAL BEHAVIOUR OF SOME COMPOSITE COATINGS OBTAINED BY ELECTROSYNTHESIS ON METALLIC SUBSTRATE

Viorel BRÂNZOI[*a], Florina BRÂNZOI [b] and Florentina GOLGOVICI[a]

[a] Department of Physical Chemistry and Electrochemistry, Faculty of Applied Chemistry and Material Science, University "Politehnica" of Bucharest, Calea Griviței 132, Bucharest, 010737 Roumania, e-mail: iv_branzoi@chim.upb.ro
[b] Institute of Physical Chemistry Bucharest, Splaiul Independentei 202, Bucharest, 060021, Roumania, fbrinzoi@chimfiz.icf.ro

Received June 12, 2008

Copolymers of aniline and pyrrole have been formed by electrochemical oxidation in acidic medium, but the composition of the polymeric chain differs from the composition of the synthesis solution. It was shown that the structure and the morphology of the obtained coatings were dependent on the feed ratio of monomers (aniline and pyrrole). The polyaniline and polypyrrole have very distinct electrochemical behaviours. The properties of those copolymers have been studied by cyclic voltammetry. The corrosion performance of composite coated aluminium was evaluated by CV and EIS. The corrosion resistance of composite coated aluminium was higher than of uncoated aluminium. The morphological structure of composite coatings was examined by metallographic microscope. It was observed the formation of a new material, namely composite coating.

INTRODUCTION

There is a lot of literature concerning the synthesis and characterisation of conducting polymers. Electrochemical synthesis of conductive polymers allows preparation of layers of polymers of desired thickness, shape and dimensions generally are not possible by chemical methods.

Thus far most promising conductive polymers have been those made from monomers of pyrrole, aniline, benzene, thiophene, acetylene.

These polymers can be easily prepared electrolytically in organic or aqueous solutions. Conductivity is usually in the semiconductor range.

The conductivity of doped polymers can be attributed to the delocalisation of Π conjugated systems.

These polymers such as polyaniline (PANI) and polypyrrole (PPY) have received great attention since its rediscovery by Shirakawa *et al*.[1] One of the key features is its wide range of proposed applications, including presently fields such as actuators, electrochromic and photovoltaic devices, secondary batteries, fuel cells, supercapacitors, ionic sensors, biosensors, electrocatalysis and corrosion protection among many other ones.[2-21] Due to their potential applications and interesting characteristics, the electrochemistry of these polymers has been intensively studied in the past years.[22-26]

Electrochemical synthesis of conductive polymers allows preparation of polymer layers of desired thickness, shape and dimensions, generally are not possible by chemical method.

Conducting polymers containing two compounds can be prepared as copolymers, composites, bilayers or blends. This is done for the improvement of the physical, chemical, mechanical and electrical proprieties of homopolymers. As we shown before, polyaniline and polypyrrole are two of the most promising conducting polymers. Both of them have a relatively high conductivity and good environmental stability.[27]

Because the oxidation potential of aniline and pyrrole are very near, we believe that simultaneous oxidation and codeposition of polyaniline and polypyrrole is possible by changing the applied potential.

In this paper, we studied the formation of polyaniline-polypyrrole composite coatings on aluminium electrode using potentiodynamic method. The electrochemical proprieties of these composite coatings were studied by cyclic voltammetry and by

* Corresponding author: iv_branzoi@chim.upb.ro

electrochemical impedance spectroscopy. The morphological structure of composite coatings was examined by metallographic microscope. It was observed the formation of a new material, namely composite coating.

EXPERIMENTAL

A model VoltaLab 40 potentiostat/galvanostat with EIS dynamic was used for the electrochemical polymerization. Electropolymerization was carried out in a three electrodes system.

A platinum electrode and a saturated calomel electrode (SCE) were used as counter and reference electrode respectively. The reference electrode was placed in a separate cell and was connected to the corrosion cell via a salt bridge, which ends as a Luggin capillary in the corrosion cell. This arrangement was used to reduce the ohmic resistance of the corrosion system. The working electrode was made from pure aluminium (99.9%). Samples with 0.64 cm^2 geometric surface aria were used. Prior to experiments, the electrodes were polished with SiC emery paper down to #4000. After polishing, the electrodes were degreased in acetone, washed with Millipore water and then introduced into the measuring cell.

Polyaniline (PANI), polypyrrole (PPY) and poly (aniline-co-pyrrole) films were electropolymerized onto an aluminium substrate by cyclic voltammetry with a scan rate of 20 mV/s. All the reactions were carried out in the scan range of -1000 up to +3000 mV versus SCE.

The electropolymerization of aniline and pyrrole monomers was carried out in a 0.1 M monomer + 0.25 M oxalic acid electrolytic solutions.

In the case of the copolymers synthesis, the concentration of aniline was maintained constant at 0.1M and the proportion in moles of pyrrole was varied from 0.1M to 0.5M. It can be observed that, the initial concentration of co-monomers (aniline and pyrrole) was varied from 1:1 to 1:5. The electrochemical characteristics of the coatings were studied by cyclic voltammetry and electrochemical impedance spectroscopy, in an aqueous solution of 0.5M K_2SO_4. The working electrode potential was cycled on the potential range of -1000 mV up to 3000 mV with scan rate of 20 mV s^{-1}.

Impedance measurements were carried out using a software program between 100 KHz and 10 mHz with an ac wave of ± 5 mV (peak-to-peak) overlaid on a dc bias potential and the impedance data were obtained at a rate of 10 points per decade change in frequency.

All tests have been performed at 25^0C under atmospheric oxygen without agitation.

RESULTS AND DISCUSSION

Electrochemical synthesis of poly (aniline-co-pyrrole) from different precursor solutions produces homogeneous and adherent black films they show great electroactivity in the cycling solutions and the voltammetric profiles are very similar to the potential values of the current peaks being located at intermediate values of the typical electrochemical responses of homopolymers.

First we obtained the PANI films on the aluminium substrate in a synthesis solution of 0.1M aniline+0.25M oxalic acid by potentiodynamic method. The electrode potential was scanned on the range of -1000 mV up to +3000 mV with a sweep rate of 20mVs^{-1} for a period 25 cycles.

Analyzing the cyclic voltammograms from figure 1, it can be observed that, at the first cycle on the anodic branch of the voltammograms appear two anodic oxidation peaks which point out the anodic oxidation of aniline and the formation of polyaniline (PANI) film. The formation process of PANI film was illustrated by us in a previous paper.[28]

It is well known that, polyaniline can exist in three different oxidation states such as leucoemeraldine (fully reduced form), emeraldine form (partially oxidized form) and pernigraniline (fully oxidized form). A very important characteristic of polyaniline consists in the fact that its structural units contain two different entities with different ponderables. Taking into account this property we can write thus:

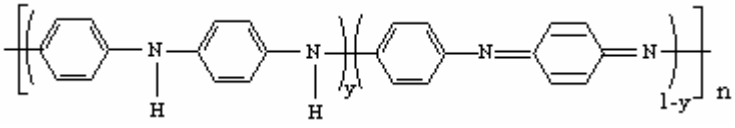

when y = 1, we have leucoemeraldine base, when y = 0 we obtained pernigraniline base and when y = 0.5 an intermediate state between leucoemeraldine and pernigraniline is obtained which is called emeraldine base.

These forms of polyaniline are dependent on the applied potential. At the increasing anodic potential sweep the oxidation forms of polyaniline are obtained and on the anodic branch of the cyclovoltammogram appear the oxidation peaks (see Figure 1).

At the reverse potential sweep, no cathodic reduction peak appears up to -1000 mV, but it can be observed that, the cathodic current begins to increase at a potential value of -650 mV (see Figure 1). The increase the number of cycles led in all the cases to decrease of the height of the anodic peaks and also, to decrease of the anodic and cathodic current (see Figure 1 and Table 1).

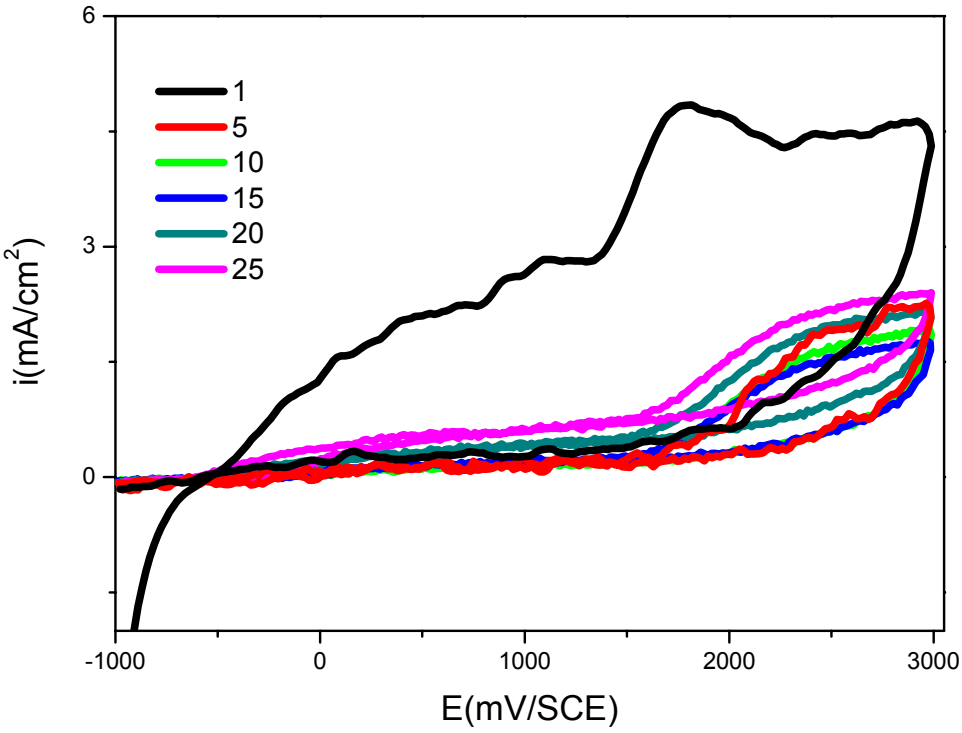

Fig. 1 – The cyclic voltammograms obtained for the aniline polymerization on the aluminium electrode surface.

Table 1

Kinetic parameters obtained from the cyclic voltammograms for aniline electropolymerisation in 0.25 M oxalic acid aqueous solutions

No. cycle	ipa_1 (mA/cm^2)	Epa_1 (mV)	ipa_2 (mA/cm^2)	Epa_2 (mV)
1	2.83	1091	7.83	1777
5	1.27	2141	1.92	2484
10	-	-	1.72	2561
15	-	-	1.83	2512
20	-	-	1.98	2508
25	-	-	2.13	2424

We can see that, after five cycles on the anodic branch of voltammogram appears only one anodic oxidation peak and its height is much lower than in the case of the first cycle. This decrease of the anodic peak height and of the anodic and cathodic current once with the increase of the cycles number is due to the formation of the Al_2O_3 passive layer which behaves as a barrier for charge transfer reaction (as we explained above in the paper).

Also, we analyzed by metallographic microscope the modified electrode PANI/Al surface and in figure 2 are given the micrographic images. Analyzing these micrographies, it can be observed very well the electrodeposited polyaniline layer and its characteristic structure formed from polymer (PANI) chains, which are uniform, distributed. These images prove once again the formation of PANI layer on the aluminium surface by cyclic voltammetry and its characteristic structure.

Further, we studied the obtainment of the polypyrrole films on aluminium substrate by using cyclic voltammetry.

In figure 3 are given the cyclic voltammograms of pyrrole polymerization in a synthesis solution of 0.25 M oxalic acid + 0.1 M pyrrole. The electrode potential was scanned on the range of -1000 mV up to +3000 mV with a sweep rate of 20 mVs^{-1} for a period of 25 cycles.

Analyzing the cyclic voltammograms from figure 3, it can be observed that, at the first cycle on the anodic branch of the voltammogram appears an anodic peak, which is very high and wide. This anodic peak points out the anodic oxidation of pyrrole and the formation of polypyrrole film. The formation process of PPY

film was illustrated by us in a previous paper [29] and is in according to this mechanism. The electropolymerization reaction appears to involve two electrons per molecule of pyrrole (Py) monomer, and it proceeds through a radical coupling mechanism.[30] During the formation a stoichiometric amount of anions provided by the supporting electrolyte is incorporated into the polymer layer to neutralize the positive charge of the PPY chains. Therefore, the nature of the anions plays an important role in conferring the electrochemical properties of the PPY films.

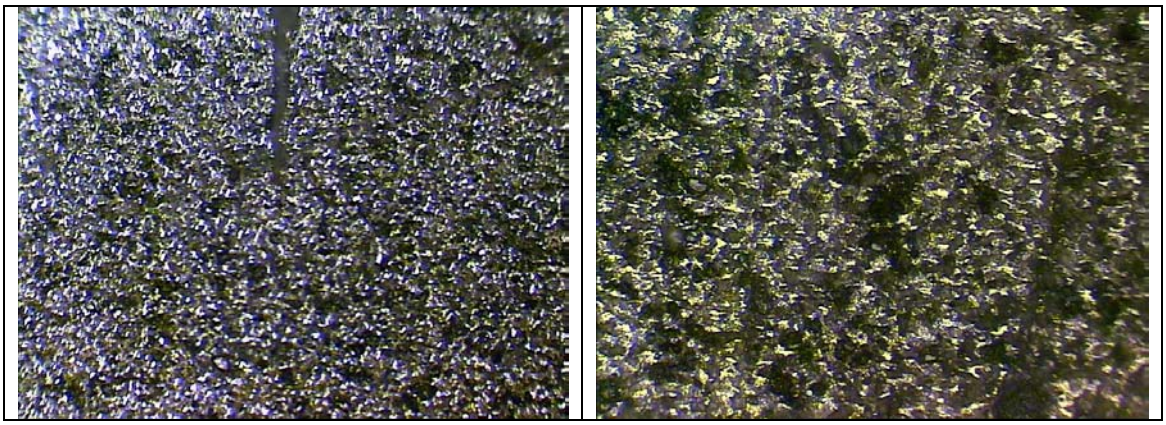

a) PANI/Al +200x b) PANI/Al + 400x

Fig. 2 – Micrographies of PANI film electrodeposited on aluminium surface after 25 cycles.

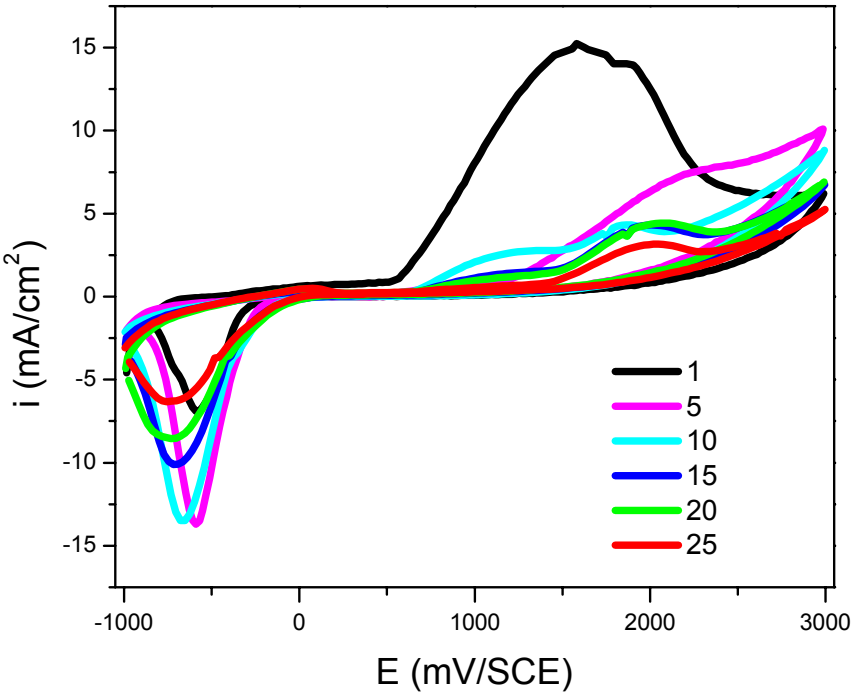

Fig. 3 – The cyclic voltammograms obtained for the pyrrole electropolymerization on the aluminium electrode surface.

At the reverse sweep electrode potential, on the cathodic branch of the voltammogram (for the first cycle) a reduction cathodic peak appears which is much lower than the anodic peak (see figure 3 and table 2). The separation potential range (ΔE_p) between the anodic and cathodic peaks is wide enough and points out the fact that, at the electrode surface take place quasi-reversible processes. The value of ΔE_p is very high because the formation of PPY film led to the increase of ohmic resistance of the electrochemical system and consequently the charge transfer reactions are impeded and ΔE_p increases. After five cycles, the cyclic voltammogram obtained has a modified shape in

comparison with the first cyclic voltammogram. In this case, at the anodic potential sweep appears an anodic oxidation peak which has a lower height than in the case of the first cycle and it is shifted to more anodic potential. On the cathodic branch of the cyclic voltammogram with number 5, the reduction cathodic peak appears in the same potential range, but in this case, it is more narrow and higher. Further, increasing the number of cycles, it can be observed that, on the anodic branch appear two anodic oxidation peaks which have much lower currents density and also, on the cathodic branch of the cyclic voltammograms appears a reduction cathodic peak. The height of this peak decreases with the increase of the cycles number (see figure 3 and table 2).

Table 2
Kinetic parameters obtained from the cyclic voltammograms for pyrrole electropolymerization in 0.25 M oxalic acid aqueous solutions

No. cycle	ipa_1 (mA/cm^2)	Epa_1 (mV)	ipa_2 (mA/cm^2)	Epa_2 (mV)	ipc_1 (mA/cm^2)	Epc_1 (mV)	ΔEp_1 (mV)
1	16.38	1634	-	-	8.60	-578	2212
5	7.91	2235	-	-	14.51	-590	2825
10	2.70	1172	4.31	1815	13.49	-651	1823
15	1.31	1035	4.37	1896	10.08	-692	1727
20	1.18	1025	4.40	2032	8.53	-704	1729
25	0.66	1007	3.14	1970	6.29	-717	1724

The decrease of the anodic current peak height with the increase of the cycles number can be explained thus: at the anodic polarization of the aluminium electrode in synthesis solution, the formation of Al_2O_3 and PPY films proceeds simultaneously. At the first cycle the anodic oxidation of pyrrole to polypyrrole in according to the mechanism given by [29] is predominant process. With the increase of the cycles number the predominant process becomes the anodic oxidation of aluminium, with formation of Al_2O_3 film, which acts as an excellent barrier inhibiting the charge transfer reactions. Hence, the formation of Al_2O_3 film inhibits the electrochemical polypyrrole formation and thus, we can explain the decreasing of the anodic oxidation current once with the increase of the cycles number. These two films interact one with the other and it can be considered that, the bilayer film was obtained consisting from a barrier oxide film of Al_2O_3 and an electronically conducting PPY film.

Further, we analyzed by metallographic microscopy the modified PPY/Al electrode surface and in figure 4 is given a micrographic image. Analysing this micrography, it can observed very well the electrodeposited polypyrrole film and its characteristic structure like as cauliflower. This image proves once again the formation of the PPY film on the aluminium substrate by cyclic voltammetry and its characteristic structure.

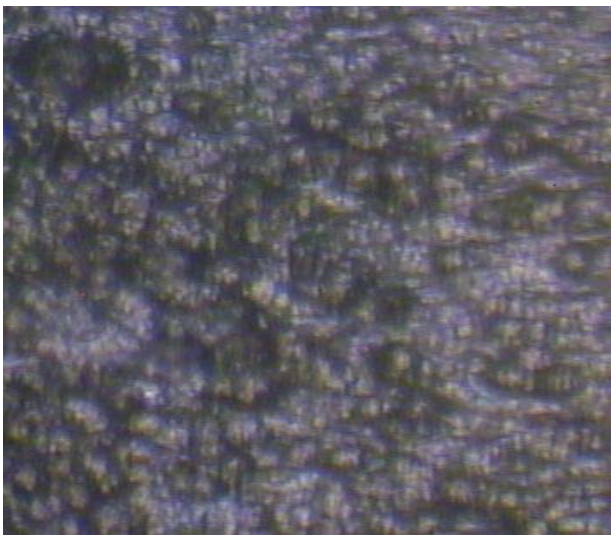

Fig. 4 – Micrography of PPY film electrodeposited on aluminum surface after 25 cycles.

Further, we studied the formation of polyaniline - polypyrrole composite coatings on aluminium substrate using the cyclic voltammetry for electrodeposition of composite polymeric film. It was shown that, the yielded structure and the morphology of the coatings were dependent on the feed ratio of the monomers (aniline and pyrrole) and on the applied potential. The resulting composite also showed significant changes in electrochemical behaviour when were compared with the electrochemical behaviour of homopolymers. Because the oxidation potentials of aniline (0.8 V vs. SCE) and pyrrole (1.2V vs. SCE) are very near, we belive that simultaneously oxidation and codeposition of polyaniline and polypyrrole is possible by changing the applied potential.

Therefore, the copolymerisation of aniline and pyrrole was performed by using repeated potential cycling between -1000 mV and +3000 mV with a sweep rate of 20mVs^{-1} for a period of 25 cycles.

In figure 5 are presented the cyclic voltammograms obtained for the polymerization of a pyrrole-aniline mixture after a certain number of cycles.

As it can be seen, the voltammogram obtained after the first polymerisation cycle presents two wide and high anodic oxidation peaks which form together a very large anodic oxidation range which point out that, in this potential range takes place the active oxidation process of aniline and pyrrole with the new composite formation. For the following cycles, it can be observed that, the shape of voltammograms change, on the anodic branch of the voltammograms appears only one oxidation peak which is much lower and is shifted to more electropositive potential. At the reverse potential sweep the anodic current decreases very much and no cathodic current appears up to the very negative values of the potential.

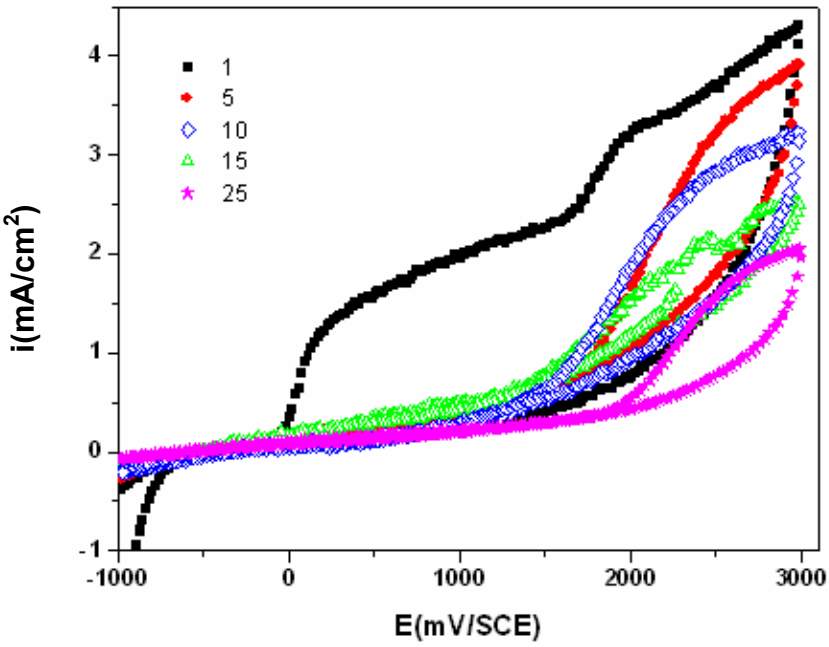

Fig. 5 – The cyclic voltammograms for polymerization of the mixture: 0.1 M pyrrole + 0.1M aniline in an aqueous solution of 0.25M oxalic acid.

The decrease of the anodic current peak height with the increase of the cycles number can be explained thus: at the anodic polarization of the aluminium electrode in synthesis solution, the formation of Al_2O_3 and composite films proceeds simultaneously. At the first cycle the anodic oxidation of aniline and pyrrole with co-deposition of composite film is the predominant process. With the increase of the cycles number the predominant process becomes the anodic oxidation of aluminium, with formation of Al_2O_3 film, which acts as an excellent barrier, inhibiting the charge transfer reactions. Hence, the formation of Al_2O_3 film inhibits the anodic oxidation of aniline and pyrrole and in this way, it can be explained the decreasing of the anodic and cathodic current once with the increase of the cycles number. The formation of Al_2O_3 layer proceeds two interfaces,

the first at the aluminium / Al_2O_3 layer and the second at the Al_2O_3 layer / composite film [poly(aniline-co-pyrrole) film]. It is assumed that, the species are continuosly generated at metal/oxide interface. Then, they migrate through growing Al_2O_3 layer toward the solution where high electric field, while oxide ions O^{2-} migrate toward the aluminium electrode. At the interface of Al_2O_3 layer/composite film, the Al^{3+} ions encounter water species to form Al_2O_3 film. In this way, it can be explained also, the decreasing height of the oxidation and reduction peaks once with the increase of the cycles number (see Figure 5 and Table 3).

This behaviour of composite polymer is different from the homopolymers behaviour (see in comparison Figures 1, 3, 5) and this fact proved that, a new material is formed namely composite material or in our case composite coating.

Further, we studied the obtainment of composite coatings from different mixture in function of the molar feed ratio of monomers. In Figures 6 and 7 are given the cyclovoltammograms for composite electropolymerization from different mixture of aniline and pyrrole.

Analyzing in comparison these electro-polymerization voltammograms, it can be observed that, the behaviour of the current-potential curves are function of the molar feed ratio of monomers and that, the composite voltammograms are very different from the homopolymers voltammograms. From analysis of these figures, we can conclude that, in comparison with the homopolymers, the formed composite has an intermediate behaviour that proved the formation of a new material.

The EIS measurements were carried out for PPY-PANI/Al modified electrodes in 0.5M K_2SO_4 solutions in relation to the cycles number of electrodeposition and in relation to the feed ratio of the monomers (aniline and pyrrole). In figure 8 are given, for exemplification the Nyquist diagrams for PPY-PANI (5:1)/Al modified electrode in 0.5M K_2SO_4 solution in relation to the cycles number of electrodeposition.

Analysing this figure, it can be observed that in all the cases, at the high and medium frequencies the capacitive loop very well definited were obtained while at the low and very low frequencies a wide inductive region is obtained. Analysing in comparison the Nyquist diagrams obtained for different cycles of electrodeposition, it can be observed that, the capacitive loop increases with the cycles number of electrodeposition and the inductive region increases in the same mode. This behaviour can explained considering that, once with the increase of cycles number the formation of the composite coating and of Al_2O_3 layer is much more well definited and much more stable. Bode diagrams from figure 9 are in concordance with the results showed by Nyquist diagrams (see in comparison figure 8 and figure 9).

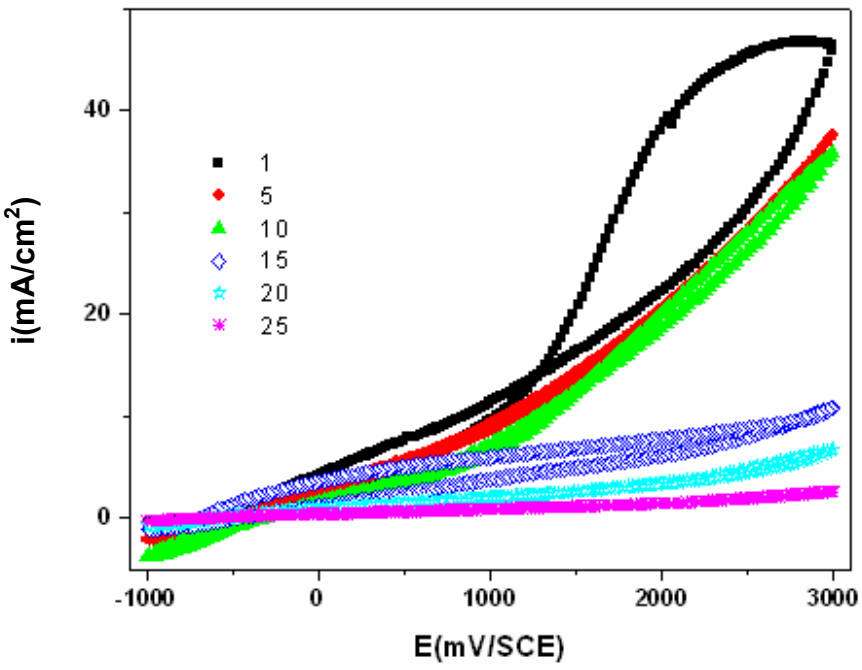

Fig. 6 – The cyclic voltammograms for polymerization of the mixture: 0.5 M pyrrole + 0.1M aniline in an aqueous solution of 0.25M oxalic acid.

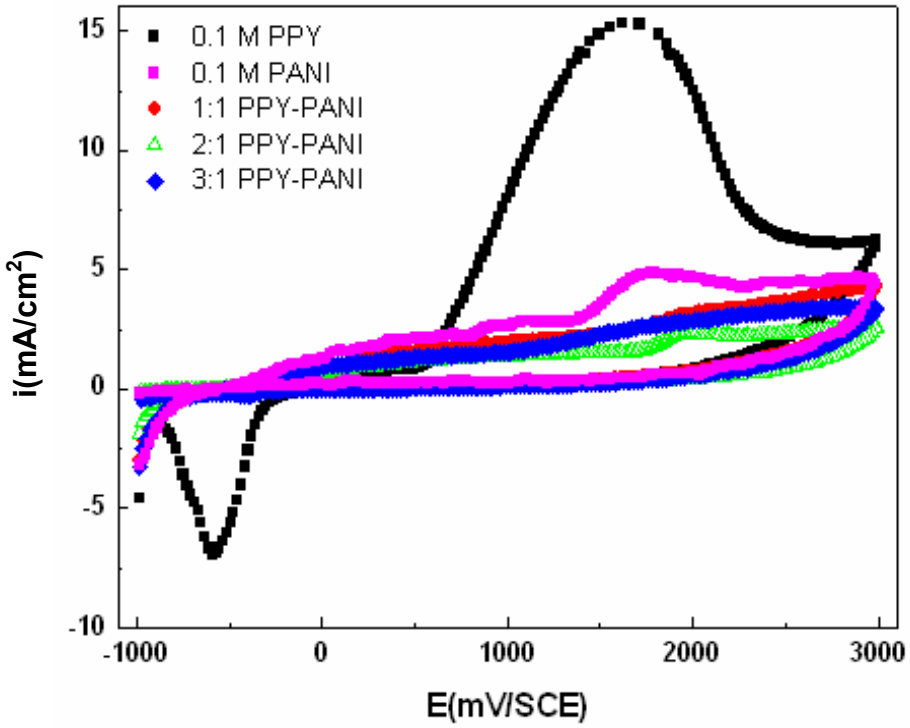

Fig. 7 – The cyclic voltammograms for PPY/Al, PANI/Al and composite PPY-PANI/Al modified electrodes in 0.25 M oxalic acid aqueous solutions.

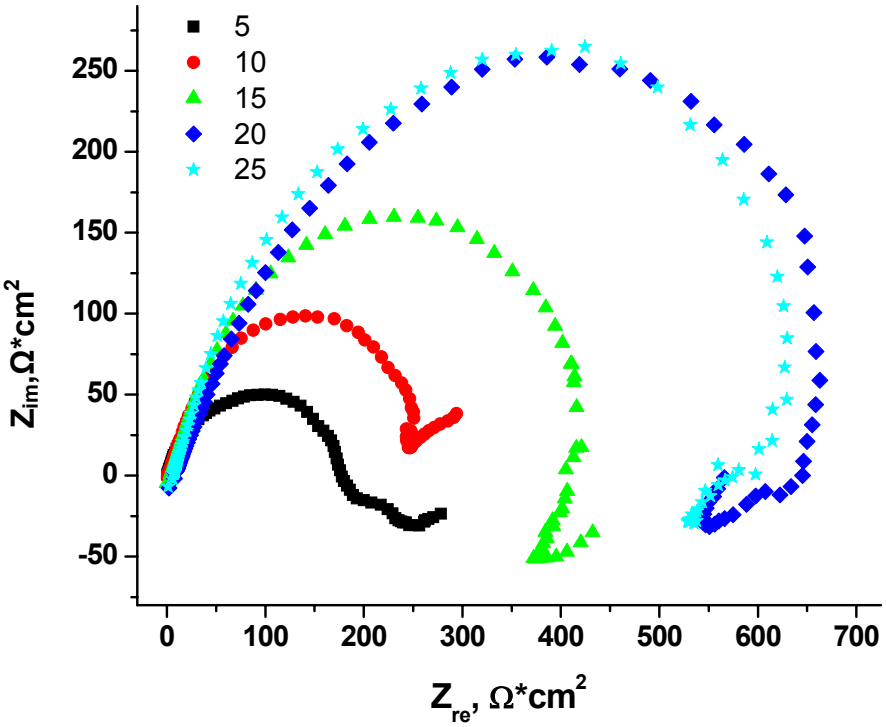

Fig. 8 – Nyquist diagrams for PPY- PANI (5:1)/Al modified electrode in 0.5 M K_2SO_4 solutions in relation to the number of electrodeposition.

Analyzing the Figure 9b, it can be observed that, on the phase angle versus logarithm frequency curve appear two maxima, respectively, two time constants. The maximum, which appears at the high and very high frequencies, is very well defined, it is very wide and high. The phase angle for this maximum has a value of approximately 75^0 that means a capacitive behaviour of the

composite/Al modified electrode. This capacitive behaviour was observed for all the composite films obtained for different cycles of electrodeposition (see Figure 9b) but, the phase angle value increases once with the increase of the cycles number of electrodeposition, that means an increase of the capacitive behaviour once with the increase of the electrodeposition cycles number. The same results are pointed out by the Bode diagrams from Figure 9a. This fact is in concordance with the results pointed out by Nyquist diagrams and cyclic voltammograms.

From Figure 9b it can also be observed that, at low and very low frequencies appears a maximum which is not well defined and the phase angle for this peak has a value of approximately 25^0, that means an inductive behaviour. This value of the phase angle decreases once with the decrease of the electrodeposition cycles number. The inductive behaviour points out the fact that, on the electrode surface takes place the adsorption of the active species from electrolyte solution followed by relaxation phenomena.

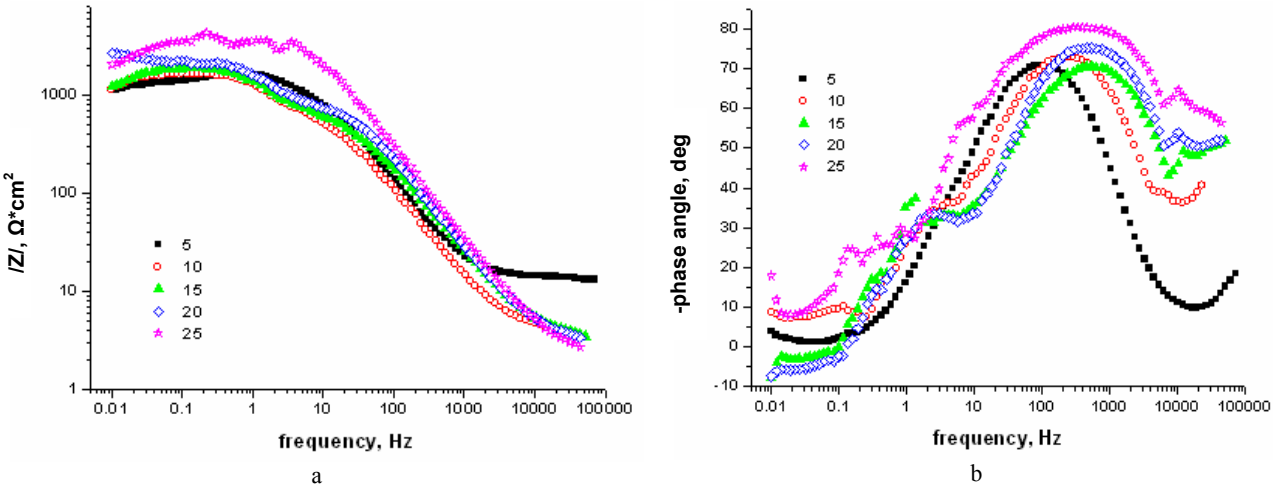

a b

Fig. 9 – Bode diagrams for PPY-PANI(5:1)/Al modified electrode in 0.5 M K2SO4 solution in relation to the number of electrodeposition cycles.

Further, we studied in comparison by EIS, the electrochemical behaviour of PPY/Al, PANI/Al and composite (PANI-co-PPY)/Al modified electrodes. In figure 10 are given in comparison the Bode diagrams for PPY, PANI, Al and composite obtained from different molar feed ratios. Analyzing this figure it can be observed that, in all the cases in the high frequencies range a maximum very well defined is obtained, but the height and the diameter of this maximum differs for the each particular case. Thus, the phase angle with the highest value is obtained for composite (PANI-co-PPY) which was electrodeposited from a synthesis solution with the feed ratio of 5:1 (Py/An) and the lowest value of the phase angle was obtained for PPY film (see Figure 10).

For the PANI film, the value of the phase angle is lower than in the cases of composite coatings with the molar feed ratio of 2:1 and 5:1 (Py/An). The phase angle values for composite with other molar feed ratios were intermediates between the values for PANI film and PPY film (see Figure 10). This fact proves once again the formation of a new composite material with a new morphological structure in comparison with the morphological structure of PANI and PPY films.

Analyzing the phase angle values (from figure 10), it can be observed that, the composite coatings obtained from mixture with molar feed ratio changeable from 5:1 up to 1:1 have the best capacitive behaviour while the PPY film has a capacitive behaviour with diffusive tendency.

Also, we analyzed by metallographic microscopy the modified electrode PPY-PANI/Al surface and in figures 11 and 12 are given the micrographic images.

As, it can be observed, the morphological structure of the composite coatings of the PPY-PANI/Al modified electrode surfaces is different from the morphological structure of the PPY/Al and PANI/Al modified electrode surfaces (see in comparison Figures 4, 8, 11 and 12). This fact proves another one that, a new material, respectively a new composite material was formed.

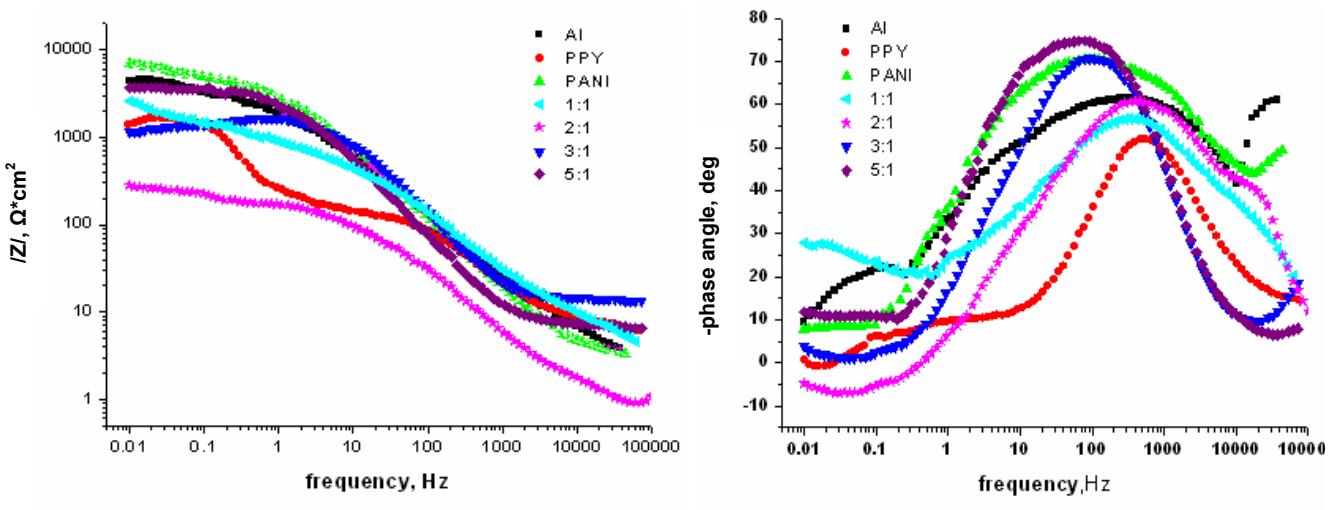

a b

Fig. 10 – Bode diagrams for PPY/Al, PANI/Al and composite PPY-PANI/Al modified electrodes in 0.5 M K_2SO_4 aqueous solutions in relation to the number of electrodeposition cycles.

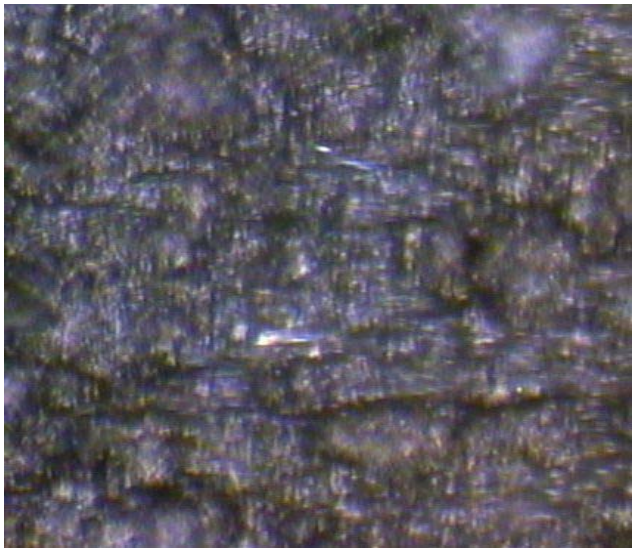

Fig. 11 – Micrographic image of pyrrole – aniline (1:1) film electrodeposited on aluminium surface after 25 cycles.

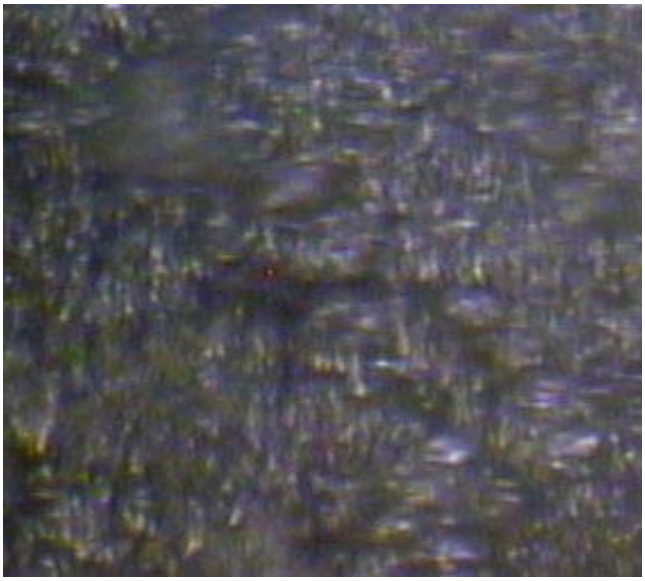

Fig. 12 – Micrographic image of pyrrole – aniline (5:1) film electrodeposited on aluminium surface after 25 cycles.

CONCLUSIONS

The electropolymerization of aniline is an anodic oxidation process.

The formation of Al_2O_3 films inhibits the electrochemical polyaniline formation and thus the decrease of the anodic oxidation current takes place.

For PANI/Al modified electrodes the increase of the number of polymerization cycles led in all the cases to decrease of the anodic peak height and to decrease of the anodic and cathodic current and in general of the average of the anodic and cathodic current.

The electropolymerization of pyrrole is also, an anodic oxidation process, which involves two electrons per molecule of monomer incorporated in the polymer chain.

The formation of Al_2O_3 film inhibits the electrochemical polypyrrole formation and thus the decrease of the anodic oxidation process takes place.

After a prolonged anodic oxidation the PPY film becomes loose and porous and the polarization resistance decreases.

The increase of the cycles number led in all the cases to decrease of the anodic peak height and of the anodic and cathodic current.

The composite coatings on aluminium substrate from pyrrole and polyaniline were obtained using the cyclic voltammetry.

The morphological structure of the composite coatings is dependent on the molar feed ratio of the monomers (aniline and pyrrole) and the applied potential.

The composite formation takes place by simultaneous oxidation and codeposition of aniline and pyrrole.

The behaviour of the composite polymer is different from the homopolymers behaviour and this fact proved that, a new material is formed, namely composite material or composite coatings.

REFERENCES

1. H. Shirakawa, E. Louis, A. G. MacDiarmid, C. K. Chiang, and A. J. Heeger, *J. Chem. Soc. Chem. Commun*, **1977,** *16*, 578.
2. S. Hung, T. Wen, and A.Gopalan, *Mater. Lett*., **2002,** *55*, 165.
3. M. C. Morvant and J. R. Reynolds, *Synth. Met*., **1998,** *92*, 57.
4. K. A. Noh, D. Kim, C. Jin, J. Kim and J. M. Ko, *J. Power Sources* **2003,***124*, 593.
5. V. Gupta and N. Miura, *Mater. Lett.* **2006,** *60*, 1466.
6. K. Lota, V. Khomenko and E. Frackowiak, *J. Phys. Chem. Sol.,* **2004,** *65*, 295.
7. J. H. Chen, W. Z. Li, D. Z. Wang, S. X. Yang, J. G. Wen and Z. F. Ren, *Carbon,* **2002,** *40*, 1193.
8. C. S. Li, D. Z. Wang, T. X. Liang, X. F. Wang and L. Ji, *Mater. Lett*., **2004,** 58, 3774.
9. G. Z. Chen, M. S. P. Shaffer, D. Coleby, G. Dixion, W. Zhou, D. J. Fray and A. H. Windle, *Adv. Mater*, **2000,** *12*, 522.
10. M. Wu, G. A. Snook, V. Gupta, M. Shaffer, D. J. Fray and G. Z. Chen, *J. Mater. Chem*., **2005,** *15*, 2297.
11. S. Sakkopoulos, E. Vitoratos and E. Dalas, *Synth. Met*., **1998,** *92*, 63
12. R. Haggenmueller, H. H. Gommans, A. G. Rinzler, J. E. Fischer and K. I. Winey, *Chem. Phys. Lett.,* **2000,** *330*, 219.
13. K. Jurewicz, S. Delpeux, V. Bertagna, F. Beguin and E. Frackowiak, *Chem. Phys. Lett*., **2001,** *347*, 36.
14. V. Gupta and N. Miura, *Electrochim. Acta,* **2006,** *5*, 1721.
15. Q. Xiao and X. Zhou, *Electrocim. Acta,* **2003,** *48*, 575.
16. J. Zeng, W. Wei, L. Wu, X. Liu, K. Liu and Y. Li, *J. Electroanal. Chem*., **2006,** *595,* 152.
17. N. Ferrer-Anglada, M. Kaempgen and S. Roth, *Phys. Stat. Sol. B,* **2006,** *243*, 3519.
18. P. Santhosh, K. M. Manesh, K.-P. Lee and A. I. Gopalan, *Electroanalysis,* **2006,** *18,* 894.
19. C. Downs, J. Nugent, P. M. Ajayan, D. J. Duquette and K. S. V. Santhanam, *Adv. Mater*., **1999,** *11*, 1028.
20. W. K. Maser, A. M. Benito, M. A. Callejas, T. Seeger, M. T. Martinez, J. Schreiber, J. Muszynski, O. Cauvet, Z. Osvath, A. A. Koos and L. P. Biro, *Mater. Sci. Eng*., **2003,** C23, 87.
21. E. Frackowiak, V. Khomenko, K. Jurewicz, K. Lota and F. Beguin, *J. Power Sources,* **2006,** *153*, 413.
22. J. Fan, M. Wan, D. Zhu, B. Chang, Z. Pan and S. Xie, *Synth. Met*., **1999,** *102,* 1266.
23. H. Hughes, G. Z. Chen, M. S. P. Shaffer, D. J. Fray and A. H. Windle*, Chem. Mater*., **2002,** *14*, 1610.
24. C. Peng, G. A. Snook, D. J. Fray, M .S. P. Shaffer and G. Z. Chen*, Chem. Comun*., **2006**, 4629.
25. Y. Zhou, B. He, W. Zhou, J. Huang, X. Li, B. Wu and H. Li, *Electrochim. Acta,* **2004**, *49*, 257.
26. G. A. Snook, C. Penh, D. J. Fray and G. Z. Chen, *Electrochem. Comun*., **2007,** *9*, 83.
27. E. T. Kang, K. G. Neog and K. L. Tan, *Prog. Polym. Sci.,* **1988,** *23*, 277.
28. V. Brânzoi, L. Pilan and F. Brânzoi, "Computational Methods and Experiments in Materials Characterisation II", WIT Press, 2005, p.51.
29. V. Brânzoi, L. Pilan, F. Golgovici and F. Brânzoi*, Mol. Cryst. Liq. Cryst.*, **2006,** *446*, 305.
30. E. M. Genies, G. Bidan and A. F. Diaz, *J. Electroanal. Chem*., **1983,** *49*, 101.

Revue Roumaine de Chimie, **2008**, *53*(11), 1007–1015

APPLICATION OF ELECTROCHEMICAL IMPEDANCE SPECTROSCOPY (EIS) TO STUDY OF PHENOLIC FILMS

Cristian PIRVU,[a] Alexandra BANU,[b] Octavian RADOVICI[b] and Maria MARCU[c*]

[a] POLITEHNICA University from Bucharest, Faculty of Applied chemistry and Materials Science, Polizu 1, Bucharest, Roumania
[b] POLITEHNICA University from Bucharest, Faculty of Management Technological Systems, Splaiul Independentei 313, Bucharest, Roumania
[c] Institute of Physical Chemistry Ilie Murgulescu, Splaiul Independentei 202, Bucharest, Roumania

Received December 18, 2007

This paper describes the phenol electrochemical oxidation that occurs with formation of phenolic films on the platinum electrode by cyclic voltammetry (CV) and electrochemical impedance spectroscopy (EIS) measurements. Both cyclic voltammetry and impedance studies were performed at room temperature, using a GAMRY PC3 potentiostat. The impedance data were recorded in a frequency range from 0.01 Hz to 100 kHz, with a.c. amplitude of 5 mV.
The capacitance and resistance curves were recorded at various frequencies, corresponding to the three regions from Nyquist plot, at high frequency (90kHz), where a kinetic stage controls the reaction, at small frequency (100Hz), where a diffusion control is present and at 2 kHz frequency for a mixed control.

INTRODUCTION

Industrial effluents containing toxic and/or biorefractory products are presently a serious environmental problem due to the increasing severity of the legislation on acceptable limits and to the lack of general treatment methods. Among aqueous industrial effluents, those containing organic pollutants cause problems due to the high activation energy barrier for chemical oxidation reactions and to the complexity of the degradation mechanisms.

Phenol is one of these compounds and it is a general protoplasmic poison that is corrosive to any living tissue it contacts. Inhalation can cause irritation to the respiratory system and associated mucosa. [1-3] Some studies have suggested that exposure to phenol causes mutations (genetic changes) in humans. While there is no evidence of carcinogenicity of this chemical in humans, it has caused cancer in mice and is considered a suspected carcinogen.[4]

The electrochemical methods can be used for partial or total degradation of toxic organic substances. Destruction of organic compounds by these ways offers the prospect of relatively simple equipment, environmental friendliness, and the possibility of high-energy efficiency by comparison with other methods.[5-7]

The chemical literature contains numerous reports of the loss of electrode activity, which accompanies the build-up of polymeric film on the surface of solid electrodes during phenol oxidation.[8-10] In a previous work[11] we proposed the following mechanism for electrochemical oxidation of phenol in sulfuric acid solutions.

The first step in the phenol (I) oxidation is a one-electron oxidation producing the phenoxy radical cation (II) which is a strongly acidic species and can deprotonate rapidly to the neutral radical (III), which, owing to its lower oxidation potential may be further oxidized to the corresponding phenoxonium ions (IV). This second electrode transfer may take place at the electrode and/or in solution.

This cation, acting as a strong electrophile, can react with water to produce hydroquinone (V).

The adjacent adsorbed phenoxy radicals (II) and the neutral radicals (III) can couple to form dimers (VI), trimers and eventually polymers that remain adsorbed on the electrode blocking the surface, *i.e.* electrochemical destruction of phenolic species is complicated due to electrode fouling producing

* Corresponding author: m_marcu2000@yahoo.com

oligomeric or polymeric nonsoluble compounds formed as a result of the coupling of phenoxy radicals generated in the initial oxidation step.

However, from a practical point of view, immobilization of phenol on the electrode surface due to electropolymerization might be used as an alternative to the electrooxidation for pollution remediation of aqueous solutions.

This paper describes the phenol oxidation that occurs with formation of phenolic films on the platinum electrode by cyclic voltammetry (CV) and electrochemical impedance spectroscopy (EIS).

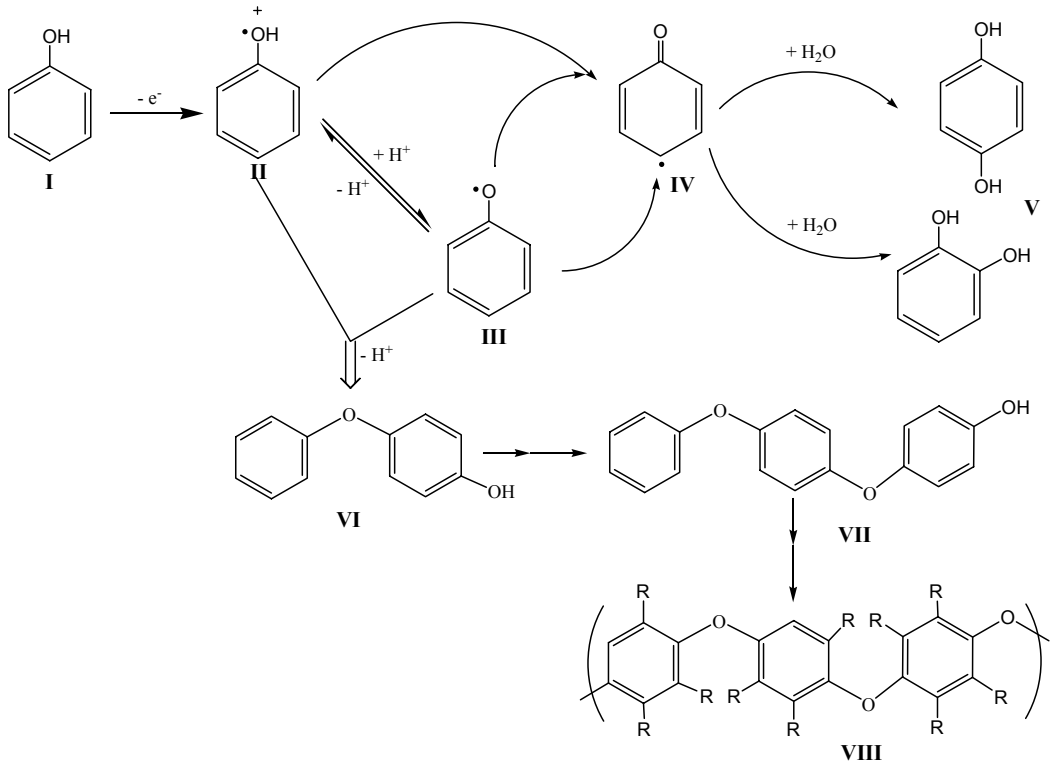

Fig. 1 – Proposed mechanism for electrochemical oxidation of phenol in sulfuric acid.
R is hydrogen or other rings of polymeric structure.

The Mott-Schottky technique was used in order to measure capacitance and resistance (*vs* d.c. potential) of electrode surface covered with a polymeric film. Evolution of capacitance and resistance *vs*. potential and *a.c*. frequency can offer us information about both adsorption and desorption ranges of electroactive species. At a different fixed frequency, small *a.c.* signal potential excitation is applied to the electrochemical cell and the impedance at the working electrode interface is measured at different values of polarization potential.

EXPERIMENTAL

The cyclic voltammetry and electrochemical impedance spectroscopy experiments were carried out in 12mM phenol in 0.5M sulfuric acid as supporting electrolyte, at room temperature, using a three-electrode system. The working electrode was Pt. Also, a platinum wire was used as counter electrode and the potentials were measured against a saturated calomel electrode placed in a separated compartment and connected with the cell by means of agar-agar bridge.

Cyclic voltammetry measurements were performed using a GAMRY PC3 potentiostat.

The investigation has been done in anodic direction from 0.2 to 1.4 V and before each scan the electrode was prepared to ensure a reproducible surface by polishing, rinsing with distillated water and ultrasonic cleaning for 4 min. in high purity water.

The impedance data were recorded using a GAMRY Instruments EIS 300, over a frequency range from 0.01 Hz to 100 kHz, with an *a.c.* amplitude of 5 mV.

The Mott-Schottky curves were obtained at various values of frequency (1 Hz, 100Hz, 1kHz, 90kHz) in the potential region corresponding to oxidation of phenol 0.2V – 1.3V.

RESULTS AND DISCUSSION

Voltammetric studies

Voltammograms obtained in acid aqueous media show an unique anodic wave at potentials

close to +1.0V and a little cathodic peak which shifted towards more chatodic potentials (figure 2). That implies the irreversibility of the system due to the fast subsequent chemical reaction. The nature of that wave and the various suggestions given by different authors about the dimerization of the radical formed indicated above, have led us to test either the existence of that kind of process and the mechanism which takes place.

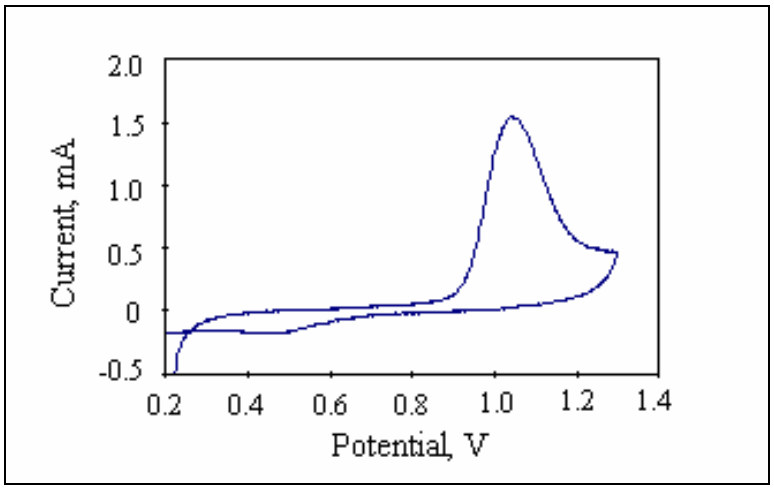

Fig. 2 – Cyclic voltammogram for 8 mM phenol in sulfuric acid 0.5M on Pt electrode.

The properties of the oxidation peak are in complete agreement with an irreversible diffusion (D) controlled reaction. So its peak current (i_p} is proportional to the square root of the sweep rate (v) see also fig. 3 as is given by:

$$i_p = mD^{1\backslash 2}v^{1/2}c \qquad (1)$$

Also a linearity of peak currents with concentration was found for lower values of concentration up to 10 mM.

On the basis of these results, it can be concluded that, with decreasing concentration and sweep rate, the peak current behaviour of phenol oxidation approaches that of an irreversible diffusion controlled reaction.

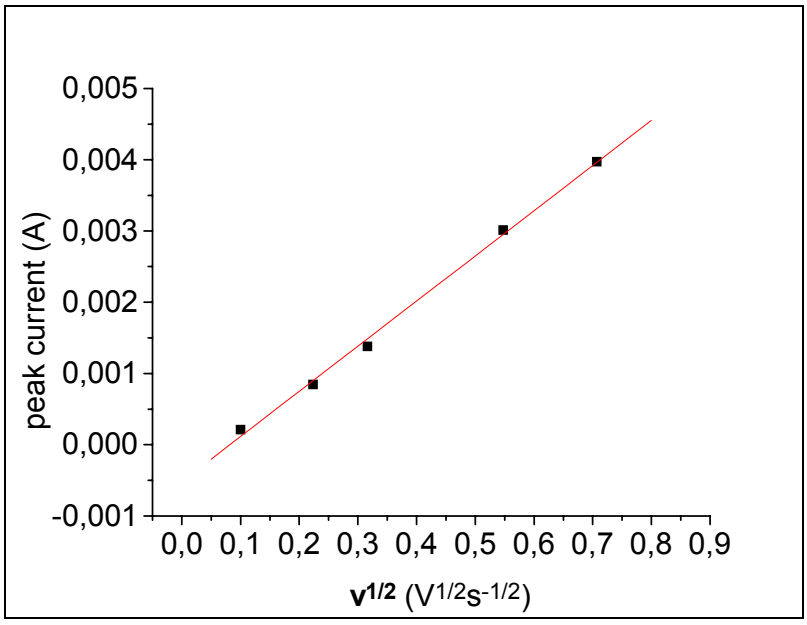

Fig. 3 – Variation of peak currents with square root of scan rates, for the oxidation of 8 mM phenol on platinum electrode.

So first of all voltammetric data show that the first current peak corresponds to a one electron reversible transfer followed by a fast dimerization of the radicals formed by EC mechanism, *i.e.*:

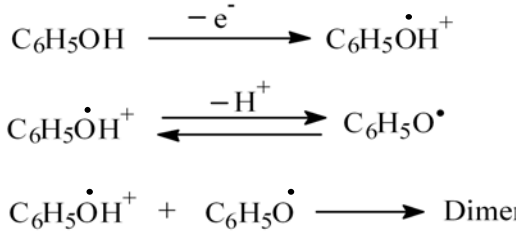

More data concerning the kinetic control were obtained by impedance spectroscopy.

Electrochemical impedance spectroscopy

The Nyquist impedance plot (figure 4) for phenol in acid solution at oxidation half wave potential, displayed Warburg impedance, indicating a diffusion effect.

In fact the impedance diagram gives a capacitive loop and a Warburg impedance, which implies that coverage on the electrode surface with adsorbed species is low and oxidation process is still proceeding on uncovered sites.

The impedance spectra with Warburg impedance and capacitive loop may be analyzed using the electrical circuits shown by figure 5 respectively.

The following figure presents an equivalent circuit specific to mixed control.

Where: R_s represents the solution resistance, R_t is charge transfer resistance, W is Warburg impedance, Cdl represents double layer capacitance and Cpc is a pseudocapacitance, Ra is pseudoresistance.

The values of elements of circuit are calculated as follows.

At very high frequencies, the Warburg impedance becomes unimportant in relation to Rt and the circuit converges to that of figure 6.

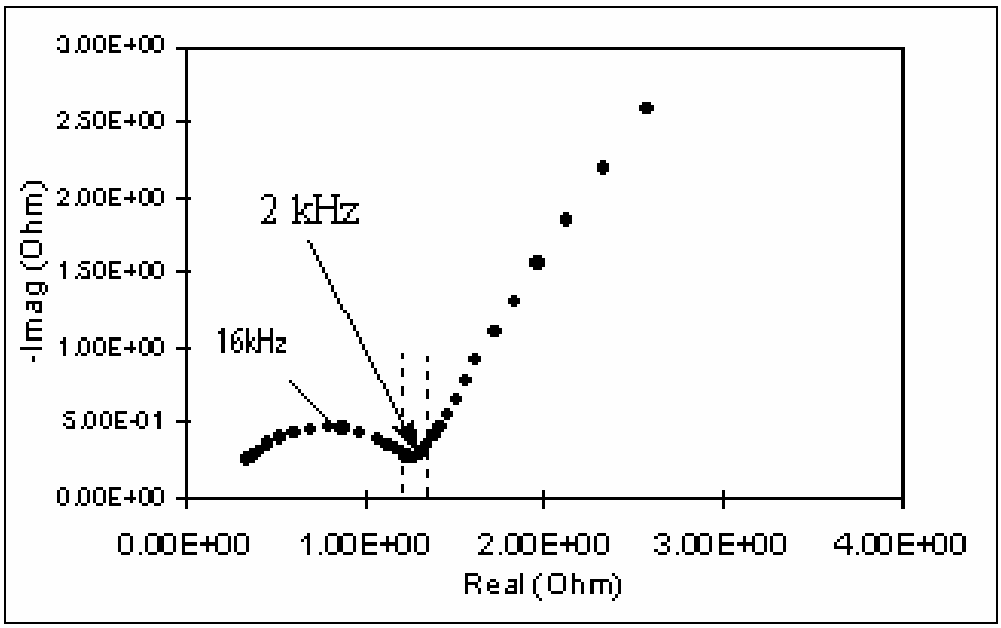

Fig. 4 – Nyquist plot for phenol in sulfuric acid on platinum electrode, at 1 V vs. ECS, frequency range 100 kHz to 0.3 kHz.

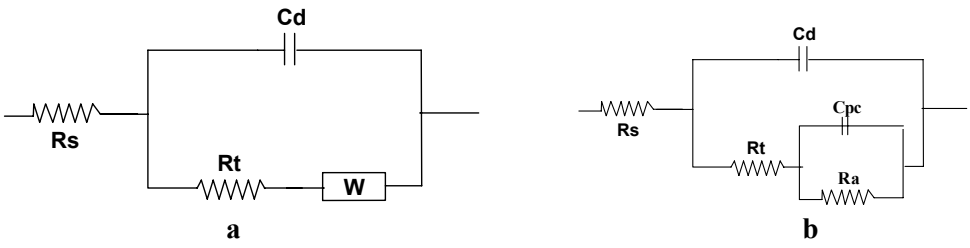

Fig. 5 – Equivalent circuit for a mixed kinetic and diffusion control.

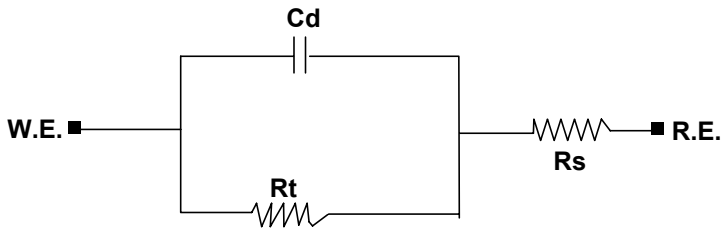

Fig. 6 – Equivalent circuit for a system in which the Warburg impedance is unimportant.

The impedance is: [12]

$$Z = R_s - j\left(\frac{(R_t}{R_t C_d \omega - j}\right) \quad (2)$$

which is expressed as the series combination of two elements Z_{Re} and Z_{Im}, real and imaginary components:

$$Z_{\mathrm{Re}} = R_s + \frac{R_t}{1 + R_t^2 C_d^2 \omega^2} \quad (3)$$

and

$$Z_{\mathrm{Im}} = \frac{R_t^2 C_d \omega}{1 + R_t^2 C_d^2 \omega^2} \quad (4)$$

Elimination of ω from this pair of equations yields

$$\left(Z_{\mathrm{Re}} - R_s - \frac{R_t}{2}\right)^2 + Z_{\mathrm{Im}}^2 = \left(\frac{R_t}{2}\right)^2 \quad (5)$$

Hence Z_{Im} vs. Z_{Re} should give a circular plot centered at

$$Z_{Re} = R_s + R_t/2 \quad \text{and} \quad Z_{Im} = 0$$

and having a radius of $R_t/2$.

R_t is defined as: [13]

$$R_t = \frac{RT}{nFi_0} \quad (6)$$

At the maximum value of Z_{Im}

$$\omega = \frac{1}{R_t C_d} \quad (7)$$

From these relations ship we have determined charge transfer kinetic parameters which are presented in table 1.

The values of these parameters, especially i_0, corresponds to a one electron reversible (fast) transfer reaction, followed by a fast dimerization of the radicals formed by an EC mechanism.

Table 1

Parameters, which were determinate at high frequencies

R_s	0.25Ω
R_t	0.75Ω
C_d	13.3μF
i_0	0.037A.cm^{-2}

Also, the low value of the charge transfer resistance, 0.75 Ω, shows a fast electron transfer reaction corresponding to phenol oxidation. This represents the first step of the reaction which is followed by polyphenol formation on the electrode surface.

At low frequencies the reactants have to diffuse farther, thereby increasing the Warburg impedance. The real and imaginary components will become

$$Z_{\mathrm{Re}} = R_s + R_t + \sigma\omega^{-1/2} \quad (8)$$

$$Z_{\mathrm{Re}} = \sigma\omega^{-1/2} + 2\sigma^2 C_d \quad (9)$$

Elimination of ω between these two equations gives

$$Z_{\mathrm{Re}} = Z_{\mathrm{Re}} - R_s - R_t + 2\sigma^2 C_d \quad (10)$$

The extrapolated line intersects the real axis at $R_s + R_t - 2\sigma^2 C_d$.

σ is the Warburg coefficient defined as: [14]

$$\sigma = \frac{RT}{n^2 F^2 A\sqrt{2}} \frac{1}{C_0\sqrt{D}} \quad (11)$$

in which:

ω - radial frequency; D –diffusion coefficient; A – surface area of the electrode; n – number of transferred electrons; C_0 – bulk concentration of the diffusing species;

The Warburg coefficient (σ) calculated from the slope of resistance *vs.* $\omega^{-1/2}$ plot (figure 8), at room temperature, is 120 $\Omega s^{-1/2}$.

Parameters which were determined at low frequencies are presented in the following table 2.

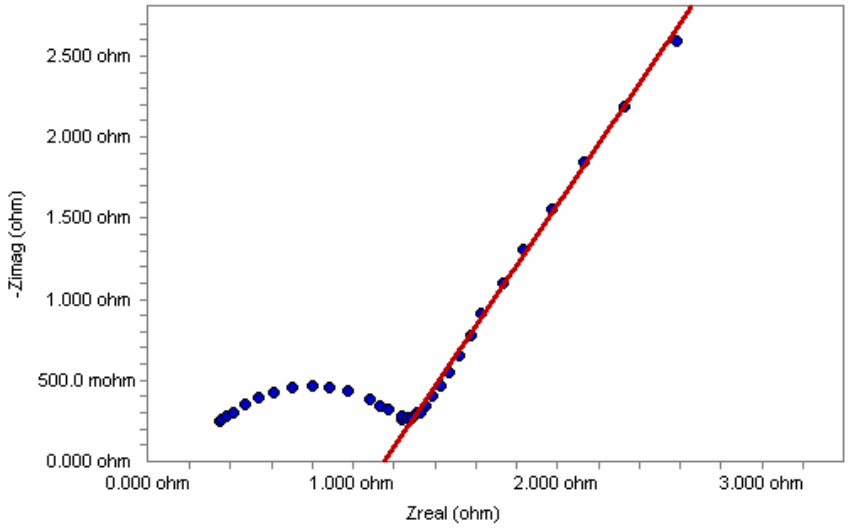

Fig. 7 – The extrapolated line which intersect the real axis at $R_s + R_t - 2\sigma^2 C_d$.

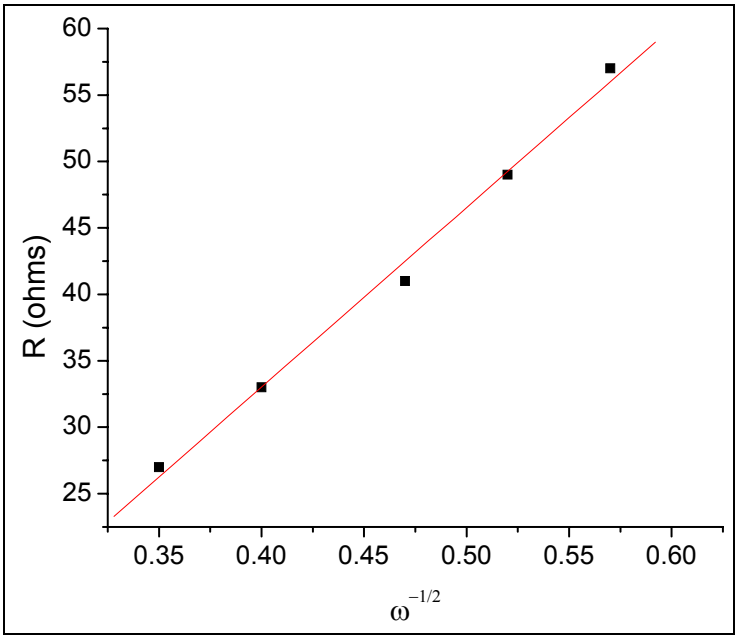

Fig. 8 – Dependence of resistance vs. $\omega^{-1/2}$

Tabel 2

Parameters which were determined at low frequencies

C_d	60 μF
σ	120 $\Omega s^{-1/2}$
D	$6.5.10^{-8}$ cm^2/s.

On the basis of the values of σ and D it can be concluded that oxidation of phenol is a irreversible diffusion (D) controlled reaction

Adsorption pseudocapacitance

The values of elements of circuit b are analyzed as follows. [15, 16]

The rate of migration of different active groups within membranes and monolayer on electrodes make necessary to consider the coupling between migration of reactants and electrode process i.e. the electrode process is coupled with a diffusional transport and possible with some reactions preceding, following or in parallel with the electrode process.

A reversible (fast) electrode reaction gives rise to a pseudocapacitance peak at the half wave potential. One defines as adsorption pseudocapacitance the case where only adsorbed constituents participate in the process.

As was shown by[1] pseudocapacitance resulting from a reversible electrode process is independent of frequency below complete surface coverage.

However when the full surface coverage is approached, the size of capacitance peak measured at medium and high frequency starts decreasing *i.e.* the capacitance peak are strongly frequency dependent when saturated monolayers (full coverage) are formed by adsorption.

This phenomenon suggests that the process giving rise to the capacitance peak is impeded at high surface coverage, while there is only little frequency dependence when the surface is only partially covered.

From the frequency dependence of pseudocapacitance it is evident that the electrode process being reversible, slow access of the electroactive groups to the active surface can be responsible for the frequency dependence at high surface concentration (coverage).

It was shown by [15] that one alternative mechanism for approach of the active species to the electrode surfaces is a diffusion process within the adsorbed layer. The diffusion mechanism gives a linear dependence of the pseudocapacitance C_{pc} on $1/\omega^{1/2}$ at high frequencies with an asymptotical approach to the echilibrum value at low frequencies.

For high frequency the expression for the pseudocapacitance C_{pc} is reduced to the form obtained for the diffusion in a semi-infinite phase, namely:

$$C_{pc} = a_s \frac{K_1}{(1+K_1)^2} \frac{F^2}{RT} (\Delta\delta + \frac{D}{2\omega})^{1/2} \quad (12)$$

where a_s is the concentration of active groups in the layer, K_1 is the equilibrium constant of the electrode process at any polarization, $\Delta\delta$ is the thickness of the electroactive monolayer, D is the internal diffusion coefficient of the active species in the polymeric layer.

As seen in (12) the pseudocapacitance varies linearly with $1/\omega^{1/2}$ through the whole frequency region.

The pseudocapacitance extrapolates to zero for $\omega \to \infty$ since at all experimental concentrations C_{pc} for $\omega \to \infty$ becomes extremely small.

Figure 9 presents the capacitance and resistance *vs.* d.c. potential applied curves, for phenol solution in sulfuric acid medium, on platinum electrode, applying different frequencies of a.c potential excitation. The Mott Schotky capacitance-resistance curves were recorded at various frequencies corresponding to the three regions from Nyquist plot, at high frequency (90kHz), at small frequency (100Hz), and at 2 kHz frequency.

In Table 3 we present the values of resistance and differential capacitance peak as a function of the frequency of the excitation signal, after five minutes of immersion of the electrode in phenol acid solution.

Table 3
The variation of resistance and capacitance at peak potential with frequency of the excitation signal

Frequency kHz	Resistance Ω	Capacitance μF
0.1	24	15
2	5.5	12
90	1.5	3

As seen from figure 9 and table 3 the above experimental pseudocapacitance values are in complete concordance with theoretical model of diffusion of active species in an adsorbed layer.

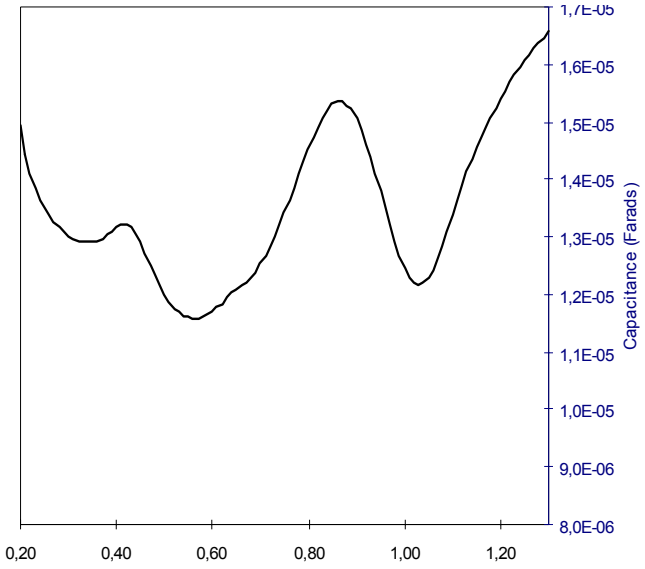

100Hz

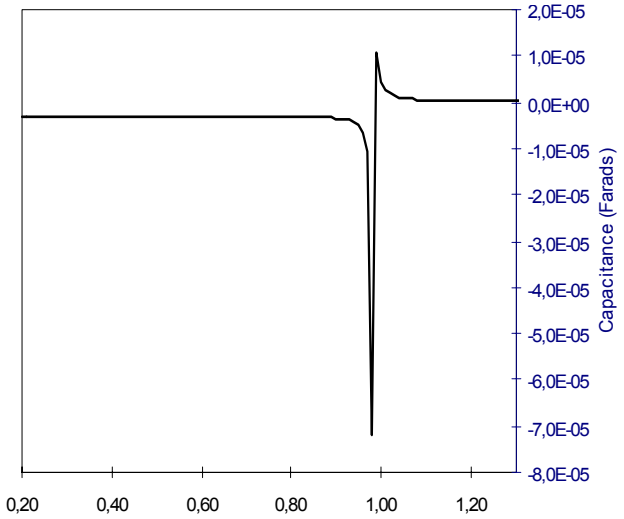

90KHz

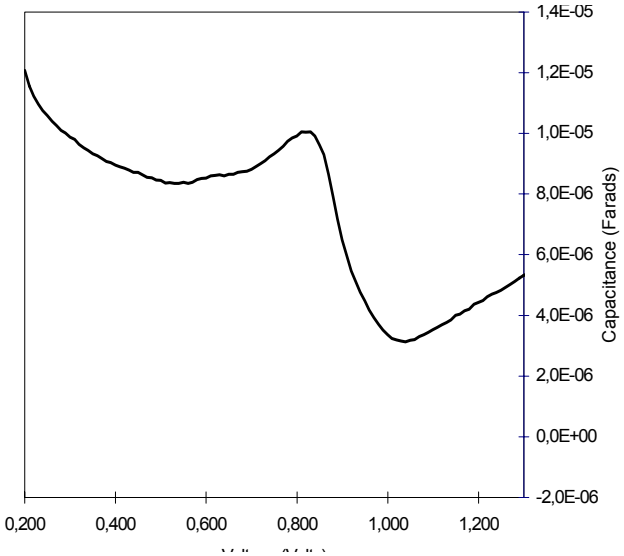

2kHz

Fig. 9 – Curves capacitance vs. *d.c*. potential applying at different frequencies of the a.c. potential excitation on Pt electrode in phenol 12mM and sulphuric acid 0.5M.

CONCLUSION

Electrochemical oxidation of phenolic species is stopped due to electropolymerisation. Ether- and quinone- type polymeric non-soluble compounds are formed as a result of the coupling of phenoxy radicals generated in the initial oxidation step. These non-soluble solide polymeric compounds block the electrode surface and lead to electrode deactivation and prevent effective total phenol deactivation.

Ortho and *para* linked polyphenol derivatives are formed in the course of electropolymerization of phenol as a result of preferable stabilization of phenoxy radicals via the *ortho* and *para* positions with respect to the original hydroxyl group.

The distribution of electropolymerization products depends on the stability of the radical formed, the structure and reactivity of the monomer molecules, reaction medium (solvent, pH solution), the electrode material, electrode potential and phenol concentration.

REFERENCES

1. L. G. Cockerman and B. S. Shane, “Basic Environmental Toxicology”, CRC Press/Lewis Publishers, New York,1994
2. A. D. Bloom and F. J. DeSerres. “Ecotoxicity and Human Healt”, CRC Press/Lewis Publishers, New York, 1995.
3. E. J. Calabrese, “Biological Effects of Low Level Exposures”, CRC Press/Lewis Publishers, NewYork, 1994.

4. J. W. Vincoli, "Risk Management for Hazardous Chemicals", Lewis Publisher, New York, 1996.
5. J. E. Vitt and D. C. Johnson, *J. Electrochem. Soc*., **1992**, *139*, 774.
6. N. Belhadj Tahar and A. Savall, in "Fundamentals and Potential Applications of Electrochemical Synthesis*",* edited by R. D. Weaver, F. Fisher, F. R. Kalhammer and D. Mazur, (The Electrochemical Society, Penning-ton, NJ), 1997, pp. 198-206
7. Ch. Comninellis and C. Pulgarin, *J. Appl. Electrochem*. **1993**, *23*, 108.
8. M. Ganttrell and D. Kirk, *J. Electrochem. Soc*., **1993**, *140*, 1534.
9. D. Pletcher and A. Alvarez-Gallegos, *Electrochim. Acta* **1998**, *44*, 853.
10. Z. Ezerskis and Z. Jusys, *J. Appl. Electrochem*., **2001**, *31*, 1117-1124.
11. C. Pirvu, A. Banu, O. Radovici and S. Nisipeanu, Proc. Of 12th Romanian International Conference on Chemistry and Chemical Engineering, Bucharest, 2001, 92-97.
12. R.E. Melnick, G. Tayhas and R. Palmore*, J.Phys.Chem. B,* **2001**, *105*, 1012-1025.
13. N. Belhadj Tahar and A. Savall, Journal of Applied Electrochemistry , **1999**, *29*, 277
14. N. Belhadj Tahar and A. Savall, J. Electrochem. Soc. **1998**, *145*, 3427.
15. I. R. Miller, Proc. Of the 1st International Symposium on biological aspects of Electrochemistry, 477-486, ed. S. Milazzo, 1971.
16. O. Pavlovic and I. R. Miller Of the 1st International Symposium on biological aspects of Electrochemistry, 513-524, ed. S. Milazzo, 1971.

Revue Roumaine de Chimie, **2008**, *53*(11), 1017–1026

THE POLYMER MOLECULAR WEIGHT AND SILICATE TREATMENT INFLUENCE UPON THE MORPHOLOGY OF NANOCOMPOSITES FOR FOOD PACKAGING

Doina DIMONIE,[*] [a] Constantin RADOVICI,[a] Ramona Marina COSEREA,[a] Sorina GÂREA[b] and Mircea TEODORESCU[b]

[a] ICECHIM Bucureşti, Spl.Independenţei, No.202, District 6, Bucharest, cod 060021, Roumania
[b] "Politehnica"University Bucharest", Faculty of Applied Chemistry and Material Science, Department of Polymer Science and Engineering, Calea Victoriei, No. 149, Bucharest, cod 010072, Roumania

Received December 20, 2007

Some results concerning the obtaining, based on melt processing techniques, of polymer nanocomposites from poly(ethylene–co–vinyl acetate) and layered silicates with improved barrier properties for food packaging it is presented. The dependence between the polymer molecular weight and the silicate treatment upon the EVA – layered silicates micro–composites morphology is analyzed.
As a consequence of the umectability in proportion with the molecular weight, microcomposites with high morphological level order are obtained if EVA with high molecular weight was used.
Because of the prevalent hydrofobicy of the EVA chains with 28 % polar groups, the biggest silicate "swelling" are obtained with untreated silicates. If the silicate was functionalisated, then, from ammonium and pirolydonym ions, the ammonium with small substituents must be prefered. In the case of big substituents the interactions with the vinyl–acetate group from EVA are weak and the silicate "swelling" degree unimportant.

INTRODUCTION

If, between the 1950 and 1995, it was the period of "macro" materials in which the leading size was the millimeter, around the 1970s, started the stage of micro-materials that have as characteristic feature the micro-meter. In 2005, begin the "nano" time that, is estimated to have an extremely long life, at least until after 2050. The main characteristics of the "macro" period were the interest for the miniature sizes. The stars of "nano" period are and will be the nano-materials, nanocomposites and biotechnologies. The main applications of "nano" materials are the packaging, the automotive industry and the constructions and in the next years, medicine, micro–electronics and still packaging.[1-3]

Many packed foods, needs, on the one hand, protection against oxygen, humidity, light, and on the other hand, the preservation of their aromes and fats, on the entire life, *i.e.* until food-stuffs consumption. The needed food-stuffs protection, is provided by the packaging barrier properties defined by the performance level, presented in table 1.

The most known packaging with the barrier properties are made of polymeric nanocomposites, and montmorillonite (MMT), a layered silicate with the thickness at the nano scale and with the width and length within the micrometers range.

Whereas, the nanocomposite permeability is expressed by the formula (1) and the passing of gases through the nanocomposite, follows the "sinous path of Neilson" (fig. 1), the **nanocomposites used as** materials with the barrier properties must be of the **exfoliated type** (fig. 2).

$$P_{nano} = (1 - \varphi)\, P_{matrice} / (1 + \alpha\, \varphi /2)^{*} \qquad \text{(formula 1)}$$

[*] Corresponding author: ddimonie@chimfiz.icf.ro

where: P_{matrix} = polymer permeability; P_{nano} = nanocomposite permeability; φ = fraction of volume for the nanoparticles; α = ratio related to the particles shape

Table 1

General estimation of the performance levels of the barrier properties for the food packaging

Performance of barrier	Light optic Density	OTR[a], cm^3 / m^2 d bar	WVTR[b], G / m^2 d
High	> 2.8	< 1.0	< 0.5
Medium	2.0 – 2.8	1.0 – 10	0.5 – 5
Low	< 2.0	> 10	> 5

[a] OTR – oxygen transmition rate; [b] WVT – water vapor transmition

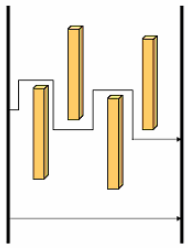

Fig. 1 – The illustration of sinous path of Neilson.

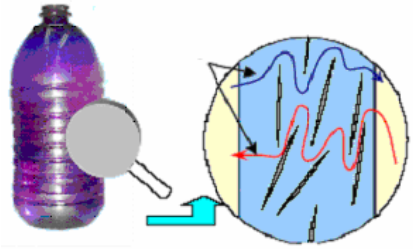

Fig. 2 – The explanation of the neccessity to perform exfoliated nanocomposites for maximizing the barrier properties.

The maximizing the barrier properties of a polymer nanocomposite, achieved by the melt processing techniques, require the solving of the following scientific and technical aspects:the compatibilisation of the silicate with the polymer matrix based on the silicate treatment, the melt compounding, inclusively by reactive techniques, of the treated layered silicates with the interest polymeric matrix; the exfoliation of the layered silicate until individual lamellas, the barrier effect maximizing by the orientation, at the melt processing, of the lamellas within the polymeric matrix, parallel with the package surface, the avoiding of the lamellas re-aggregation during the packaging manufacture (films or bottels). The packaging obtaining must avoid loosing of silicates exfoliation and lamellas orientation. Also it must be done the characterization of the nanocomposites and packaging by using the advanced nano-scale evaluation methods and devices and the estimation of the physico-mechanical properties, thermal stability and barrier properties with visualisation of the morphologic structures in relation to the obtained properties.

The polymer nanocomposites with improved barrier properties, are used both, as films and as adhesives. The multi-layers structures (fig. 3) with improved barrier properties are extensively used in the packaging production.

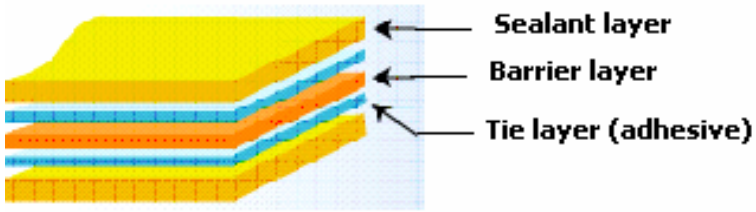

Fig. 3 – Multilayer polymeric structure used as food packaging.

The ethylene–vinyl acetate co-polymer (EVA) can be used as a layer with barrier properties and as an adhesive intermediary layer within the composition of the multi-layered structure designed for the packaging production.[4-8]

A part of the results obtained for the preparation, by the melt processing techniques, of multi-layers food packaging with the improved barrier properties, from nanocomposites based on the ethylene – vinyl acetate copolymer (EVA) and montmorillonite (MMT), will be presented below.

EXPERIMENTAL

The aim of the performed works was the study of the EVA molecular weight and of the silicates treatment influence upon the EVA – MMT composites morphology. As it is known, depending on the silicate exfoliation degree, the resulted polymer–silicates systems can be of the following types: micro-composites or the conventional composites (fig. 4a), intercalated nanocomposites (fig. 4b) and exfoliated nanocomposites (fig. 4c).[9] Because the results shown below, do not refer to the TEM micrography, on which basis, good estimations upon the morphology type can be made, for discussing the obtained polymer – silicate systems the micro-composite nomenclature will be used in the following presentation.

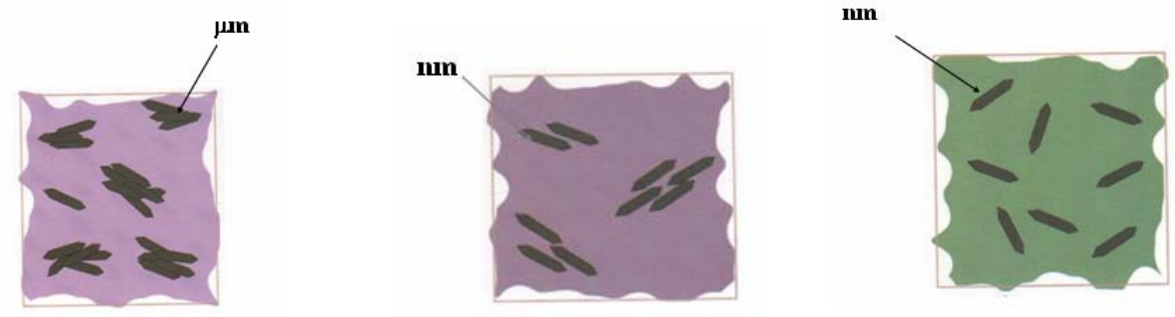

a) b) c)

Fig. 4 – Types of layered polymer–silicate systems: a) microcomposites (polymer are not intercalated between the silicate layers); b) intercalated nanocomposites (polymer chains are intercalated between the clay layers); c) exfoliated nanocomposites (the clay layers are completely distributed in the polymer matrix).[8,9]

1. Materials

a. The ethylene–vinyl acetate copolymer with different molecular weights, provided by the Du Pont company (Table 2). Knowing that the most technological expression of the molecular weight is the melt flow index (MFI),[10] the reference at different EVA molecular weight, will be done using the MFI values.

b. Treated and non- treated montmorillonite (Tables 3, 4 and fig. 6). The used silicates have not a homogeneous morphologies, because they contain galleries with different sizes, except of bentonite and Cloisite 15 A.

c. Additives for the EVA melt processing.

Table 2

The used EVA types

Grades / Applications	Vinyl acetate content, [%]	Tmelting, ^{0}C (Boetius)	MFI, g/10 min.	Density, g/10 min.	Hardness, ^{0}Sh A
Elvax 260 / industrial application	28	78 – 85	6	0.955	85
Elvax 220 W/ industrial application	28	65 – 70	150	0.951	69
Elvax 210 W / industrial application	28	62 – 65	400	0.951	62
Elvax 205 W / industrial application	28	60 – 70	800	0.951	75

Table 3

Treated and non- treated montmorillonite

Silicate grades	Chemical formula	XRD basal spacing, Å
Bentonite	natural, non-functionalised Montmorillonite $M_x Al_{4-x} Mg_x) Si_8 O_{20} (OH)_4$(M= monovalent cation; x = degree of isomorphous substitution (values 0.5 – 1.3)	11.7
Nanocor I 28[11]	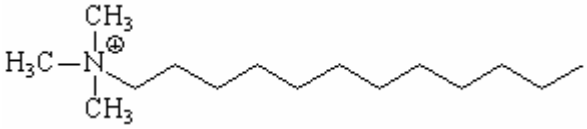 Trimethyl dodecyl ammonium Particles with the diameter of 8–10 µm with density of 1,9 g/cm^3 [10]	28
Nanocor I 33[11]	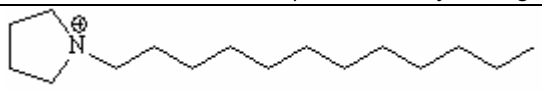 Dodecyl pyrolidone	30.29

Table 3 (continued)

Cloisite 15 A	Dymethyl, 2-ethylhexyl (hydrogenated tallowalkyl) ammonium Hydrogenated tallow: ~ 65 % C 18; ~ 30 % C16; ~ 5 % C14 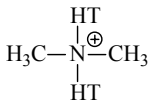 HT = Hydrogenated tallow	31.5
Cloisite 93 A	$CH_3N+ (HT)_2 H$ Hydrogenated tallow: 65 % C; ~ 30 % C 16; ~ 5 % C14 Anion: $^-HSO_4$ 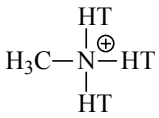 Methyl dihidrogenated tallow ternary ammonium	23.6

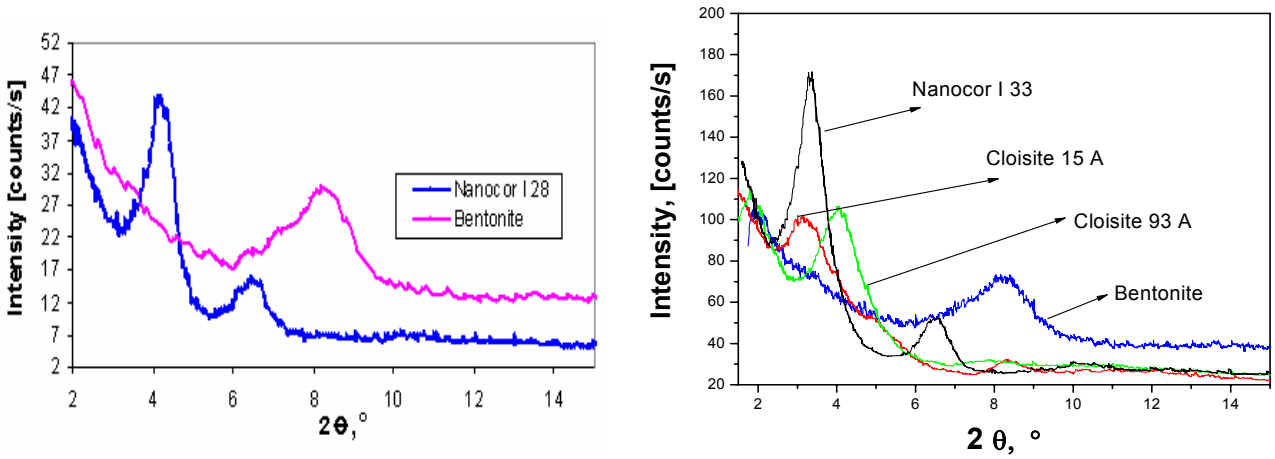

Fig. 5 – The diffractograms of the used silicates.

Table 4

The XRD basal spacing

Silicate	2 teta, ^{0}	d, Å
Cloisite 15 A	3.21; 8.24	**31.9**
Cloisite 93 A	1.78; 4.05; 7.9	57.6; **25.3;** 13
Nanocor I 28	1.76; 4.2; 6.36;	58; **24.4;** 16.1
Nanocor I 33	3.35; 6.64; 10.8	30.6; **30.29**; 30.23
Bentonite	8.26;	**12.43**

2. Microcomposites obtaining

Compounding within a Bradender plastographs at 125 – 130°C, 100 rpm and outlining in sheets, by rolling on without friction on a laboratory roller has been employed.

3. Characterisation

The morphology was analysed by X rays diffraction (RDX). It was recorded the variation of the radial diffraction intensity dependence by the diffraction angle, at the room's temperature. It was explored the 2 – 14 ^{0} diffraction angle domain, working with 0.03^0 step, scanning speed = 8 s /step, and a filter with λ = 1.7921 Å. For computing the interbasic distance (d) it was used the Law of Bragg [12] (formula 2).

$$d = n\lambda / 2 \sin \text{theta} \qquad \text{(formula 2)}$$

where: d – basal spacing; n – constant; λ – wavelength of X ray; theta – the angle between the incident ray and the diffusion plane.

RESULTS

The X rays diffractograms of the micro-composite obtained from **EVA with different molecular weight and Cloisite 15 A** are presented in fig. 7. The XRD basal spacings on these microcomposites are presented in table 7.

The diffractograms show, for all the situations, an identical arrangement of the amorfous morphology, at **10.06 Å.**

It is also noticed that, regardless the value of the polymer molecular weight, the diffraction takes place, in all cases, approximately at the same diffraction angles (5.13 **Å** and 2.53 – 2.66 **Å**). Depending on the EVA molecular weight, the diffractograms differ each other, by the height, width and the area of the diffraction peaks. The smallest diffraction peaks, are met for the microcomposites in which EVA has the smallest molecular weight (MFI= 800 g/10 min.). The height of the 2.53 **Å** diffraction peak is approximately 50 counts/s, that means approx. 3 times lower than the similar peak from 2.66 Å of the micro-composite in which the polymer has the biggest molecular weight (MFI = 6 g/10 min.). These results show a dependence with the polymer molecular weight of the order degree of the morphological structures that have the same difraction maximum. So much less the area of the diffraction peak, more reduced the order degree of the sample morphology.

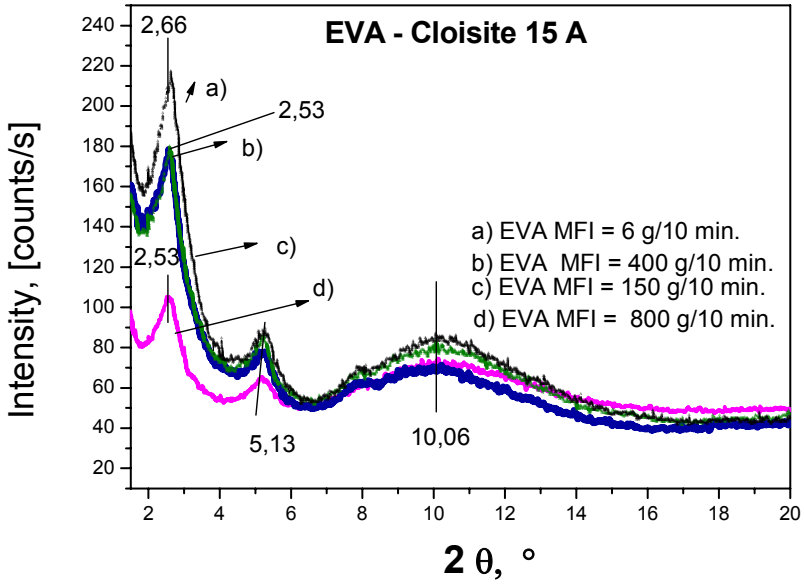

Fig. 6 – The XRD diffractograms related to the microcomposites of EVA with different molecular weights and 3 % Cloisite 15 A.

Table 5

The XRD basal spacing of the micro- composites of EVA with different molecular weights and 3 % Cloisite 15 A

EVA MFI, g/10 min.	2 teta, 0	Dx, Å
6	2.56; 5.14; 7.71;	40.1, 20; 13.3
150	2.58; 5.18;	39.7; 19.8
400	2.62; 5.24;	39.1; 19.6
800	2.62;8.21	39.1; 19.6

[x] Bolded Value = main gallery

According to fig. 5 and Table 4, Cloisite 15 A is a silicate with a homogeneous morphology, because it has only one basal spacing size, respectively of **31.9 Å.** Within the EVA micro - composites, Cloisite 15 A suffered a spacing until **40.1 Å** in case of EVA with MFI = 6 g/10 min. and until **39.1 – 39,7 Å** for EVA with lower molecular weights (table 5). All the performed microcomposites are inhomogeneous because they contain galleries with different sizes.

Comparing the basal spacing size of the Cloisite 15 A in the native condition, to those from the micro–composites with EVA with different molecular weights, it is noticed that through the melt compounding, it was achieved an increase of the basal spacing size of **7 – 8 Å.** This means that the interactions between the acetate group from the copolymer with the ammonium groups from the Cloisite 15 A galleries, determined galleries spacing of approx. **8 Å**.

The X rays diffractograms of the micro–composites based on EVA with different molecular weights and 4 % **Cloisite 93 A** are presented in the fig.7. The basal spacings of these micro–composites are shown in Table 5.

An identical ordness of the amorphous phase, at approx. 10 Å distance, in all situations can be observed. Regardless of the polymer molecular weights, the diffraction take place at the same angles (approx. 5.62 Å and approx. 2.96 Å respectively). The height, width and diffraction peak area make the differences between the diffractograms (fig.7). The smallest diffraction peaks are recorded for the micro – composite in which the polymer has the smallest molecular weight (MFI= 800 g/10 min.). It can be observed, in this situation too, the dependence of the order degree of the morphological structures whith the same diffraction peaks on the molecular weight. Much the diffraction peak has a smaller height, more the order degree is lower.

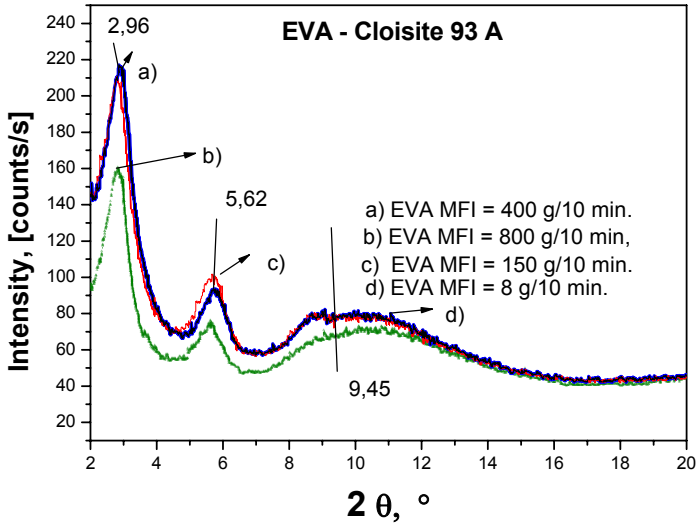

Fig. 7 – The X rays diffractograms for the EVA micro - composites with different molecular weight and 3 % Cloisite 93 A.

Table 6

The XRD basal spacing of the micro- composites of EVA with different molecular weight with 3 % Cloisite 93 A

EVA MFI, g/10 min.	**2 teta, ^{0}**	**D^x, Å**
6	2.93; 5.79	**35**; 17.7;
150	2.85; 5.68;	**36**; 18.1;
400	2.88; 5.74;	**35.6**; 17.9;
800	2.88; 5.74;	**35.5**; 17.9;

^{x} Bolded Value = main gallery

Cloisite 93 A is a silicate with a non-homogeneous morphological structure as it contains galleries of different size (basal spacing by 57.6; **25.3;** 13 Å) (fig. 5, table 4). The morphological order of the 4 micro – composites with EVA does not depend on the molecular weights (fig. 7, table 6). All these micro-composites have a similar morphological order with galleries of about **35 – 36 Å** and **17 – 18 Å.** This means that the gallery spacing, in all cases, is by approximately **10 – 11 Å** regardless the EVA molecular weight.

Considering the Cloisite 15 A and Cloisite 93 A degree of "swelling" into the studied micro – composites, it can be underlined that the interactions between the vinyl acetate groups from EVA and the functional groups from the Cloisite 15 A and Cloisite 93 A galleries are characterized by small values and order of magnitude.

The X rays diffractograms of the **EVA - Nanocor I 28** micro – composites, are presented in the fig. 8 and their basal spacings in the table 7. These diffractograms show, for all the variants, an identical order of the amorphous phase, at a distance of 10.1 Å. The micro – composite

diffractogram in which the polymer has the biggest molecular weight (MFI = 6 g/10 min.) does not show any maximum of diffractions (fig. 8, a curve). If the polymer has a smaller molecular weights (MFI = 150, 400, 800 g/10 min.) then the diffractograms put into evidence the diffractions at the same angles for all the three different situations (2.21 - 2.39 Å and at 5.04 Å). These values are different from those of the individual silicate and shifted to small values of the diffraction angle.

These peaks have a small height (50 – 90 counts/s) and a similar width. The different height of the diffraction peaks from 2,21 -.2,39 Å indicates greater morphological order in case of the polymer with a higher molecular weights. Practically, the height of these peaks decrease with the decreasing of the polymer molecular weight. The diffraction peak of the micro–composite in which the polymer has the lower molecular weight (MFI = 800 g/10 min.) is by the smallest height.

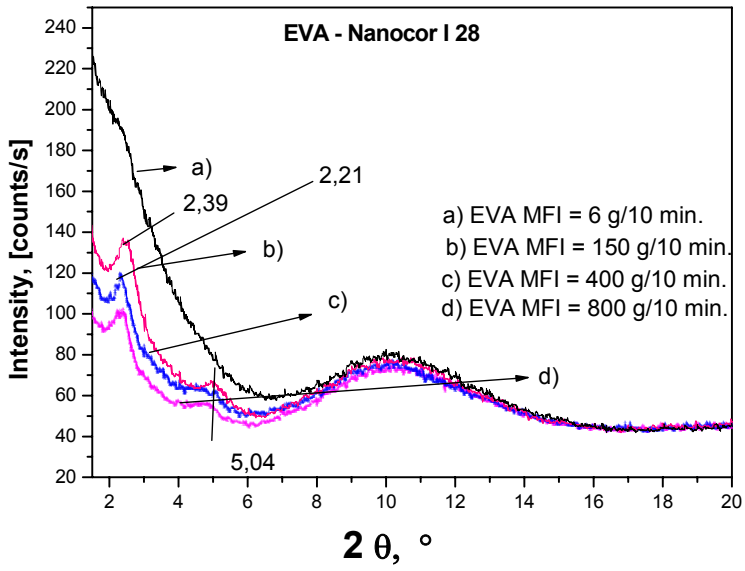

Fig. 8 – Diffractograms of X rays for the EVA microcomposites with different molecular weight and 3 % Nanocor I 28.

Table 7

The XRD basal spacing of the micro- composites of EVA with different molecular weights and 3 % Nanocor I 28

EVA MFI, g/10 min.	2 teta, ^{0}	d, Å
6	-	-
150	2.38; 4.8;	**43.5;** 21.5
400	2.32; 4.65;	**44.2;** 22.1
800	2.48; 4.95;	**41.4;** 20.7

Comparing the basal spacing of Nanocor I 28 in the native state with those from the EVA micro - composites, it can be noticed that by melt processing with EVA, a silicate " swelling" by **16 – 20 Å** (the basal spacings of 24.4 Å in native state and of 41 – 44 Å in micro–composites) was performed. This means that the functional groups from the Nanocor I 28 galleries, interact more efficiently with the acetate groups from EVA than in case of the other silicates (Cloisite 15 A and Cloisite 93 A). In other words the substituents from the ammonium ion used for the layered silicate galleries treatment, control the interaction with the polymer.

The X rays diffractograms of the EVA micro–composites with the **Nanocor I 33,** are shown in fig. 9 and their basal spacings in table 8. These diffractograms indicate that for all situations, there is an identical orientation of the amorphous phase, at a distance of 10.1 Å. The diffractograms indicate that for all the 4 micro - composites, regardless the value of molecular weight, the diffraction maximum for similary angles: 2.95 – 3.02 Å and 5.78 – 5.99 Å. In this case too, the height, the width and the area of diffraction peaks differ.

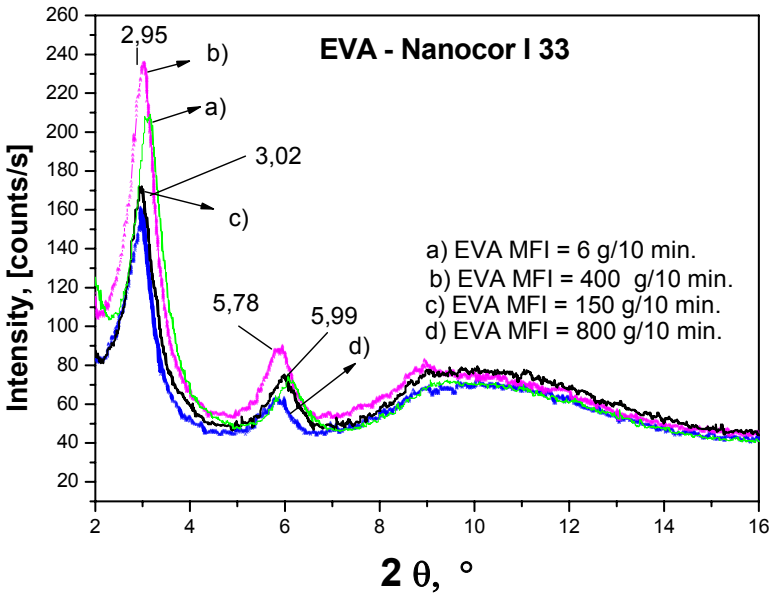

Fig. 9 – The X rays diffractograms of the microcomposites of EVA with different molecular weights and 3 % Nanocor I 33.

Table 8

The XRD basal spacing of the micro- composites of EVA with different molecular weights and 3 % Nanocor I 33

EVA MFI, g/10 min.	**2 teta, ^{0}**	**d, Å**
6	3.03;6.04;	33.8; 17;
150	2.98; 5.95;	34.4;17.2
400	2.96; 5.9;	34.7; 17.4
800	2.95; 5.89;	34.8; 17.4

Nanocor I 33 is relatively more homogenous than the other studied silicates, whereas the interbasic distance is by **30.29** – 30.6 Å (fig. 5, table 4). The micro–composites have a heterogeneous morphology because, nearby the main galleries of 33 – 34 Å, there are others of approx. 17 Å. Regardless the molecular weight, in all the 4 studied micro–composites the basal spacings have approximately the same size of **33 – 34 Å,** that means a galleries "swelling" with only **2 Å**. This small galleries enlargement is a prove that the **dodecyl pyrolidone** functionality of Nanocor I 33 are not compatible with the vinyl acetate groups from EVA.

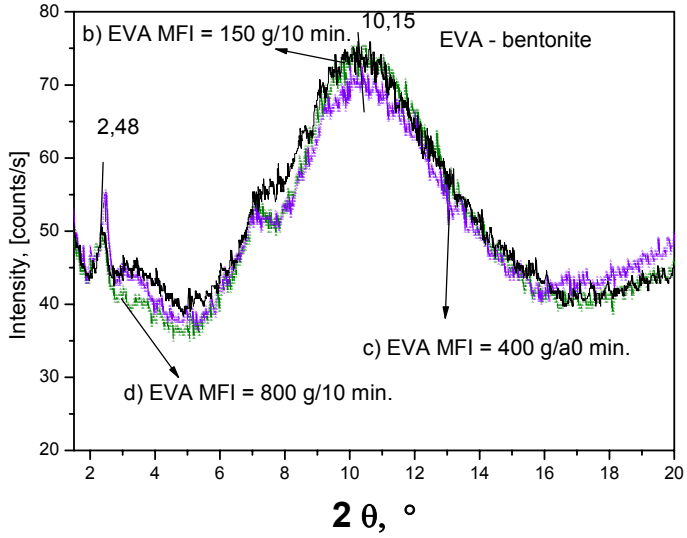

Fig. 10 – The X rays diffractograms of the microcomposites of EVA and 3% bentonite.

On the diffractograms of the micro-composites of EVA with bentonite (fig. 9) a very wide maximum at 10.15^0 with the intensity of 75 counts/s and other smaller at 2.48^0 with the intensity of 65 counts/s appears. Data from Table 9 proves that if EVA has MFI = 6 g/10 min., then at the melt compounding with bentonite, a silicate enlargement from 12.43 Å to 30 Å, i.e. a swelling of **27 – 27 Å** takes place. If the polymer molecular weight is smalller then, regardless the molecular weight, the bentonite galleries swelling is only by approx. 30 Å.

Table 9

The XRD basal spacing of the micro- composites of EVA and 3% Bentonite

EVA MFI, g/10 min.	2 teta, ^{0}	d, Å
6	8.4	30.2
150	2.35; 7;	43.6; 14.7
400	2.34; 3.37; 7.04;	43.8; 30.4; 14.6
800	2.44; 7;	42; 14.7

DISCUSSION

It is known that EVA is a statistical copolymer, based on ethylene and vinyl acetate (formula 3) which is obtained industrially by radical copolymerization at high pressure.[13] The copolymer properties are controled by the vinyl acetate content and by the molecular weight values.

The higher the content of vinyl acetate, the higher the flexibility, the low temperature impact resistance, and the capacity of fillings accepting.

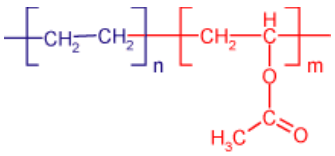

(formula 3)

In the performed experiments, EVA with 28% acetate groups was used. The obtained results showed that this type of EVA, better incorporated the non treated silicates. If the silicates were treated then the functional groups of ammonium type which contain small radicals more efficient are. Functionalizing of the silicate galleries with the pyrolidon ions is not efficient. The explanation of this result is connected to the predominant non-polar and hydrophobic character of EVA with 28 % polar groups in the molecular chains.

The molecular mass of EVA is another parameter which controls the polymer properties. The bigger the molecular weights, the higher the fluidity and the wettability are.

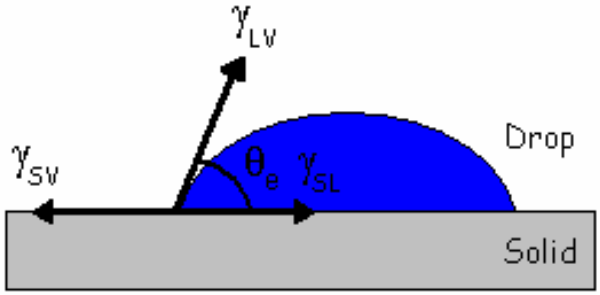

Fig. 11 – Graphic representation of the contact angle as an expression of liquid wettability (polymeric melt)[14].

As it is known, the wettability is given by the value of contact angle between a liquid drop within the thermic equilibrium with an horizontal surface (fig. 11).[14] If the wetting angle θ has a value lower than 90^0 then the fluid has good wetting properties. If the wetting angle is between 90^0 and 180^0 A then the fluid has bad wetting properties.

The thermodynamic wetting equilibrium depends on the interface tension and is defined by the formula 6.

$$0 \leq \theta \geq 90 \qquad \text{(formula 4)}$$

$$90 \leq \theta \geq 180 \qquad \text{(formula 5)}$$

$$\gamma_{s,v} = \gamma_{s.l} + \gamma_{l,v} \cos\theta \qquad \text{(formula 6)}$$

where: $\gamma_{s,v}$ represents the gas – solid interface tension, $\gamma_{s.l}$ is the solid – liquid interface tension and $\gamma_{l,v}$ the liquid – gas interface tension. Considering solid the silicate galleries and liquid the polymer melt, all the above-mentioned can explain the compatibility between the plymer melt and silicate galleries.

In all silicate – EVA pairs that differ through the molecular weights, it was noticed the same diffraction peaks, but depending on the molecular weight the peaks, have different height, width and specific area. The highest peaks were met in the cases of the biggest EVA molecular weight because of the higher wetting character of these macromolecular chains. The most eloquent situation was in the case of Nanocor I 28 when, for EVA with MFI = 6 g/10 min. the diffractogram didn't show any diffraction peak (fig. 8 a). All the above-mentioned results will be re-analysed from the TEM perspective coupled with the thermal analysis.

CONCLUSIONS

Some results concerning the obtaining of polymeric nanocomposites with improved barrier properties for food packaging based on melt processing techniques based on poly (ethylene–co–vinyl acetate) and layered silicates are presented. The study concerning the dependence between the polymer molecular weight and the silicate treatment on the EVA – layered silicates micro–composites morphology is detailed.

As a consequence of the wettability in proportion with the molecular weight values, the micro–composites with high morphological order level are obtained based on EVA with high molecular weight.

Because of the prevalent hydrofobicity of the EVA macromolecular chains with 28 % polar groups, the biggest silicate "swelling" are obtained with un treated silicates. If the silicate was treated, then, between ammonium and pyrolidon ions, the ammonium groups with the smaller substituents must be prefered. In case of big substituents the interactions with the vinyl – acetate group from EVA are weak and the silicate "swelling" unimportant

Because of the wettability in proportion with the molecular weight, EVA with higher molecular weight reinforced with multilayered silicate lead to the micro–composites with higher content of ordered phase. This dependence is more pronunced in the case of silicates with treated galleries which is more compatible with the polymer.

REFERENCES

1. Y. Mai and Z. Yu, "Polymer nanocomposites", Woodhead Publishing, 2006.
2. S. Auerbach, K. A. Carrado and P. K. Dutta, "Handbook of Layered materials", Marcel Dekker Inc, New York, Basel, 2004.
3. L.Kovarova, "Barrier Properties and Morphology of Surlyn/Montmorillonite Nanocomposites, Proceeding of the 8th Polymers for Advances Technologies international Symposium, Budapest, Hungary, 13 – 16 September, 2005.
4. Rahul K., *J. Non-Newtonian Fluid Mech*., 2005, *128*, 116-125.
5. Ranjit Prasad, *Polym. Eng. Sci.,* 2004, *44,* 1220-1230.
6. Cheol Hwan Jeon, *Polym. Intl.,* 2003, *52*, 153–157.
7. Il Soon Suf, *J. Appl. Polym. Sci*., 2004**,** *94,* 1057–1061.
8. Doina Dimonie, *Rev. Mat. Plast.*, 2006, *43*, 132 – 137.
9. D. Louvier, Nanotechnology& packaging: overview, SFN Technology Meeting, Bern University of Applied Sciences – Swiss College of Agriculture, 12th dec. 2006.
10. L.Karger, "Polypropylene an A-Z references", Kluwer Academic Publishers, 1999.
11. "Nanocor", Arlington Heights, IL, *The Free Library* 01 July 2002. 19 December 2007**.**
12. http://www.eserc.stonybrook.edu/projectJava/Bragg.
13. http://www.specialchem4adhesives.com/tc/ethylene-copolymers/.
14. http://www.ksvltd.com/content/index/keyca.

Revue Roumaine de Chimie, **2008**, *53*(11), 1027–1039

PRACTICAL ASPECTS ASSOCIATED WITH THE USE OF JACOBI POLYNOMIALS IN THE SIMULATION OF QUASI-REVERSIBLE ELECTRODE PROCESSES WITH LINEAR POTENTIAL SCAN AND DIFFUSIONAL CONTROL IN ONE DIMENSION

Dan DRAGU* and Mihai BUDA

Department of Applied Physical Chemistry and Electrochemistry, Faculty of Applied Chemistry and Materials Science, "POLITEHNICA" University of Bucharest, Calea Grivitei 132, 010737, Bucharest, ROMANIA

Received March 8, 2008

This paper emphasizes some practical aspects regarding orthogonal collocation techniques as used for model of a cyclic voltammetry experiment for a quasi-reversible electrode process with one-dimensional diffusion control. The influence of model's parameters is underlined and their influence over simulation accuracy is discussed.
The main model's parameters taken into account are the number of collocation points and their distribution for various types of Jacobi orthogonal polynomials. The influence of the number of potential/time discretization points and the length of diffusion limit layer is also discussed.
The differences between explicit and implicit discretization and the importance of the method used for computing the orthogonal constants are underlined.

INTRODUCTION

A system of differential equations with boundary conditions can be solved numerically through a wide range of techniques. It has long been known that one of the most efficient methods is the orthogonal collocation, provided the model's functions can be reasonably well approximated by a polynomial.

The advantages of this technique were underlined by Villadsen and Stewart,[1] while Michaelsen and Villadsen[2] described a simplified procedure for computing the constants associated with the collocation points. A particular case was further adapted to electrochemical experiments by Whiting and Carr,[3] and developed later by Speiser.[4–6]

Both Whiting and Carr and Speiser use in their simulations Legendre polynomials, a particular case of Jacobi polynomials. A very good description of orthogonal collocation methods used in electrochemical experiments can be found in Britz.[7]

THEORETICAL ASPECTS

The orthogonal collocation method for solving a differential equation is based on approximating a given function with a polynomial. This is were both the strength and the weakness of the method lie: for well-behaved functions, (*i.e.*, functions that can be reasonably well approximated by a polynomial), orthogonal collocation will give accurate results even with only a few discretization points, whereas for ill-behaved functions (*e.g.* exponentially varying functions, which are not well described by a polynomial), the method will generally fail even with a large number of discretization points. The chosen polynomial will give the exact value of the function at the collocation nodes; care must be taken that the polynomial's roots, which give the collocation nodes, are to be found in the interval of interest, or else a change of variable may be required (such as for the shifted Legendre polynomials).

For a given function $f:[a;b]\to R$, with the boundary conditions $f'(a)=y_1$ and $f'(b)=y_2$ one can find a polynomial approximation as follows:

* Corresponding author: dandragu@yahoo.com

$$f(x) \approx P(x) = \sum_{j=0}^{n+1} a_j \cdot x^j;\ f(x)\Big|_{x_i} = P(x_i) = \sum_{j=0}^{n+1} a_j \cdot x_i^{\ j};$$

$$\frac{\partial f(x)}{\partial x} \approx P'(x) = \sum_{j=0}^{n+1} j \cdot a_j \cdot x^{j-1};\ \left.\frac{\partial f(x)}{\partial x}\right|_{x_i} = P'(x_i) = \sum_{j=0}^{n+1} j \cdot a_j \cdot x_i^{\ j-1};$$

$$\frac{\partial^2 f(x)}{\partial x^2} \approx P''(x) = \sum_{j=0}^{n+1} j \cdot (j-1) \cdot a_j \cdot x^{j-2};\ \left.\frac{\partial^2 f(x)}{\partial x^2}\right|_{x_i} = P''(x_i) = \sum_{j=0}^{n+1} j \cdot (j-1) \cdot a_j \cdot x_i^{\ j-2};$$

where x_i are the collocation nodes, $i=0..n+1$ ($x_0 = a$ and $x_{n+1} = b$) . The degree of the polynomial $P(x)$ is thus $n+2$ and can be written as $P(x)=(a-x)(b-x)P_n(x)$, where the polynomial $P_n(x)$ has the degree n and n real and distinct roots over the interval $(a;b)$.

The above equations can be written as $F = Q \cdot v$; $\frac{dF}{dX} = R \cdot v$; $\frac{d^2F}{dX^2} = S \cdot v$, where F is the vector of the function values at each collocation node, v is the vector of containing the a_j coefficients, and Q is a Vandermonde matrix having as elements the roots of the orthogonal polynomial P_n.

Equation $F = Q \cdot v$ is equivalent with $Q^{-1} \cdot F = Q^{-1} \cdot Q \cdot v = v$.

We can write:

$$\frac{dF}{dX} = R \cdot Q^{-1} \cdot F = A \cdot F \qquad (1)$$

and

$$\frac{d^2F}{dX^2} = S \cdot Q^{-1} \cdot F = B \cdot F \qquad (2)$$

Thus, it is enough to calculate the collocation points x_i only, without calculation of a_j coefficients. As P_n is an orthogonal polynomial it will have exactly n real distinct roots in the orthogonality interval.

Michelsen and Villadsen[2] proposed another approach for $P_n(x)$ based on Lagrange interpolation formula. Thus, $P_n(x) = \prod_{i=1}^{n}(x - x_i)$, and the initial $n+2$ degree polynomial $P(x)$ becomes $P(x) = \prod_{i=0}^{n+1}(x - x_i)$. The target function f can be approximated as:

$$f(x) \approx \sum_{j=0}^{n+1} \frac{P(x)}{(x - x_j) \cdot P'(x_j)} \cdot f(x_j) .$$ The equations (1) and (2) are still valid, but their coefficients are calculated through an explicit formula and not through inverse matrix Q^{-1}:

For i=j : $a_{i,i} = \frac{1}{2} \cdot \frac{P''(x_i)}{P'(x_i)}$ $b_{i,i} = \frac{1}{3} \cdot \frac{P'''(x_i)}{P'(x_i)}$

and

For i <> j: $a_{i,j} = \frac{1}{x_i - x_j} \cdot \frac{P'(x_i)}{P'(x_j)}$

$$b_{i,j} = \frac{1}{x_i - x_j} \cdot \left(\frac{P''(x_i)}{P'(x_j)} - 2 \cdot a_{i,j} \right)$$

A recurrence formula can thus be found for polynomials $P(x)$:

$$P_i(x) = (x - x_{i-1}) \cdot P_{i-1}(x);\ P_0(x) = 1;\ i=1..n+1;$$

In a similar way, a recurrence formula can be found for derivatives also for $i=2..n+1$ (the derivatives must be equal to zero at $x=x_{i-1}$):

$$P_i'(x) = (x - x_{i-1}) \cdot P_{i-1}'(x)$$
$$P_i''(x) = (x - x_{i-1}) \cdot P_{i-1}''(x) + 2P_{i-1}'(x)$$
$$P_i'''(x) = (x - x_{i-1}) \cdot P_{i-1}'''(x) + 3P_{i-1}''(x) \text{ with } P_1'(x) = 1;\ P_1''(x) = 0;\ P_1'''(x) = 0 .$$

One of the main advantages of this method is the high stability of solution when computing the coefficients for large n values.

In any approach, one has to compute the roots of an n degree orthogonal polynomial. The roots are usually computed using a Newton algorithm. The initial guess of x_i is chosen between the two roots of the immediately inferior degree polynomial. A simplified algorithm, which doesn't require the computation of the roots for all polynomials with degree smaller than n , can be found in. [9]

The system of differential equations to be solved numerically using orthogonal collocation is:

$$\begin{cases} \dfrac{\partial c_O(x,t)}{\partial t} = D_O \cdot \dfrac{\partial^2 c_O(x,t)}{\partial x^2}; \quad J_O(x,t) = -D_O \cdot \dfrac{\partial c_O(x,t)}{\partial x} \\ \dfrac{\partial c_R(x,t)}{\partial t} = D_R \cdot \dfrac{\partial^2 c_R(x,t)}{\partial x^2}; \quad J_R(x,t) = -D_R \cdot \dfrac{\partial c_R(x,t)}{\partial x}; \\ J_O(0,t) = -J_R(0,t); \\ J_O(0,t) = k_1 \cdot c_O(0,t) - k_2 \cdot c_R(0,t); \\ k_1 = k^0 \cdot \exp\left(-\alpha \cdot \dfrac{n_e F}{RT} \cdot (E(t) - E^{0'}) \right); \\ k_2 = k^0 \cdot \exp\left((1-\alpha) \cdot \dfrac{n_e F}{RT} \cdot (E(t) - E^{0'}) \right); \end{cases}$$

which accounts for the electrode reaction for a planar electrode, in a diffusional controlled process:

$$O + n_e\ e^- \rightleftharpoons R$$

Once the above system is solved, the electrical current associated to the electrode process with can be calculated as $I(t) = n_e F A J_O(0,t)$.

$E(t) = \begin{cases} E_i - v \cdot t,\ t \le t_s,\ E(t_s) = E_s \\ E_s + v \cdot t,\ t > t_s \end{cases}$ is the applied potential function and the target functions are $c_O(x,t)$ and $c_R(x,t)$. To the first boundary condition already described (for x=0, *i.e.* the electrode), a second one is added, corresponding to the semi-infinite diffusion condition, $x \to \infty$: $c_O(\infty,t) = c_O^*$, $c_R(\infty,t) = c_R^*$, and two initial conditions, $c_O(x,t_0) = c_O^*, x \in [0,\infty)$, $c_R(x,t_0) = c_R^*, x \in [0,\infty)$. For the significances of the terms see the Annex 1.

The second boundary conditions is given for $x \to \infty$. In fact, following a redox reaction at the electrode, the concentrations of the species involved will alter significantly only in the limit imposed by the thickness of diffusion layer, x_L. Beyond this limit, the concentrations can be considered to remain constant. Therefore, the interval for the target functions $c_O(x,t)$ and $c_R(x,t)$ can be redefined as $[0,L]$, where $L=x_L$, or further on, [0,1] if one uses x_L as a parameter to render the differential equations dimensionless. Thus, in order to be able to use orthogonal polynomials with roots in a different interval, a change of variable is needed to shift their zeroes in the [0,1] interval.

The general Jacobi polynomials are defined as:

$$g(x) = \int_{-1}^{1} (1-x)^{\alpha} \cdot (1+x)^{\beta} \cdot P_n(x) \cdot P_m(x) dx = 0$$

.

and have roots in the [-1,1] interval. Mapping the polynomials to the [0,1] interval requires the change in variable X=0.5(x+1), so as the "shifted" Jacobi polynomials become:

$$g(X) = \int_0^1 (1-X)^{\alpha} \cdot X^{\beta} \cdot P_n(X) \cdot P_m(X) dX = 0\,.$$

The coefficients of the Jacobi polynomial are further normalized in order to transform the leading coefficient $a_0 x^0$ equal with $(-1)^n$. The recursive calculation formulas for $P_n(x)$ and $P'_n(x)$ become:[2]

$$P_n(x) = (c_n - x) \cdot P_{n-1}(x) - d_n \cdot P_{n-2} \text{ and } P'_n(x) = (c_n - x) \cdot P'_{n-1}(x) - P_{n-1}(x) - d_n \cdot P''_{n-1}(x)\,,$$

$$c_1 = \frac{\beta+1}{\alpha+\beta+2},\ c_j = \frac{1}{2} \cdot \left(1 - \frac{(\alpha+\beta)(\alpha-\beta)}{(\alpha+\beta+2j)(\alpha+\beta+2j-2)} \right), j=2..n\,;$$

$$d_1 = 0\,,\ d_2 = \frac{(\alpha+1)(\beta+1)}{(\alpha+\beta+3)(\alpha+\beta+2)^2}\,,$$

$$d_j = \frac{(j-1)(j+\alpha-1)(j+\beta-1)(j+\alpha+\beta-1)}{(2j+\alpha+\beta-1)(2j+\alpha+\beta-2)^2(2j+\alpha+\beta-3)}, j=3..n\,.$$

$$P_{-1}(x) = 0,\ P_0(x) = 1,\ P'_0(x) = 0,\ P'_1(x) = -1\,.$$

The target functions $c_O(x,t)$ and $c_R(x,t)$, will be defined thus in the dimensionless interval [0,1]. Recommended value[10] for maximum distance where concentration changes still took place is $L = 6\sqrt{D \cdot T_m}$, where T_m is necessary time for a full cycle of potential scanning between E_i, a switch value E_s, and again to E_i.

In order to eliminate time dependence for a simplified equation system, we choose to discretize potential values through N_P equal discretization points, where N_P has a conveniently chosen value (see below).

$$\begin{cases} \dfrac{\Delta c_O(X)}{\Delta T} = \dfrac{D_O}{L^2} \cdot \dfrac{\partial^2 c_O(X)}{\partial X^2}; \quad J_O(x) = -\dfrac{D_O}{L} \cdot \dfrac{\partial c_O(X)}{\partial X} \\ \dfrac{\Delta c_R(X)}{\Delta T} = \dfrac{D_R}{L^2} \cdot \dfrac{\partial^2 c_R(X)}{\partial X^2}; \quad J_R(x) = -\dfrac{D_R}{L} \cdot \dfrac{\partial c_R(X)}{\partial X}; \\ J_O(0) = -J_R(0); \\ J_O(0) = k_1 \cdot c_O(0) - k_2 \cdot c_R(0); \\ k_1 = k^0 \cdot \exp\left(-\alpha \cdot \dfrac{n_e F}{RT} \cdot E\right); \\ k_2 = k^0 \cdot \exp\left((1-\alpha) \cdot \dfrac{n_e F}{RT} \cdot E\right); \end{cases}$$

Where $\Delta c = c' - c$, c = concentration at the moment t, c' = concentration at the moment $t + \Delta T$, $\Delta T = T_m / N_P$.

Applying collocation method, the equations

$$\frac{\Delta c_{O,R}(X)}{\Delta T} = \frac{D_{O,R}}{L^2} \cdot \frac{\partial^2 c_{O,R}(X)}{\partial X^2}$$

become $\dfrac{\Delta c_{O,R}(X)}{\Delta T} = \dfrac{D_{O,R}}{L^2} \cdot B \cdot C_{O,R}$.

The form for an explicit approach is:

$$c'_{O,R}(X_i) - c_{O,R}(X_i) = \frac{\Delta T \cdot D_{O,R}}{L^2} \cdot \left(b_{0,i} \cdot c_{O,R}(0) + b_{n+1,i} \cdot c_{O,R}(1) + \sum_{j=1}^{n} b_{j,i} \cdot c_{O,R}(X_j) \right),$$

while for the implicit one:

$$c'_{O,R}(X_i) - c_{O,R}(X_i) = \frac{\Delta T \cdot D_{O,R}}{L^2} \cdot \left(b_{0,i} \cdot c'_{O,R}(0) + b_{n+1,i} \cdot c'_{O,R}(1) + \sum_{j=1}^{n} b_{j,i} \cdot c'_{O,R}(X_j) \right)$$

A further important point to be discussed is the results validation. We chose as reference the dimensionless current function $\chi(\sigma t)$ proposed by Nicholson and Shain.[8] This values are calculated for a reversible electrode reaction. Therefore we chose k^0 = 1, enough to accomplish reversible criteria of Bard,[10] Λ>10, $\Lambda = \dfrac{k^0}{\sqrt{D \cdot v \cdot n_e F / RT}}$.

The relation between $\chi(\sigma t)$ and I is $\sqrt{\pi} \cdot \chi(\sigma t) = I(t) \cdot \dfrac{1}{n_e \cdot F \cdot A \cdot c_O^* \cdot \sqrt{D_O \cdot \sigma}}$. The values for $\sqrt{\pi} \cdot \chi(\sigma t)$ are tabulated in the literature. Other simulation data are: start potential E_i = 0,5 V; switch potential E_s = 0,0V; surface area, A = 0,01 cm^2; scan rate v= 0.1 V/s; temperature, T = 298 K; formal potential, $E^{0\prime}$ = 0,025V; transfer coefficient, α=0,5; initial concentration of the oxidized species c_O = 1 mM; initial concentration of the reduced species, c_R = 0 mM;diffusion coefficients of the species $D_O = D_R$ = 1.0×10^{-5} cm^2/s.

RESULTS AND DISCUSSION

We shall discuss first the solutions obtained using particular forms of Jacobi polynomials (Legendre, Chebyshev I, Chebyshev II, Gegenbauer). The results are shown in Figures 1-5.

The particular case of Legendre polynomials will be discussed more extensively, since these polynomials are most often used in literature and give the best results.

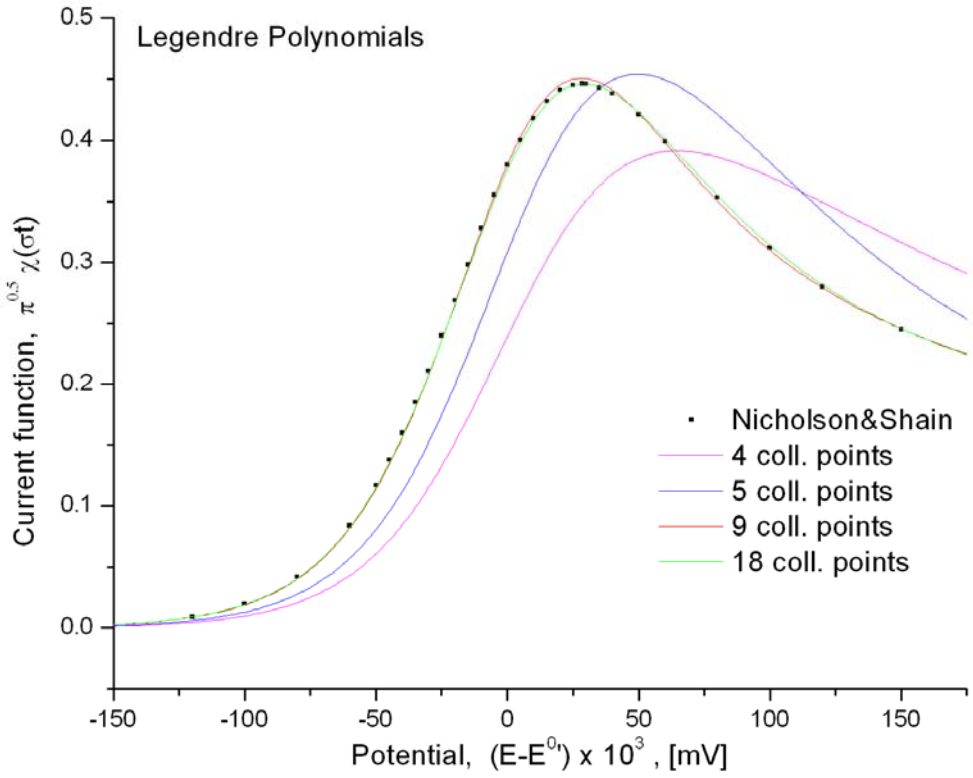

Fig. 1

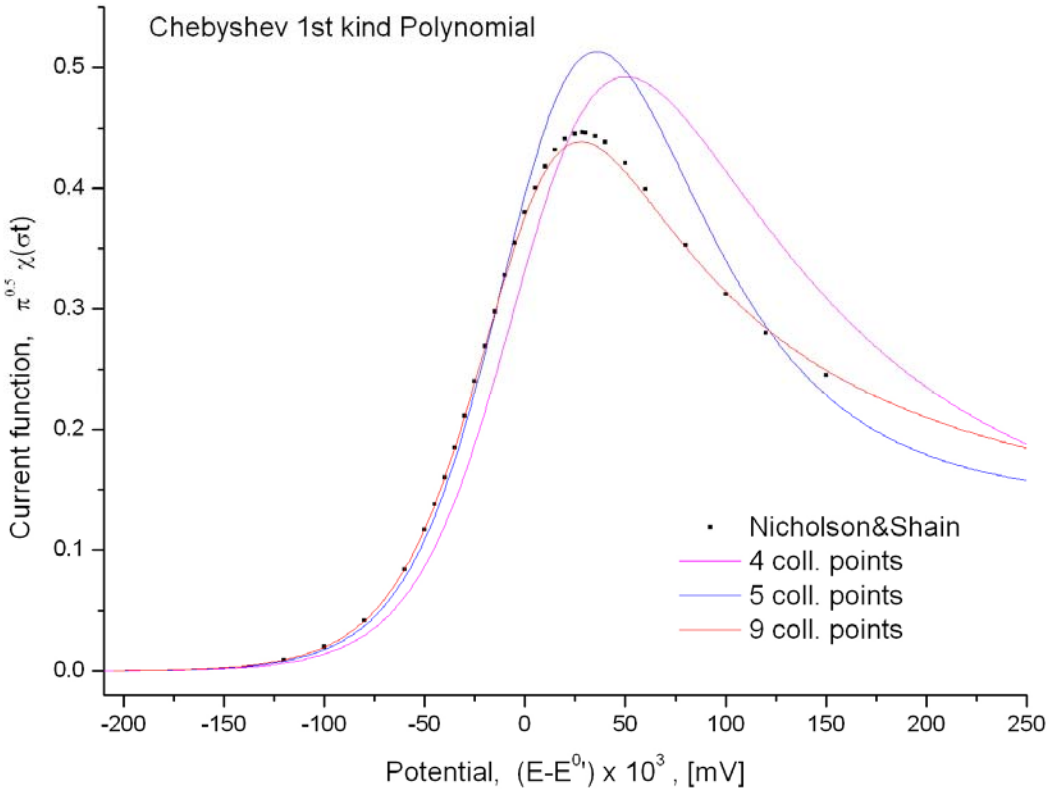

Fig. 2

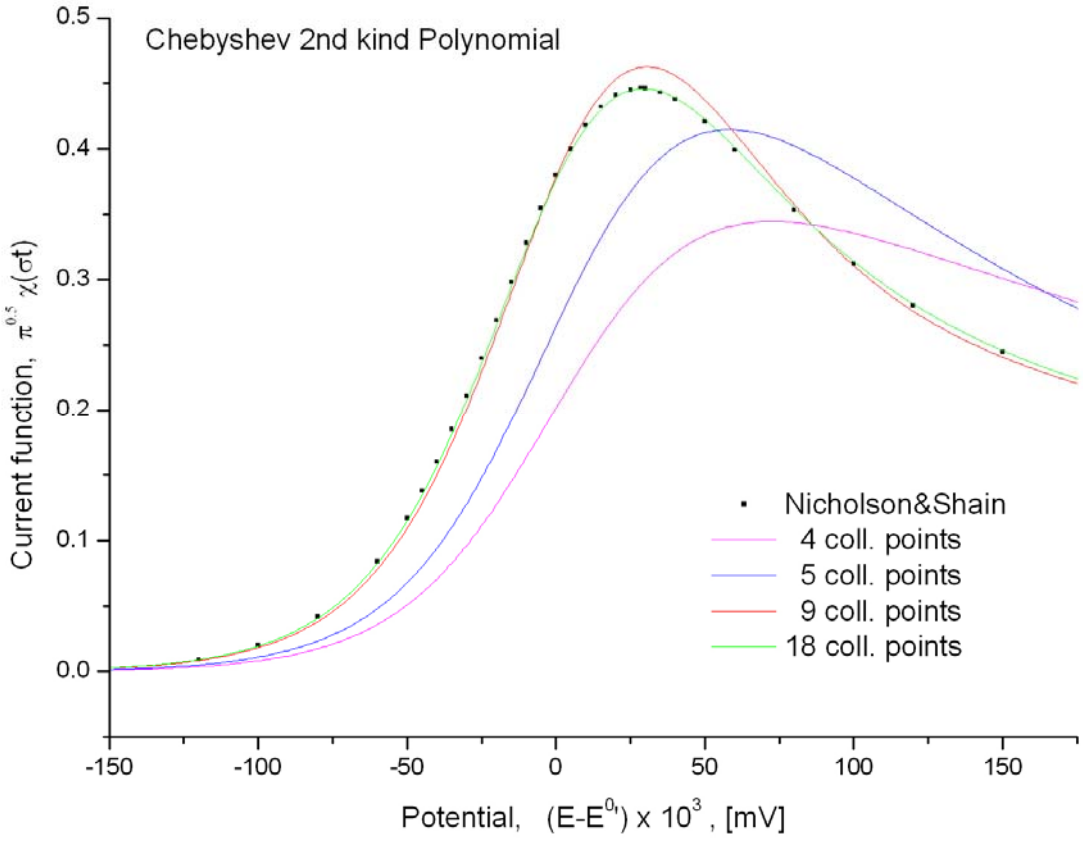
Chebyshev 2nd kind Polynomial
Current function, $\pi^{0.5}\chi(\sigma t)$
Potential, $(E-E^{0'}) \times 10^3$, [mV]
Nicholson&Shain
4 coll. points
5 coll. points
9 coll. points
18 coll. points

Fig. 3

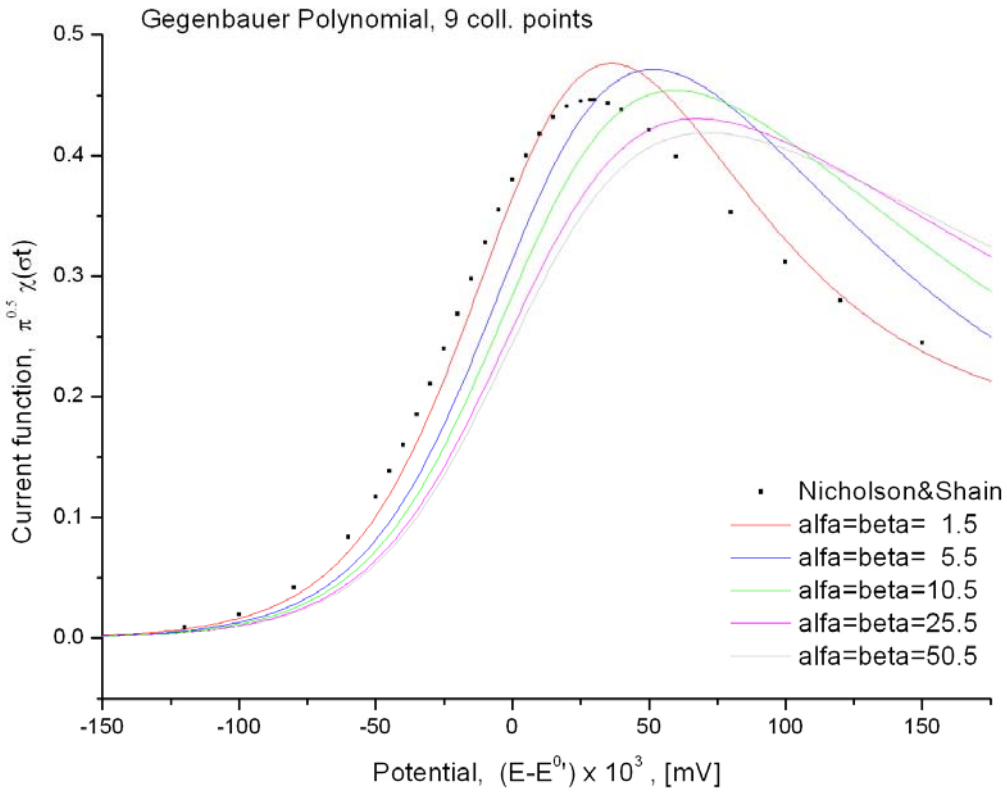
Gegenbauer Polynomial, 9 coll. points
Current function, $\pi^{0.5}\chi(\sigma t)$
Potential, $(E-E^{0'}) \times 10^3$, [mV]
Nicholson&Shain
alfa=beta= 1.5
alfa=beta= 5.5
alfa=beta=10.5
alfa=beta=25.5
alfa=beta=50.5

Fig. 4

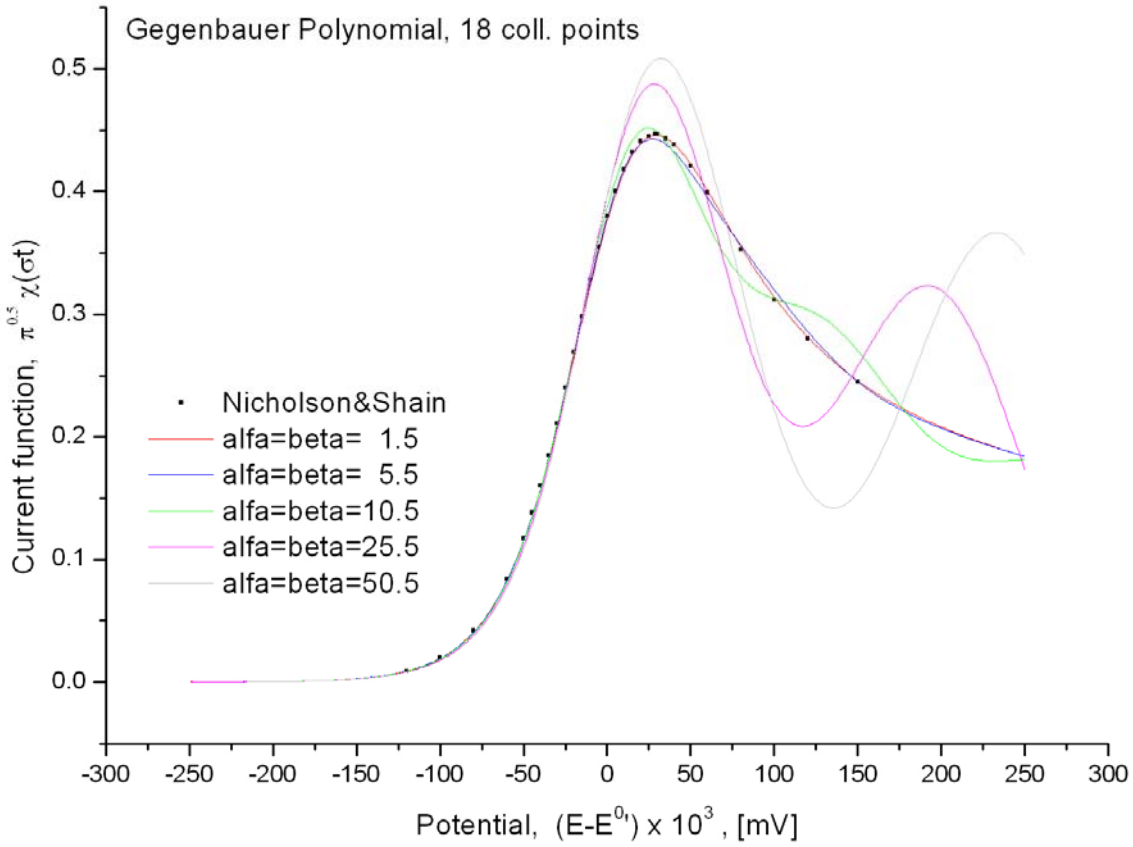

Fig. 5

Legendre polynomials will give very good results even when using just 9 collocation nodes. For Chebyshev polynomials, up to 18 collocation nodes are required. However, the solution tends to become unstable for Chebyshev polynomials of 1st kind. Increasing the number of collocation nodes doesn't lead to improve performances of Gegenbauer polynomials with large values of α and β.

The main reason for these results lie in the distribution of the collocation nodes. When the collocation nodes are concentrated closer to x=0, the accuracy of the solution is improved. This is a direct consequence of the fact that the concentrations change mostly close to x=0. For Gegenbauer polynomials, when $\alpha = \beta$, the nodes are evenly distributed around 1/2; increasing the values of α and β, the nodes tend to be concentrated around 1/2 (Figure 6). If only the value for α is increased, the nodes are concentrating closer to x=0, while an increase of β concentrates the nodes towards x = 1 (Figure 7). 5 collocation points may still provide reasonable accuracy, as long as the nodes are concentrated at x=0 (Figure 8), even if the errors increase slightly for longer times (the right part of potentials domain): this is to be expected, since for longer experimental times, the concentration profile will start to change significantly further away from x = 0.

Under certain circumstances, the solution is prone to oscillations (Figure 9). These oscillations are mostly eliminated with increasing of the value for N_P. In the absence of the oscillations, small errors are obtained for a relative small value of N_P (Figure 10), and a slightly increased value for N_P over a reasonable limit, doesn't affect considerable the accuracy of the solution (Table 1). The oscillations appear because increasing values for α and β on one hand, and increasing number of collocation points on the other. Another important factor generating oscillations is the method used for calculation of the coefficients for matrixes A and B. From this point of view, the recursive method is better when large number of collocation points are used (Table 2).

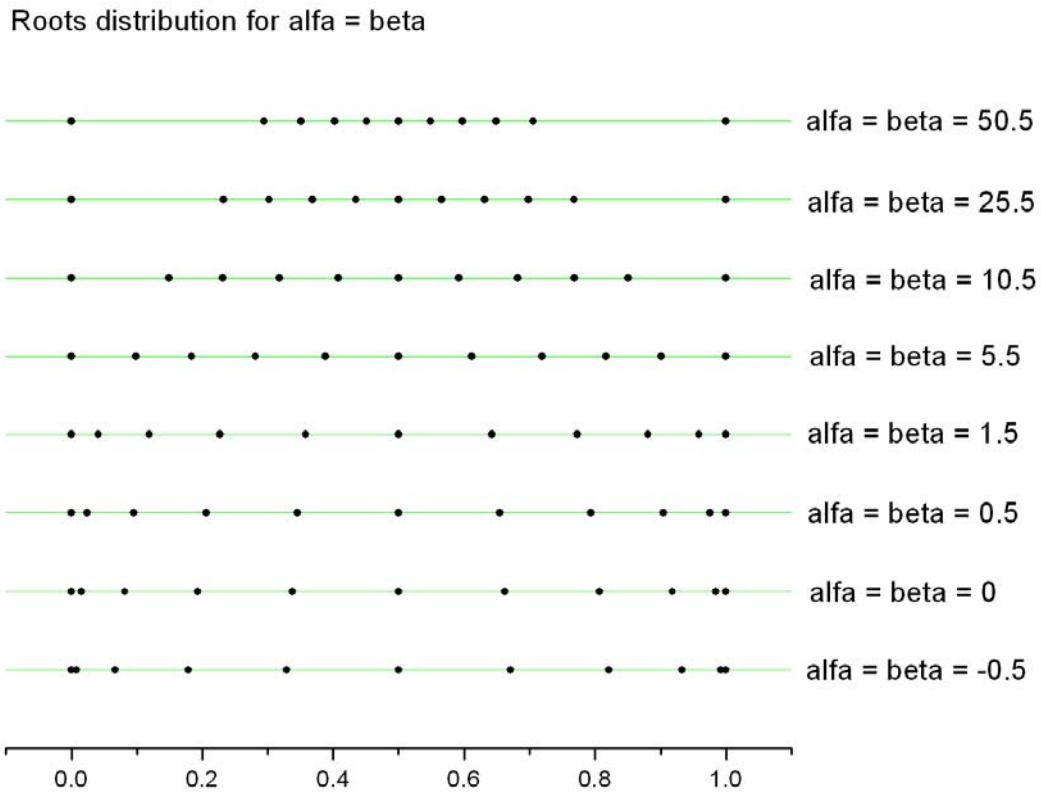
Roots distribution for alfa = beta
alfa = beta = 50.5
alfa = beta = 25.5
alfa = beta = 10.5
alfa = beta = 5.5
alfa = beta = 1.5
alfa = beta = 0.5
alfa = beta = 0
alfa = beta = -0.5
0.0
0.2
0.4
0.6
0.8
1.0

Fig. 6

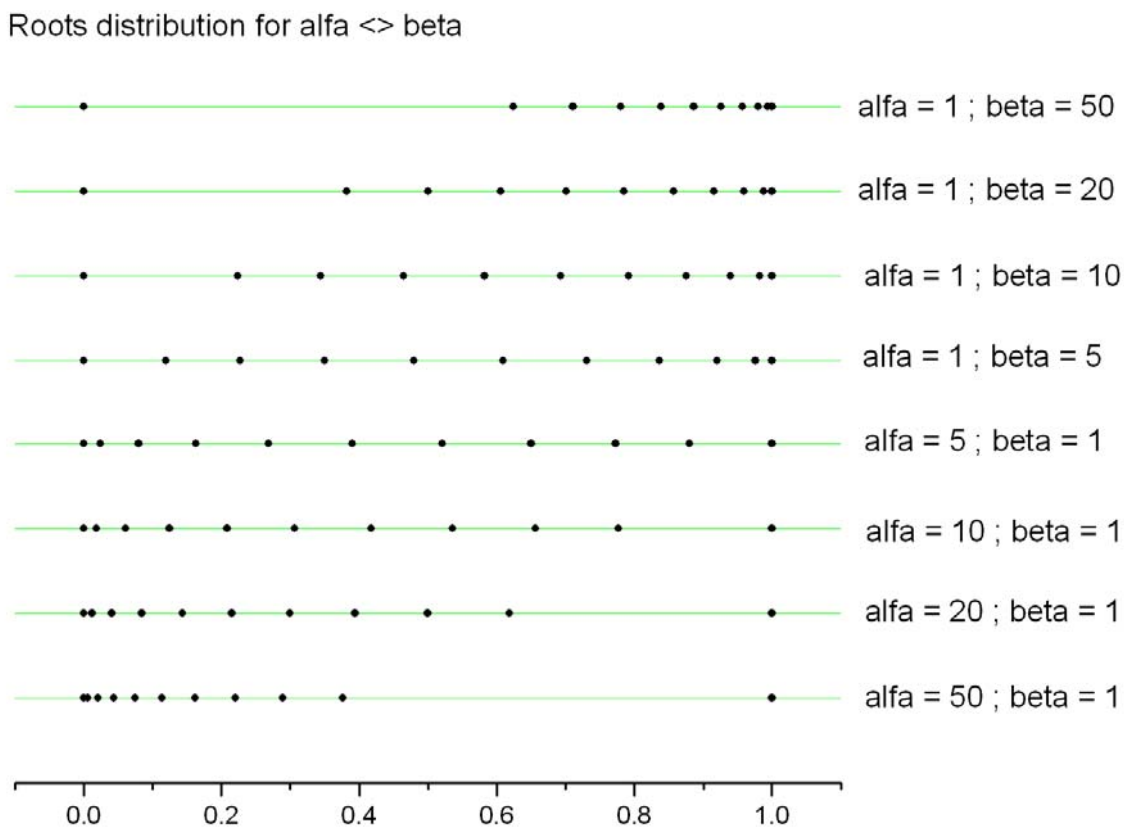
Roots distribution for alfa <> beta
alfa = 1 ; beta = 50
alfa = 1 ; beta = 20
alfa = 1 ; beta = 10
alfa = 1 ; beta = 5
alfa = 5 ; beta = 1
alfa = 10 ; beta = 1
alfa = 20 ; beta = 1
alfa = 50 ; beta = 1
0.0
0.2
0.4
0.6
0.8
1.0

Fig. 7

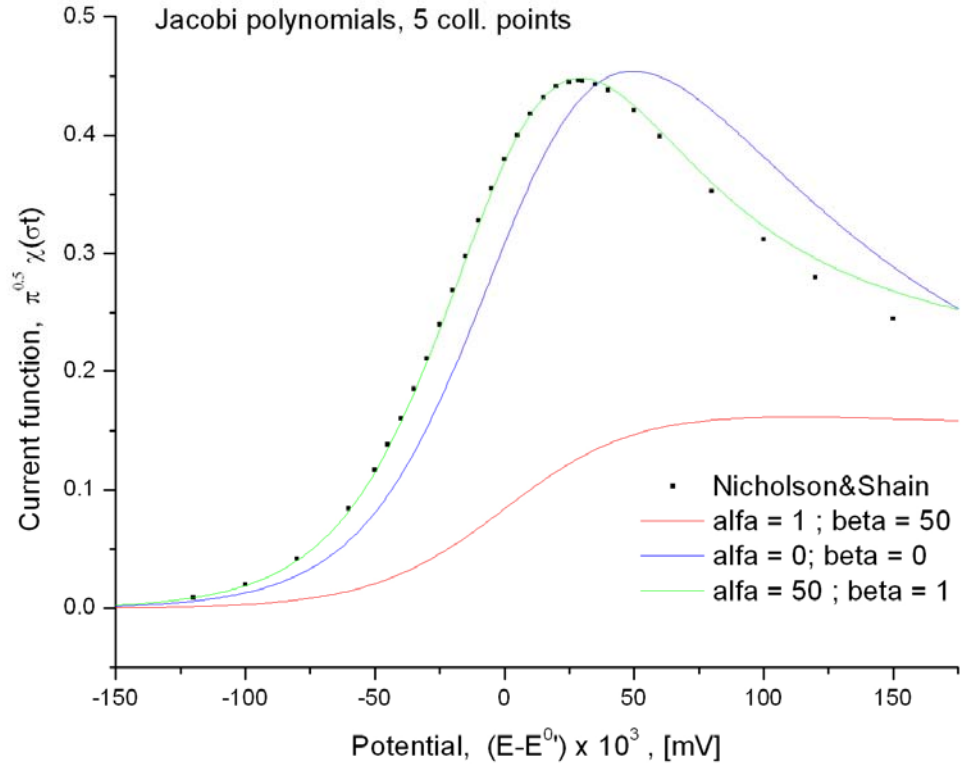
Jacobi polynomials, 5 coll. points
Current function, $\pi^{0.5}\chi(\sigma t)$
Potential, $(E-E^{0\prime}) \times 10^3$, [mV]
Nicholson&Shain
alfa = 1 ; beta = 50
alfa = 0; beta = 0
alfa = 50 ; beta = 1
0.5
0.4
0.3
0.2
0.1
0.0
-150
-100
-50
0
50
100
150

Fig. 8

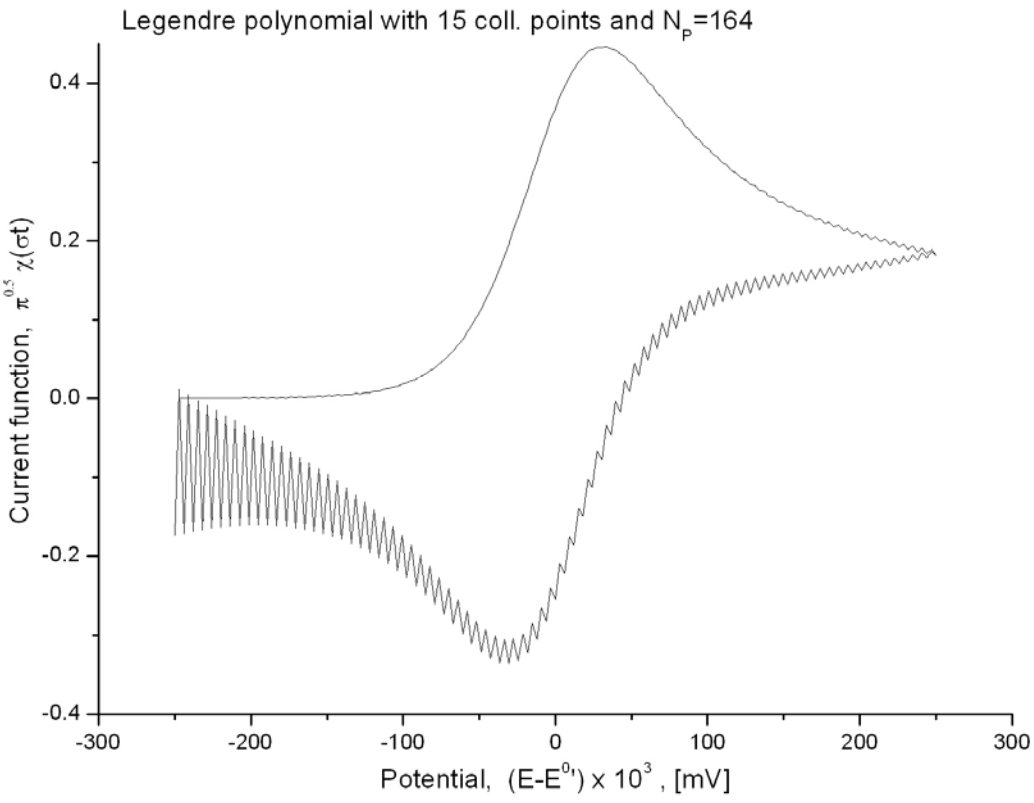
Legendre polynomial with 15 coll. points and N_P=164
Current function, $\pi^{0.5}\chi(\sigma t)$
Potential, $(E-E^{0\prime}) \times 10^3$, [mV]
0.4
0.2
0.0
-0.2
-0.4
-300
-200
-100
0
100
200
300

Fig. 9

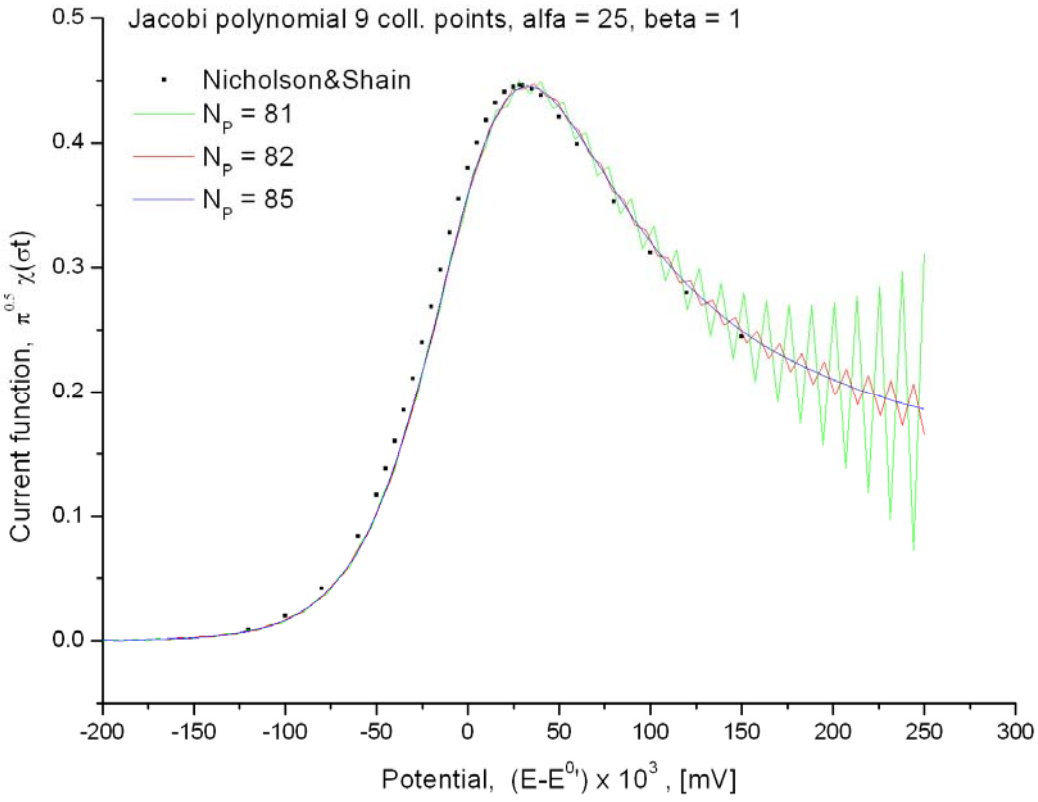

Fig. 10

Table 1

Comparison between reference values calculated by Shain&Nicholson and the values calculated using different types of orthogonal collocation methods. In order to emphasize the small differences between reference and new values we substitute ±1 and ±2 with ±* and ±**.

		Np=1000		**Np=500**		**Np=100**		**explicit**		**implicit**	
$E-E_0$	Shain &							Np=500		Np=500	
	Nicholson	n = 9		n = 9		n = 9		n = 9		n = 9	
		α = 25		α = 25		α = 25		α = 0		α = 0	
		β = 1		β = 1		β = 1		β = 0		β = 0	
	(x 10^3)	(x 10^3)		(x 10^3)		(x 10^3)		(x 10^3)		(x 10^3)	
-120	9	–		–		–*		–		–	
-100	20	–*		–*			-3	–*		–*	
-80	42	–*		–**			-6	–**		–**	
-60	84	–*		–**			-10		-3		-3
-50	117	–*		–**			-13		-3		-4
-45	138	–**			-3		-15		-4		-5
-40	160	–*			-3		-17		-4		-5
-35	185	–**			-4		-19		-4		-6
-30	211	–*			-3		-19		-4		-5
-25	240	–**			-4		-21		-4		-6
-20	269	–**			-4		-21		-4		-5
-15	298	–*			-3		-21	–**			-4
-10	328		-3		-4		-22		-3		-4
-5	355	–**			-4		-20	–*			-4
0	380	–**			-4		-19	–			-3
5	400	–*		–**			-15	+**		–*	
10	418	–*		–**			-13		+3	–	
15	432	–*		–**			-10		+3	–	
20	441	–*		–**			-7		+4	+*	
25	445	–		–			-3		+5	+**	
28.5	**446.3**		**-0.4**		**-0.4**		**–2.3**		**+4.3**		**+1.8**
30	446	–		–		–*			+4	+*	
35	443	–		+*		+**			+4	+**	

Table 1 (continued)

40	438	–	–	+4		+3	+*	
50	421	–	+*	+6	+*		–	
60	399	+*	+**	+8	–		–*	
80	353	+*	+*	+8		-3		-3
100	312	+*	+*	+7	–**		–*	
120	280	+*	+*	+6	–*		–	
150	245	–	+*	+4	–		+**	

Table 2

Maximum number of collocation nodes as the result of the method of calculation of the matrix *B* coefficients (recursive or through Q^{-1}):

	N_p=500	N_p=1000	N_p=5000	N_p=10000	N_p=50000
recursive,α=25,β=1	18	23	30	30	30
inverse,α=25,β=1	18	22	22	22	22
recursive,α=0,β=0	19	23	35	42	50
inverse,α=0,β=0	19	22	22	22	22

As for the thickness of the Nernst layer, L, large variations between $L = 1.5\sqrt{D \cdot T_m}$ and $L = 21\sqrt{D \cdot T_m}$ have not significant influence over the simulations. For a value of $L = 0.6\sqrt{D \cdot T_m}$ we record a slightly increase of errors in the right side of the potential range, and only an increase of $L = 40\sqrt{D \cdot T_m}$ generates significant errors (Figure 11). Similar results are obtained when Legendre polynomials are used. A variation of the scan rate between 10 and 1000 mV is equivalent with a variation of L between $L = 1.8\sqrt{D \cdot T'_m}$ and $L = 19\sqrt{D \cdot T'_m}$, T'_m is experimental time for a scan rate of 100 mV/s.

When small values of L are used, the solution is strongly oscillating. Therefore, for $L = 0.6\sqrt{D \cdot T_m}$, a number of N_P=50000 was chosen for compensation, and for $L = 1.5\sqrt{D \cdot T_m}$, N_P=25000. The length of the diffusion layer has also influence over the maximum number of collocation points for a fix value of N_P (Table 3).

Table 3

Maximum number of collocation points as the result of the method of calculation of the matrix *B* coefficients (recursive or through Q^{-1}) for different values of L:

	A	$L = x \cdot \sqrt{D \cdot T_m}$	N_p=500	N_p=1000	N_p=5000	N_p=10000	N_p=50000
recursive, β=1	25	x=3	10	13	25	29	29
inverse, β=1	25	x=3	10	13	16	16	16
recursive, β=1	50	x=3	-	9	17	17	17
inverse, β=1	50	x=3	-	9	13	13	13
recursive, β=1	25	x=6	18	23	30	30	30
inverse, β=1	25	x=6	18	22	22	22	22
recursive, β=1	50	x=6	12	16	17	17	17
inverse, β=1	50	x=6	12	16	17	17	17
recursive, β=1	25	x=9	24	30	30	30	30
inverse, β=1	25	x=9	24	27	27	27	27
recursive, β=1	50	x=9	17	17	17	17	17
inverse, β=1	50	x=9	17	17	17	17	17

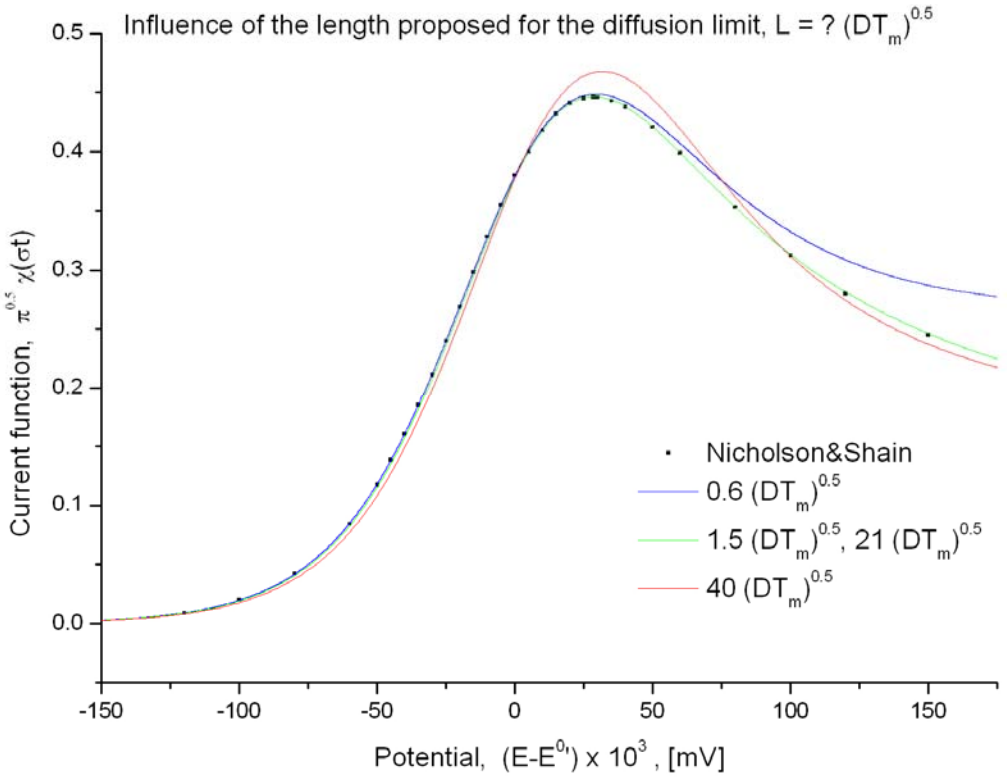

Fig. 11

For a fix set a values for the pair α and β, there is a maximum number of collocation points which allow for a stable solution. The increase of either N_P or diffusion limit L is not affecting this value (Table 3). From the tabulated data in Table 3 we can deduce an optimal set of values associated with collocation method for simulating an cyclic voltammetry experiment. Hence 9 collocation points and N_P=1000 discretization potential points are enough for covering bigger variation of values of the pair α and β and bigger variation of the length of the diffusion layer, L.

Implicit approach of the system brings no differences when α=25 and β=1 comparing with the explicit approach. However, small differences are recorded when Legendre polynomials with small number of collocation points are used (Table 1).

The simulation time for collocation method rarely exceed 1 second. For an Jacobi polynomial with α=25, β=1 N_P=25000 and 18 collocation points, the computation time on a Intel Core Duo processor with 2200 MHz is only 0.823 seconds. At least from this point of view, collocation methods are very efficient.

The software used for simulation was built in C++ and the source code is available on request. An important observation is that all variables used in program were defined in double precision.

CONCLUSIONS

The main advantage when the roots of a general Jacobi orthogonal polynomial is used for simulating a cyclic voltammetry process is given by the possibility to concentrate the collocation points closed to boundary x=0. When a simple electrochemical process is simulated, there are small differences between general Jacobi with $\alpha>\beta$ and widely used Legendre polynomials. For a more complex electrochemical process, it may become important to be able to choose a Jacobi type of polynomial. The oscillations associated with collocation method can be easily eliminated increasing the number of discretization points of potential (or time) domain. A reasonable variation of the diffusion layer L has very little influence over the accuracy of the method.

ABBREVIATIONS

v – potential scan rate;
t – time;
E_i – starting potential;
E_s – switching potential;
D_O – diffusion coefficient for O;
D_R – diffusion coefficient for R;

J_O – flux for O;
J_R – flux for R;
k^0 – standard electrochemical rate constant;
$k^{0'}$ – dimensionless rate constant;
α – transfer coefficient;
F – Faraday constant;
R – ideal gas constant;
n_e – number of electrons transferred;
T – temperature;
$E0'$ – formal potential;
I –electrical current;
L – length of the diffusion limit layer.

REFERENCES

1. J.V.Villadsen and W.E.Stewart, *Chem.Eng.Sci.*, **1967**, *22*, 1483.
2. M.L.Michelsen and J.Villadsen, *Chem.Eng.J.*, **1972**, *4*, 64.
3. L.F.Whiting and P.W.Carr, *J.Electroanal.Chem.*, **1977**, *81*, 1.
4. B.Speiser and A.Rieker, *J.Electroanal.Chem.*, **1979**, *102*, 1.
5. B.Speiser, *J.Electroanal.Chem.*, **1980**, *110*, 69.
6. B.Speiser,S.Pons and A.Rieker, *Electrochim.Acta*, **1982**, *27*, 1171.
7. D. Britz, "Digital Simulation in Electrochemistry", Springer, Berlin, 2005.
8. R.S.Nicholson and I.Shain,*Anal.Chem,* **1964**, *36*, 706.
9. Whilliam H.Press, Brian P.Flannery, Saul A.Teukolsky and William T.Vetterling, "Numerical Recipies in C: The Art of Scientific Computing", Cambridge University Press, 1992.
10. Allen J.Bard and Larry R.Faulkner, "Electrochemical Methods. Fundamentals and Applications",John Wiley&Sons, 2001.

ANNEX 1
Orthogonal polynomials

A sequence of polynomials $P_0, P_1, \ldots, P_n$, are orthogonal one with each other, if $\int_{x_1}^{x_2} W(x) \cdot P_n(x) \cdot P_m(x) dx = 0$ for $m<>n$, where m and n are polynomials degree. The function $W : [x_1, x_2] \to \Re$ is the residual function, and the domain $[x_1 , x_2]$ is the orthogonality interval.

The roots of every orthogonal polynomial lies strictly between the roots of the next degree polynomial in the sequence. Each n degree polynomial can be recursive expressed with the help of the smaller degree next two polynomial in the sequence:

$$b_1 \cdot P_n = (b_2 \cdot x + b_3) \cdot P_{n-1} - b_4 \cdot P_{n-2}.$$

The constants b_1, b_2, b_3 and b_4 are explicitly defined for every particular kind of orthogonal polynomial sequence.

Jacobi polynomials are orthogonal polynomials with $W : [-1,1] \to \Re$, $W(x) = (1-x)^{\alpha} \cdot (1+x)^{\beta}$; $\alpha > -1; \beta > -1$ and recursive coefficients are:

$$b_1 = 2n(n+\alpha+\beta)(2n+\alpha+\beta-2);$$
$$b_2 = (2n+\alpha+\beta-2)(2n+\alpha+\beta-1)(2n+\alpha+\beta);$$
$$b_3 = (2n+\alpha+\beta-1)(\alpha+\beta)(\alpha-\beta);$$
$$b_4 = 2(n+\alpha-1)(n+\beta-1)(2n+\alpha+\beta);$$

More particular Jacobi polynomials can be obtained when:

$\alpha = \beta = 0$ (Legendre polynomials);
$\alpha = \beta = -1/2$ (Chebyshev 1st degree polynomials);
$\alpha = \beta = 1/2$ (Chebyshev 2nd degree polynomials);
$\alpha = \beta = \gamma - 1/2,\ \gamma > -1/2$ (Gegenbauer polynomials).

Revue Roumaine de Chimie, **2008**, *53*(11), 1041–1049

COMPARATIVE STUDY OF DIFFERENT EXTRACTION METHODS FOR EVALUATION OF BIOAVAILABILITY OF TERRESTRIAL SEDIMENT – BOUND METALLIC ELEMENTS

Gabriela Geanina VASILE [a *] and Ion Gh. TĂNASE [b]

[a]National Research and Development Institute for Industrial Ecology ECOIND, 90-92 Road Panduri, 050663, Bucharest, ROUMANIA
[b]University of Bucharest, Faculty of Chemistry, 90-92 Road. Panduri, 050663, Bucharest, ROUMANIA

Received January 22, 2008

The objective of this paper is to compare different extraction methods for evaluation of bioavailability of some metallic elements, such as: Cd, Cu, Ni, Pb and Zn from the lake sediments collected from Roşia Montana aria and also from Săsar river and Racoş stream, situated in Baia Mare aria. The paper contains also information about mobility tests applied to a BCR Certified Reference Material 701, lake sediment. The experimental data proved that NFX31 – 120/1-92 (EDTA and NH_4OAc solution) can be successfully used for estimate the release of metallic elements from terrestrial sediments polluted by mining activities.

INTRODUCTION

Persistent and potentially harmful products have been widely dispersed and concentrated in different spheres of the environment (water, air, soil, sediment, living organism) as the result of human activities. Among the most dangerous of these are toxic metals. Such materials have been accumulated in materials dredged from waterways, harbors, in industrial sites, in landfills, in lake sediment, stream beds and deltas deposited.[1] Some organisms have accumulated high enough level of metals to do harm to themselves or to human that use them as a food source. [1]

Metals are known to concentrate in sediments of natural aquatic systems and this accumulation is postulated to be caused by different mechanisms (ion-exchange, outer and inner-sphere surface complexation, precipitation or co-precipitation) with various geochemical phases such as: organic matter, oxy-hydroxides of iron, aluminum and manganese, phyllosilicate minerals, carbonates and sulfides. [2]

Only a fraction of the metal present in sediment is mobile or bio-available, therefore the determination and monitoring of specific chemical forms of metals in environmental samples are extremely important in order to assess the toxic effects in aquatic systems and geochemical pathways. Among the factors involved in metal availability are the identity of the metal, its chemical form (type of binding, oxidation state), the nature of the suspended material, the type of organism taking the metal and the physical and chemical condition in the water (*e.g.* pH, pE).[1]

The increasing concern to assess the bio-available metal fraction (and thus to estimate the related phyto-toxic effects) and the mobility of trace metals upon disposal of sediment is reflected by a considerable increase in the frequency of analysis over the last 10 years.[3-8] Single and sequential extraction schemes have been designed in order to assess the different retention / release of metals in soil and sediment samples.[9-15]

The objective of this paper is to compare different extraction methods for evaluation of bioavailability of some metallic elements, such as: Cd, Cu, Ni, Pb and Zn from the lake sediments collected from Roşia Montana aria and also from Săsar river and Racoş stream, situated in Baia Mare aria. The sediment samples were collected from two sites, both polluted by mining activities. Also, the paper contains data about mobility tests applied to BCR Certified Reference Material 701, lake sediment.

* Corresponding author: e-mail: ecoind@incdecoind.ro

The extraction methods tested were two standard methods (SR ISO 14870/99[16], NF X 31 – 120/92[17]), used in environmental study for evaluation and monitoring the mobile metallic species from soil, sediment and sludge [12, 18, 19] and a BCR method for mobile metallic elements extracted from lake sediment, proposed by Standard Measurement and Testing Program of the European Community.

The standard methods use buffer solution with neutral pH and extract the mobile metallic elements from the matrix. In 0.11 M acetic acid solution used by the BCR method for lake sediment are released exchangeable metallic elements, water-soluble and weak acid soluble fraction (carbonates).

Assuming that bioavailability is related to solubility, then metal bioavailability decreases in the order: water-soluble > exchangeable > carbonates.

EXPERIMENTAL

The sediment samples were collected from 8 artificial lakes situated in Roşia Montana aria, in the proximal vicinity of a gold and silver mining site. The samples were taken from 1.5 to 10.5 m within the lakes using a Van Veen Bottom Sampler and were stored in plastic recipients. All samples were kept in cooling boxes at 4^0 C during transportation and the analyses were performed immediately after receiving the samples in the laboratory.

From another site polluted by mining activities, were collected 2 sediment samples, one from Racoş stream, situated in the neighbor of a mining sterile dump and the other one from Săsar river, also situated in the aria polluted with metallic elements. In table 1 there are present the symbol of the samples and location for each of them.

Dry sediment (at room temperature) with particle dimension lower than 60 μm was digested with a mixture of aqua regia[18] in a Microwave Laboratory System Ethos Millestone.

The total and fractionated concentration of metals (Cd, Cu, Cr, Pb, Ni, Zn) was determinated by an UNICAM SOLAAR 929 atomic absorption spectrometer. Air/acetylene type flame was used for all the elements, with exception of Cr. For this element was used a protoxide/acetylene flame. All the chemicals used were of analytical reagent grade (Merck quality).

The working procedure for mobile forms of metallic elements was as follows: for methods no. 1 and 2 (table 2): 4 g of dry sediment (particle size < 60 μm) were mixed with 40 mL of buffer solution. The obtained suspension was shaken at 20ºC for two hours with 40 rpm. In the BCR method, 1 g of dry sediment was mixed with 40 mL of 0.11 M CH_3COOH for 16 hours at 20º C and 30 rpm. The sediment was in complete suspension during the extraction procedure. The solution was centrifuged and then analyzed with AAS methods. For each experiment of extraction a blank sample (i.e. a container with no sediment) was prepared through the entire procedure and were used external standard, prepared from reference standard material - Merck quality in the corresponding extraction solution, for calibration curve.

Table 1

The location of the collected sediment samples

Symbol	Description	Location
L 1	Sediment collected from Mare Lake, depth 10.5 m	Roşia Montana
L 2	Sediment collected from Ţapului Lake, depth 2 m	Roşia Montana
L 3	Sediment collected from Corna Lake, depth 3.2 m	Roşia Montana
L 4	Sediment collected from Cartuş Lake, depth 2.1 m	Roşia Montana
L 5	Sediment collected from Brazilor Lake, depth 5.8 m	Roşia Montana
L 6	Sediment collected from Ţarina Lake, depth 3.5 m	Roşia Montana
L 7	Sediment collected from Anghel Lake, depth 6 m	Roşia Montana
L 8	Sediment collected from Găuri Lake, depth 1.5 m	Roşia Montana
R 1	Sediment collected from Săsar River, in the vicinity of a mining site	Baia Mare
R 2	Sediment collected from Racoş Stream, in the vicinity of a mining sterile dump	Baia Mare

Table 2

The extraction methods used for mobile metallic elements

No.	Method	Solution of extraction	Condition
1	SR ISO 14870/99	0.005 M DTPA, 0.1 M TEA, 0.01 M $CaCl_2$, pH = 7.3	Report sediment : solution = 1:10, 2 hour shake at 40 rpm
2	NF X 31 – 120/1-92	0.01 M EDTA, 1 M NH_4OAc, pH = 7.2	Report sediment : solution = 1:10, 2 hour shake at 40 rpm
3	BCR method for lake sediment	0.11 M CH_3COOH, pH = 2.8	Report sediment : solution = 1:40, 16 hour shake at 30 rpm

The sediment dry weight was determined on a separate sub-sample, approximately 1 g, by drying at 105º ± 2º C until constant weight. For each analytical results were applied a correction to "dry matter" (d.m., quantity of metal per g dry sediment).

For the availability comparison tests, each method was applied to the sediment samples (L1 ÷ L8 -lake sediments, R 1 and R 2 – river sediment, BCR CRM 701) using single chemical extraction procedure.

In the study was applied a sequential extraction procedure to BCR CRM 701, lake sediment. In table 3 are present the steps and solutions used in chemical sequential extraction procedure.

Table 3

The steps of the sequential extraction procedure

Step	Solution of extraction	Condition
first	0.005 M DTPA, 0.1 M TEA, 0.01 M $CaCl_2$, pH = 7.3 **or** 0.01 M EDTA, 1 M NH_4OAc, pH = 7	Report sediment : solution = 1:10, 2 hour shake at 40 rpm
second	Distillated water, pH~5	Report sediment : solution = 1:10, 2 hour shake at 40 rpm
third	0.11 M CH_3COOH, pH = 2.8	Report sediment : solution = 1:40, 2 hour shake at 40 rpm

Table 4

The "total concentration" of metallic elements from L1 to L 5 - lake sediments

Element	M.U.	L 1	L 2	L 3	L 4	L 5	Reference values according to Roumanian Order 161/2006
Cd	mg/Kgd.m.	< 0,5	< 0,5	< 0,5	< 0,5	< 0,5	0.8
Cu	mg/Kg d.m	**244±5.2**	**42.1±0.9**	**63.8±1.4**	**131±2.8**	**181±3.9**	40
Cr total	mg/Kg d.m	33.2±1.3	33.2±1.3	15.9±0.6	11.1±0.4	10.8±0.4	100
Ni	mg/Kg d.m	35±1.1	15±0.5	12.1±0.4	**37**±1.2	30.3±0.9	35
Pb	mg/Kg d.m	47.6±2.3	23.4±1.1	25.2±1.2	29.2±1.4	41.2±2.0	85
Zn	mg/Kg d.m	**154**±7	92.5±4.3	106±4.9	**423**±20	**453**±21	150

In order to estimate the values of uncertainty for each concentration of mobile metallic elements, an uncertainty budget was developed. The different uncertainty sources and their influence on the expanded uncertainty are present in the following formula (GUM method):

$$U_{expanded} = k * u_{cs} = k * \sqrt{(u_c^2 + u_v^2 + u_{rep}^2 + 1/u_{mass}^2 + 1/u_{rec}^2)}$$

where:
k = coverage factor, value 2 for 95% level of confidence;
u_{cs} = combined standard uncertainty;
u_c =concentration uncertainty (instrument calibration, flasks, pipettes, reference standard material);
u_v = 50 mL volumetric flask (calibration, temperature);
u_{rep} = repeatability uncertainty (mass, volume, absorbance, extraction recovery);
u_{mass} = weight uncertainty (balance calibration, linearity);
u_{rec} = extraction recovery uncertainty.

RESULTS

The "total concentrations" of metallic elements dissolved in aqua regia (mixture of nitric acid and hydrochloric acid in the report 1:3) were compared with the reference values for the sediment quality according to the Roumanian Order 161/2006[19] (tables 4 and 5). For the lake sediments, only Cu, Zn and Ni (one sample) contents were higher than the reference value. In the river sediments were recorded very high concentration of Cd (in Săsar river), Cu, Pb and Zn. These data collected from Baia Mare aria conduct to conclusion that mining activities has a harmful action to the surrounding environment.

In the figures 1–10 are present the comparative concentration of mobile metallic elements, extracted from the sediments with three different single chemical extraction procedures (see table 2).

In all test experiments, Cr metallic element was not founded in mobile state inside the sediment structure, either lake or river sediment. Ni element was founded in mobile fraction only in four lake sediments, there are: L2, L4, L5 and L8.

In the figures 11-12 there are data about the sequential extraction procedure (table 3) versus single chemical extraction with the BCR method applied to BCR CRM 701 sediment.

In order to compare the values obtained with three single chemical extraction applied to BCR CRM 701- lake sediment with the certified values, in table 6 are present the comparative results.

Table 5

The "total concentration" of metallic elements from L6 to L 8 - lake sediments, R1 and R2 – river sediments

Element	M.U.	L 6	L 7	L 8	R 1	R 2	Reference values according to Roumanian Order 161/2006
Cd	mg/Kgd.m.	< 0,5	< 0,5	< 0,5	**10.8**	**1.2**	0.8
Cu	mg/Kg d.m	**61.4±1.3**	**69.1±1.5**	**48.2±1**	**432±9**	**391±8**	40
Cr total	mg/Kg d.m	25.7±1	13.5±0.5	13.9±0.5	19.1±0.7	28.6±1.1	100
Ni	mg/Kg d.m	18.7±0.6	6.2±0.2	19.8±0.6	< 2	< 2	35
Pb	mg/Kg d.m	35.1±1.7	50.7±2.5	47±2.3	**708±35**	**643±31**	85
Zn	mg/Kg d.m	131±6.5	120±5.6	**217±10**	**1972±92**	**607±28**	150

Table 6

Comparative results from BCR CRM 701 – lake sediment

Element	M.U.	Experimental data			Certified value BCR method
		SR ISO 14870/99	NFX 31-120/92	BCR method	
Cd	mg/Kg d.m.	4.85 ± 0.24	5.16 ± 0.25	6.88 ± 0.34	7.34 ± 0.35
Cu	mg/Kg d.m	100 ± 3.1	145 ± 4.5	43.4 ± 1.5	49.3 ± 1.7
Ni	mg/Kg d.m	6.96 ± 0.30	9.47 ± 0.40	13.7 ± 0.6	15.4 ± 0.9
Pb	mg/Kg d.m	35.7 ± 2.0	55 ± 3	3.46 ± 0.19	3.18 ± 0.21
Zn	mg/Kg d.m	84 ± 4.5	171 ± 9	196 ± 10	205 ± 6

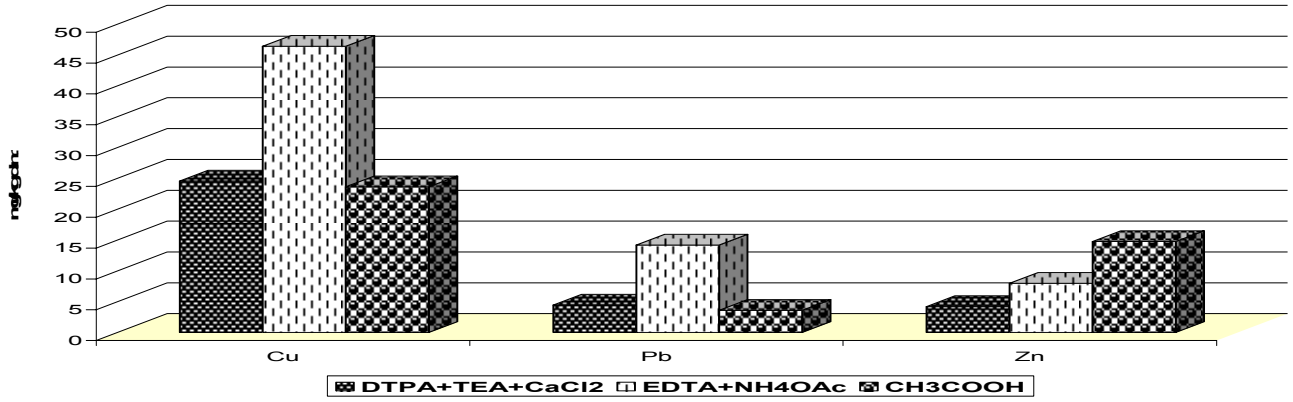

Fig. 1 – The mobile metallic elements from L1 sediment.

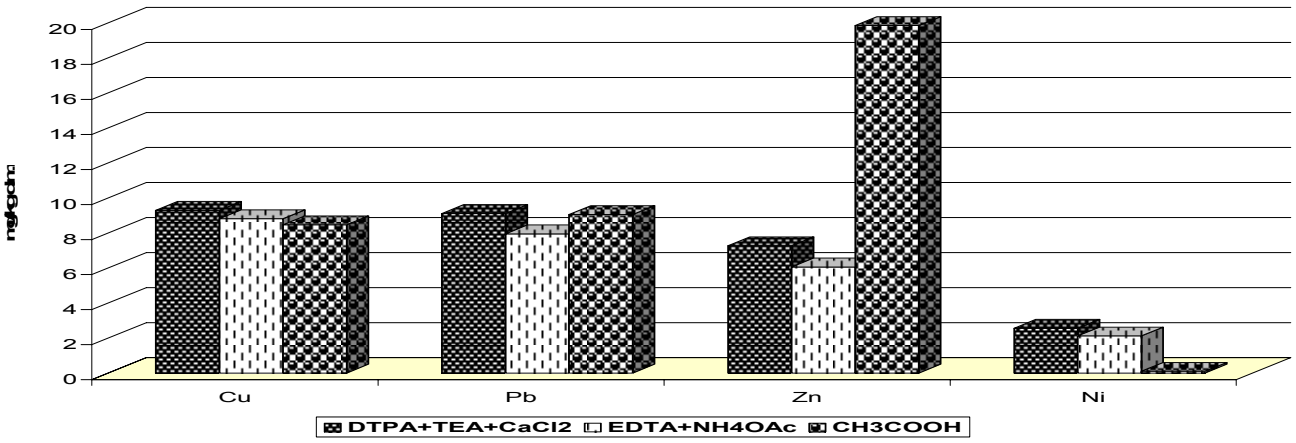

Fig. 2 – The mobile metallic elements from L2 sediment.

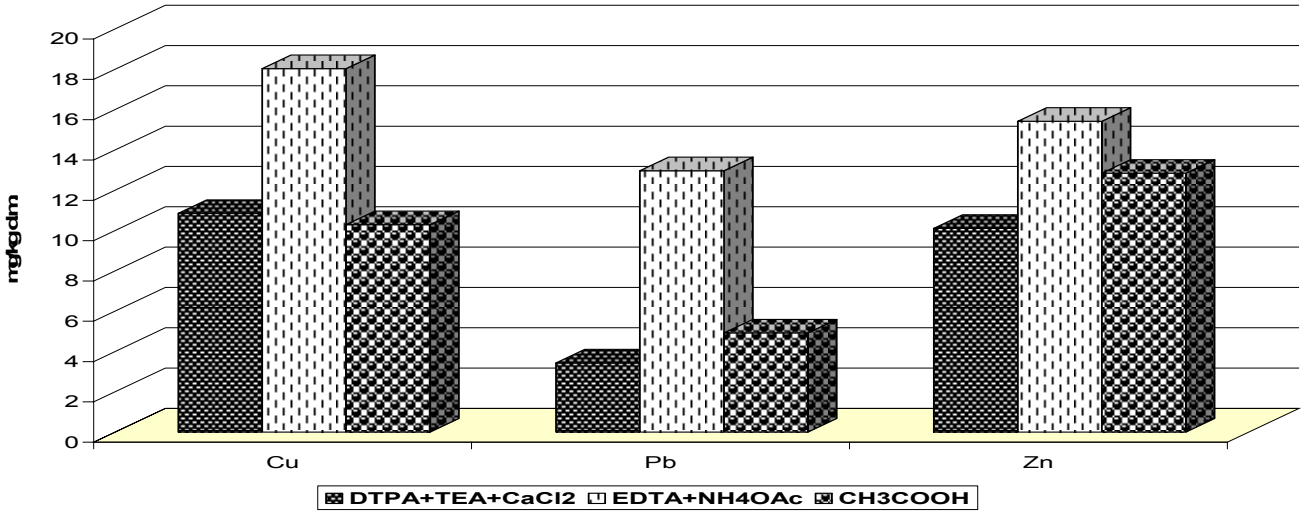

Fig. 3 – The mobile metallic elements from L3 sediment.

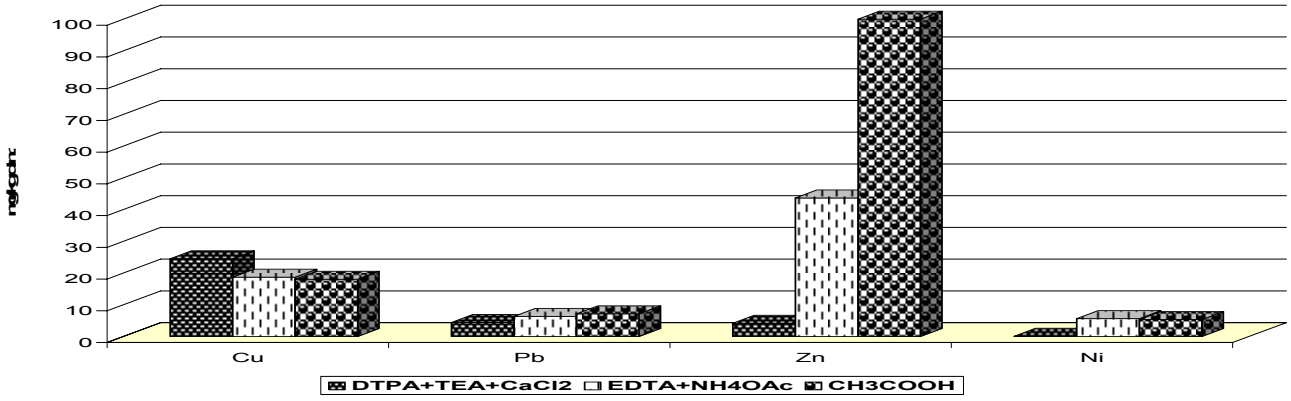

Fig. 4 – The mobile metallic elements from L4 sediment.

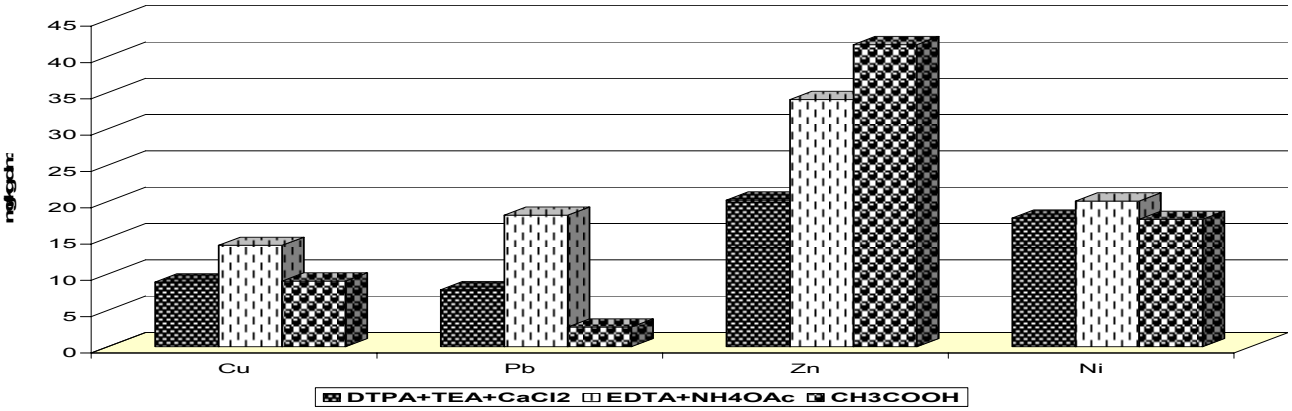

Fig. 5 – The mobile metallic elements from L5 sediment.

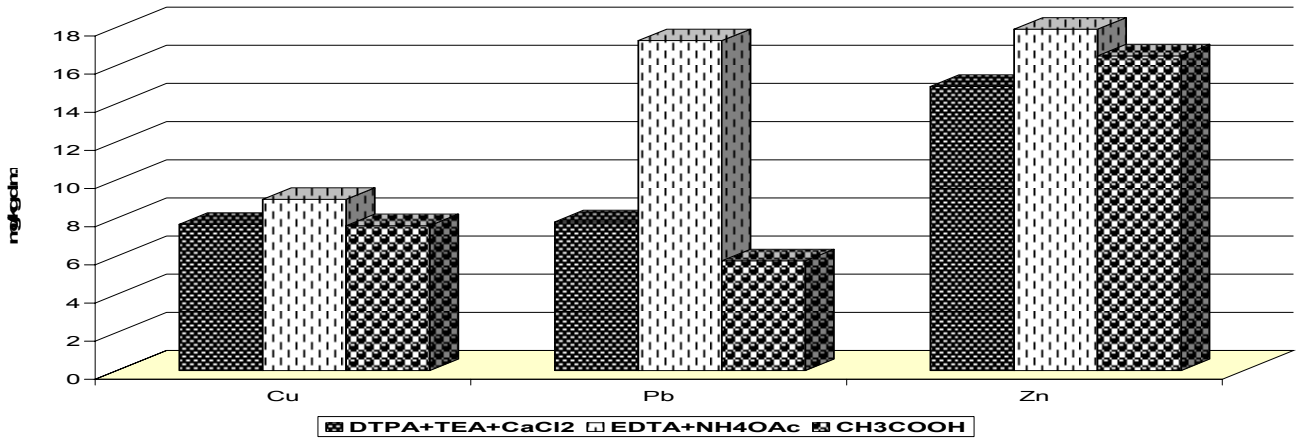

Fig. 6 – The mobile metallic elements from L6 sediment.

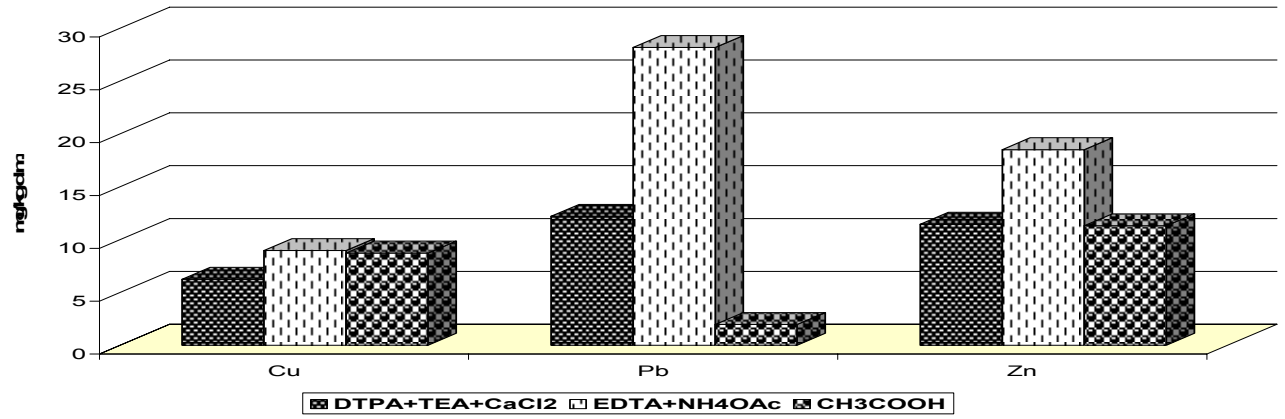

Fig. 7 – The mobile metallic elements from L7 sediment.

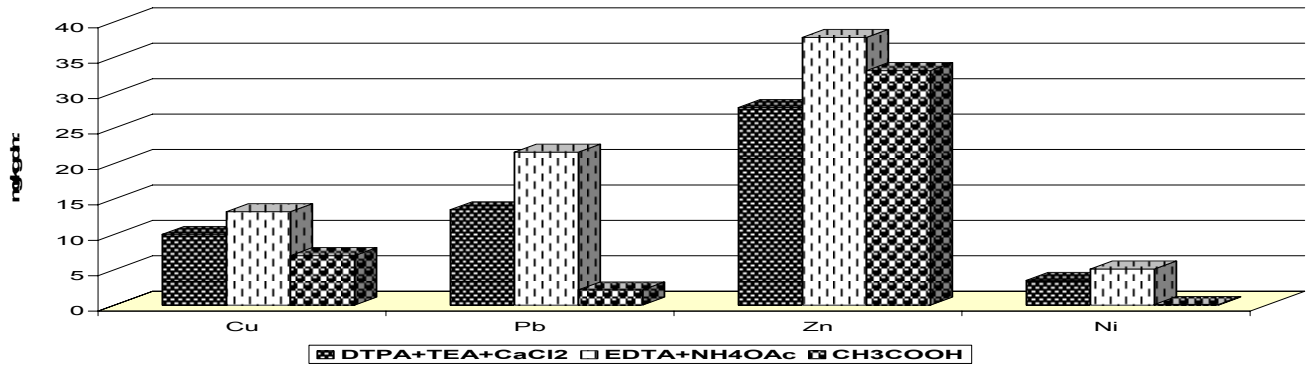

Fig. 8 – The mobile metallic elements from L8 sediment.

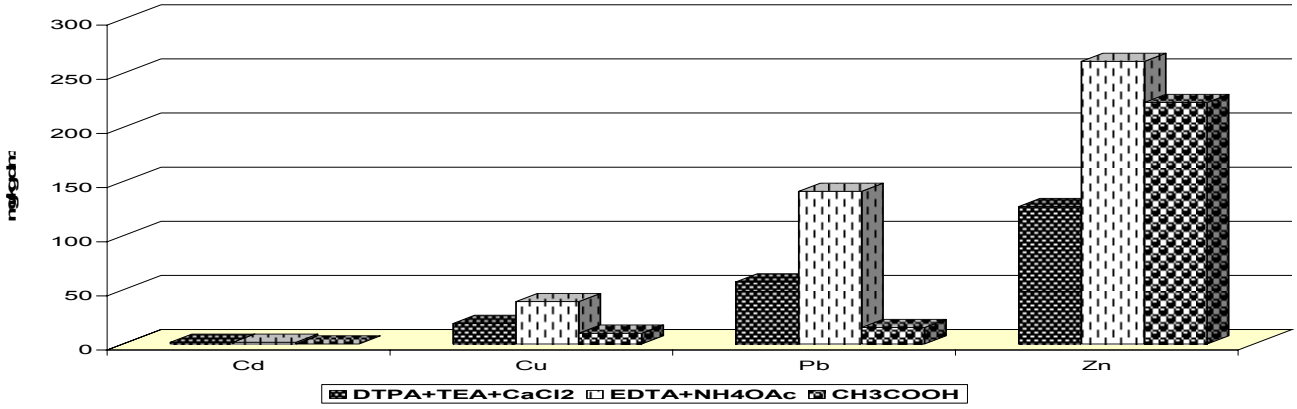

Fig. 9 – The mobile metallic elements from R1 sediment.

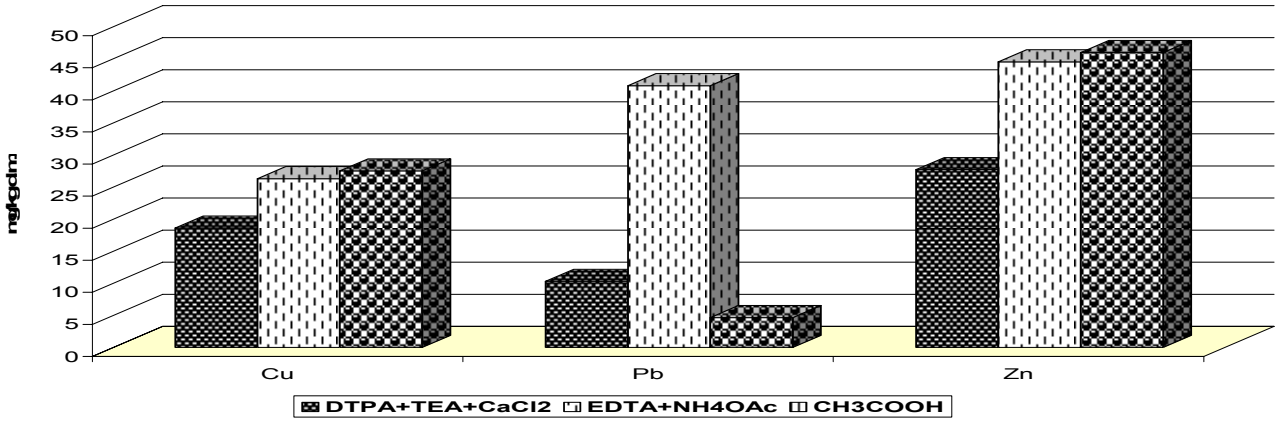

Fig. 10 – The mobile metallic elements from R2 sediment.

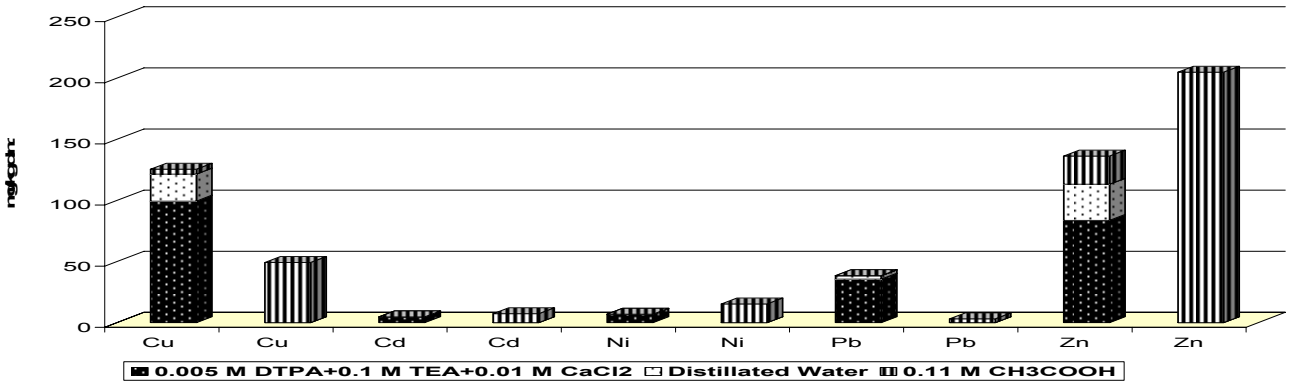

Fig. 11 – Comparative concentrations for sequential extraction (DTPA solution, distillated water and CH3COOH) and single chemical extraction with 0.11 M CH3CCOH from CRM BCR 701, lake sediment.

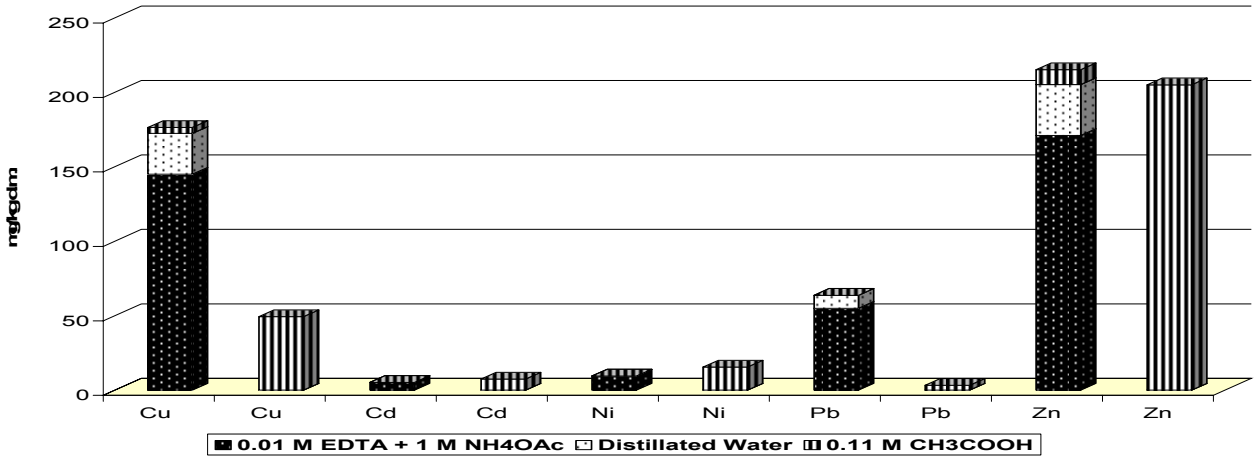

Fig. 12 – Comparative concentrations for sequential extraction (EDTA solution, distillated water and CH3COOH) and single chemical extraction with 0.11 M CH3CCOH from CRM BCR 701, lake sediment.

DISCUSSION

The aim of this study was to investigate which method is appropriate for these types of sediments and to observe the differences between the obtained results with three single chemical extraction procedures. The experimental data (figures 1 – 10) show that in the lake sediments, the 0.11 M acetic acid solution extract more quantity of Zn than EDTA method(L1, L2, L4, L5) or similarly contents (L3, L4, L7, L8). The EDTA solution release highest quantity of mobile Ni; also, for the mobile Cu and Pb, the EDTA method extract more quantity (L1, L3, L5-L8) than the other two methods.

In Brazilor Lake was recorded high concentration of exchangeable Ni, obtained with all three methods (20 mg/Kg d.m, represent 66%.), even if the total concentration is under the reference value; in Cartuş Lake, where the total Ni was over the reference value, the mobile Ni (5.5 mg/Kg d.m.) represent only 15 % from the "total concentration". The higher value for de mobile Zn content was obtained in Cartuş Lake (100 ppm) and represent approximately 24% from the total concentration (431 ppm). Even if in L5 sediment (Brazilor Lake) was high concentration of total Zn (453 ppm), three times more than the reference value, the mobile Zn was only 10% from the total content, without problem for the environment. The same situation was recorded for the other two sediments with high concentration of total Zn situated over the reference value; L1 and L8, where the mobile Zn represent 9.5%, respectively 15%.

The highest value for mobile Cu (46 ppm) was obtained in Mare Lake, where 19% from the total concentration (244 ppm) was found; for the other sediment samples, the values for mobile Cu were situated in the range 7 – 19 ppm.

In both river sediments (figures 9, 10), for mobile Pb contents the extraction order was EDTA > DTPA > acetic acid. The EDTA solution extract 10 times more Pb than 0.11 M acetic acid; also, for mobile Cu in Săsar river the EDTA method release higher quantity than DTPA and acetic acid solutions; for mobile Zn, EDTA and acid acetic solutions extract similarly contents, higher than DTPA solution.

In Săsar river was founded 1.5 mg/Kg d.m. of mobile Cd (with DTPA and EDTA solutions), that represent a potential source of pollution for the quality of surface water; also high quantity of mobile Pb (140 mg/Kg d.m) and Zn (261 mg/Kg d.m) were recorded, these mobile concentration been higher than the reference values for the total content of metals in the sediment structure according Roumanian Order no. 161/2006.

The aim of the sequential chemical extraction procedure was to clarify the differences between the tested methods. In BCR CRM 701 lake sediment (figures 11, 12) the sequential procedure shows that after first extraction, for the mobile Cu and Pb, the extracted concentrations increase in order EDTA > DTPA > acetic acid. For the other elements (Cd, Ni and Zn), the order was the following: acetic acid > EDTA > DTPA. The efficiency of extraction was 3 times higher in EDTA solution than in 0.11 M acetic acid for Cu and 17 times higher for mobile Pb. The quantity of mobile Zn release by BCR method is only with 1.2 times more than the concentration obtained with EDTA solution. For the mobile Cd and Ni, the values obtained were situated in the same range.

The other two extraction solutions used in sequential procedure release significant concentration of Cu and Zn (distillated water) and low contents for the same metals in 0.11 M acetic acid. This fact conducts to the conclusion that after the first extraction can be used a second step with distillated water and the total content of mobile metallic elements can be a sum of this two fractions.

CONCLUSIONS

The paper proposed a method for extraction of mobile metallic elements[17] from different terrestrial sediment. In the paper were compared the results obtained with three different extraction methods applied to eleven sediments: CRM BCR 701, eight sediments collected from Roşia Montana aria and two surface waters sediments.

The exchangeable fraction corresponds to the form of metals that is most available for plant uptake and can be release by changing the ionic strength of the medium.[2] The method NF X 31 – 120/1-92 use an organic complexant (EDTA) and the solution can modify the ionic strength in the sediment structure using different mechanism (ion-exchange, complexation) and also, can release more quantity of metallic elements than 0.11 M acetic acid (method BCR).

The metal content bound to carbonates is sensitive to pH changes and can became mobile when pH is lowered.[2] For this reason, 0.11 M acetic acid (pH=2.8) can release higher quantity of metallic carbonates then the other two solutions with the neutral pH. This case was recorded for Zn, higher quantity of Zn was obtained in this solution.

The experimental data proved that NFX31 – 120/1-92 (EDTA and NH_4OAc solution) can be successfully used for estimate the release of metallic elements from terrestrial sediments polluted by mining activities.

REFERENCES

1. S. E. Manahan, “Environmental Chemistry”, Seventh Edition, Lewis Publishers, Florida, 2000, 190-245.
2. A.V. Filgueiras, I. Lavilla and C. Bendicho, *J. Environ. Monit*., **2002,** *4*, 823-857.
3. I. Lavilla, A.V. Filgueras and F. Valverde, *Water, Air, Soil Pollut.*, **2006**, *172,* 273-293.
4. B. Gumgum and G. Ozturk, *Chem. Speciat. Bioavail.*, **2001**, *13*, 25-29.
5. G. Vasile, Liliana Cruceru and Jana Petre, *Rev. Chim. (Bucharest)*, **2005,** *56*, 790-794.
6. A. Schuquillo, R. Rubio and G. Rauret, *Anal. Bioanal. Chem,* **2005**, *382*, 353-359.
7. G. Vasile, E. Mihăila and M. Nicolau, *Rev. Chim. (Bucharest)*, **2006,** *57*, 967-972.
8. A. Cazzolino and M. Gabellini, *Chem. Speciat. Bioavail.*, **2006**, *18,* 95-103.
9. G. Rauret, J.F. Lopez-Sanchez, R. Rubio and C. Davidson, A. Ure, Ph. Quevauviller, *J. Environ. Monit*., **1999,** *1*, 57-61.
10. A. Mocko and W. Wackawek, *Anal. Bioanal. Chem.,* **2004,** *380*, 813-817.
11. J. Gautheyron and M. Pause, “Handbook of Soil Analysis – Mineralogical, Organic and Inorganic Methods”, Springer, Holland, 2006, p. 551 – 637.
12. J. R. Dean, “Methods for environmental trace analysis”, Northumbria University, Newcastle, UK, 2003, p. 76-88.
13. S. R. Cook and A. Parker, *Water, Air, Soil Pollut.*, **2006**, *170,*95-105.
14. F.M.G. Tack and M.G. Verloo, *Chem. Speciat. Bioavail.*, **1999**, *11,* 43-50.
15. X. Li, Z. Sheu, O.W.H. Wai and Y. Li, *Chem. Speciat. Bioavail.*, **2000**, *12,* 17-25.
16. ***, SR ISO 14870-1999, “Soil quality : Extraction of microelements in buffer solution of DTPA”;
17. ***, NF X 31 – 120/1992, “Soil quality: Measurement of heavy metals from soil after extraction with a mixture of ammonium acetate and EDTA”.
18. A.K. Gupta and S. Sinha, *J. Hazard Mater*, **2007**, *149*, 144-150.
19. M.H. Feng, X.Q. Shen, S. Zhang and B. Wen, *Environ. Pollut*., **2005,** *137*, 231-240.
20. *** SR ISO 11466-99, “Soil quality: Extraction of micro elements with aqua regia”.
21. The Ministry of Environmental and Water, “Order no. 161/2006 for the approval of the Norm concerning the reference objectives for the surface water quality classification (including quality standards for sediments)”, Official Monitor of Roumania, Part 1, No 511 bis.

Revue Roumaine de Chimie, **2008**, *53*(11), 1051–1057

HDPE-EPDM THERMOPLASTIC VULCANIZATES. MECHANICAL AND IR SPECTROMETRIC PROPERTIES

Zenovia MOLDOVAN,[a*] Florica IONESCU,[b] Ioana VASILESCU,[c]
Simona LIȚESCU[c] and Laurenția ALEXANDRESCU[b]

[a]University of Bucharest, Faculty of Chemistry, Department of Analytical Chemistry, 4-12 Regina Elisabeta Blvd., Sect.3, Cod 030018-Bucharest, Roumania
[b]Research Development National Institute for Textile and Leather -Division Leather and Footwear Research Institute, 93 Ion Minulescu St., Sect 3, Cod 031215-Bucharest, Roumania
[c]University "Politehnica" of Bucharest, Faculty of Chemistry, Department of Analytical Chemistry, 1 Gheorghe Polizu St., Sect. 1, Cod 011061-Bucharest, Roumania

Received February 11, 2008

The present work is concerned with the preparation and characterization of some thermoplastic vulcanizates based on high-density polyethylene (HDPE) and ethylene-propylene-diene terpolymer (EPDM). The polymer blends were obtained using binary vulcanizating accelerators systems. One of the components was tetramethylthiuram disulfide (TH) and the second one, 2-mercaptobenzothiazole (M) or 2,2'–dithiobenzothiazole (DM). An important part of our study is focused on the mechanical properties of the prepared thermoplastic vulcanizates. These properties were then correlated with the IR spectra obtained by applying the ATR-FTIR technique. The polymer blend containing as cure system Sulfur+TH+M in the weight ratio 0.41/1.8/0.8 and 1/1.2/0.7 were found to have better properties, especially tensile strength, modulus 300% and tear strength.

INTRODUCTION

The appearance of thermoplastic elastomers (TPEs) in the 1950s[1] provided a new dimension to the field of polymer science and technology. The field of TPEs based on rubber thermoplastic composites has grown along two different product-lines or classes: one consists of simple blends and is commonly designated as thermoplastic elastomeric olefins (TEO) according to ASTM D5593.[2] In the other class the rubber phase is dynamically vulcanized, giving rise to a thermoplastic (TPV) or dynamic vulcanizate (DV) according to ASTM D5046.[3] Morphologically, TPVs are characterized by the presence of finely dispersed crosslinked rubber particles distributed in a continuous thermoplastic matrix.[4,5] If the rubber particles are sufficiently vulcanized, the physical and chemical properties of the blend are generally improved.

The dynamic vulcanization process was first reported by Gessler[6] in 1962 and further developed by Fisher[7], Coran et al.[8, 9] and Abdou-Sabet and Fath.[10] The thermoplastic vulcanizates presents improved physical and chemical properties, such as: higher values of Shore "A" hardness, modulus 300%, stress at break, tear strength and lower value of strain at break, greater stability of phase morphology in the melt, more reliable thermoplastic processing, greater resistance at high temperature and to attack by fluids e.g., hot oils, alkaline and acid solutions.

Polyethylene-ethylene-propylene-diene terpolymer (PE-EPDM) composites have both practical and theoretical significance. To be able to utilize all the advantages offered by such composites, the basic processes taking place during their formation must be known.

In this paper, a tentative explanation which tries to help to understand better the relations between structure and properties of PE-EPDM composites is given. For this purpose, a correlation between IR spectra and physico-mechanical properties of the prepared thermoplastic elastomers was proposed.

* Corresponding author: z_moldovan@yahoo.com

RESULTS AND DISCUSSION

It is widely recognized that the formulation has a strong influence on the properties of polymer composites. For this reason, the effect of the type of cure system and of the ratio of cure agents on the physico-mechanical properties of the prepared polymer blends was investigated. The EPDM-HDPE composites were obtained by different chemical methods of vulcanization and in different formula. All polymer samples have the same ratios (parts by weight) EPDM:HDPE:ZnO:stearic acid:2,2,4–trimethyl-1,2-dihydroquinoline:Irganox 1010 = 50:50:5:0.4:1:1. The cure agents are given in Table 1. We mention that usually when the ratio of sulfur to accelerator is less than one the receipt is known as Efficient Vulcanization System (EV).

Table 1

Cure agents in formulation of some microstructured polymer blends (parts by weight)

Cure agents	Cure system / Symbol of polymer blends									
	Conventional cure system						Semi-EV system		EV system	
	S1	S2	S7	S8	S12	S13	S17	S18	S22	S23
Sulfur	2	2	2	2	2	2	1	1	0.41	0.41
TH	1	1	0.5	0.5	0.5	0.5	1.2	1.2	1.8	1.8
M		0.5		1		0.3		0.7		0.8
DM	0.5		1		0.3		0.7		0.8	

Shore "A" Durometer Hardness is the measure of elastic modulus of the polymer blend. This parameter is often indirectly obtained by measuring the elastic indentation of prescribed size and shape pressed into the surface under specified loading conditions. Higher values of this parameter correspond to harder compounds and vice versa. As can be seen in Figure 1, the values of this parameter were not significantly different for all the investigated composites; the loading with cure agents and the presence of HDPE gives a greater hardness to the cured compounds.

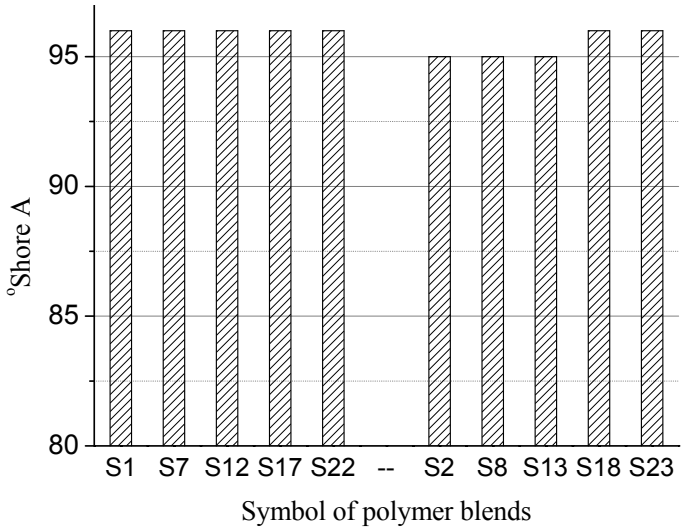

Fig. 1 – Shore "A" Durometer Hardness.

Stress at 300% (Modulus) and tensile strength (stress-at-break) for all polymer composites were investigated. The importance of 300% modulus lies in the fact that it can be taken as an index of the sum of chemical and physical crosslinks, such as chain entanglements.[11] As it is shown in Figure 2, the value of modulus at 300% is higher for the compounds S17, S18 and S23.

The stress-at-break values for all polymer composites are shown in Figure 3. The highest tensile strength corresponds to the compounds S17, S18 and S23. The other compounds, i.e., S1, S2, S13 showed nearly equal or low tensile strength values. This suggests that the strain crystallization behavior of the first mentioned composite samples was encouraged by the use of the semi-EV and EV procedures of compounding. The cure conditions obtained by semi EV and EV systems always results in higher tensile values.

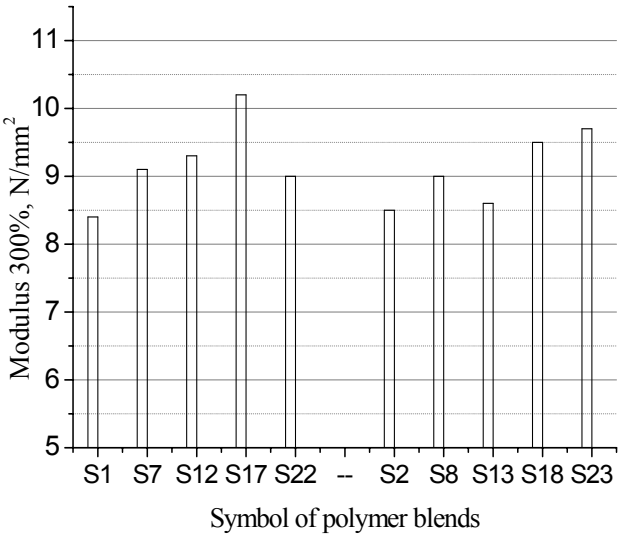

Fig. 2 – Stress at 300% strain (modulus), N/mm^2.

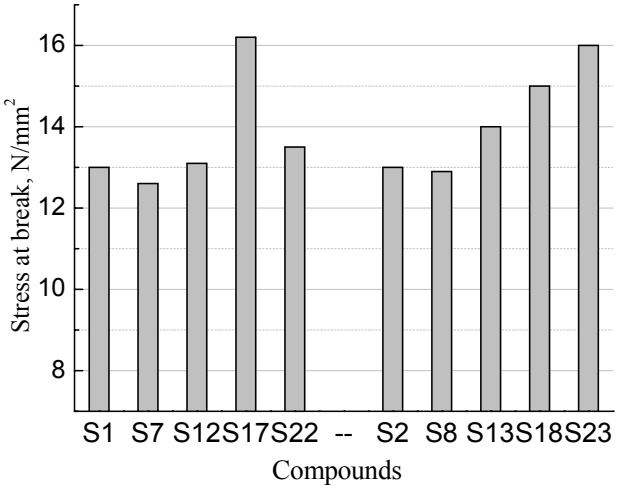

Fig. 3 – Stress at break, N/mm^2.

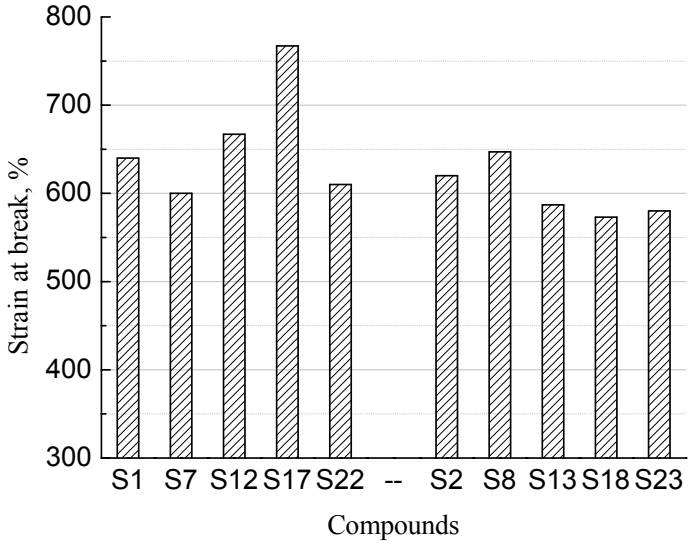

Fig. 4 – Strain at break, %.

Strain at break (elongation, %). Strain at maximum elongation, *i.e.*, the extensibility of the studied composites is illustrated in Figure 4. It is known that the elongation of the polymer blend decreases with the increases of crosslinking[12] (which is confirmed from its elongation, % value).

The results illustrated in Figure 4 seem to confirm this assumption. The effect of crosslink

density on the extensibility is evident in the case of the compounds S18 and S23, which have the lower value of elongation. On the other hand, the following ratios vulcanizing accelerators/sulfur can be seen in Table 1: 0.75 for the conventional cure systems S1, S2, S7, S8; 1.85 for the semi-EV cure systems S17, S18; 6.34 for EV cure systems S22, S23. So, even the conventional systems have higher sulfur loading, but more efficient seem to be the semi-EV and EV cure systems, which contain lower amounts of sulfur. This behavior could be explained as follows: too many crosslink junctions (assured by the polysulfide bonds) will hinder the structural regularity needed for crystallization (it is the case of samples S1, S2, S8, S12, S17), which have higher values of strain at break. The highly crosslinked compounds can not crystalline easily because of the immobility of the network structure. In the case of semi-EV system S18 and EV system S23 the crosslinking obtained is beneficial, providing the mobility to align the chains on deformation; as a result, the strain at break is lower. On the other hand, the semi-EV and EV systems (containing the accelerators TH+M, in samples S18 and S23) seem to be more efficient than those containing TH+DM (in samples S17, S22). This could be a consequence of the moderate action of M (see the value of elongation for S18 and S23 comparative with S17 and S22).

Tear behavior. The tear strength values for the polymer composites are presented in Figure 5. As we can see, the tearing strength values are influenced by the sort of sample. As a confirmation of this assumption, the literature data reported that tear strength values depend on the type of sample itself, filler type and test conditions.[11-15] The compounds S13, S18, S22, S23 have higher tear strength values than the others. This behavior could be explained by the strain crystallization of the mentioned compounds.

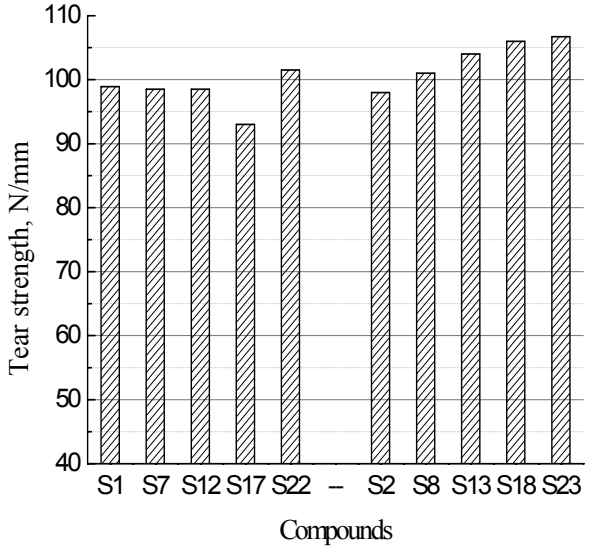

Fig. 5 – Tear strength, N/mm.

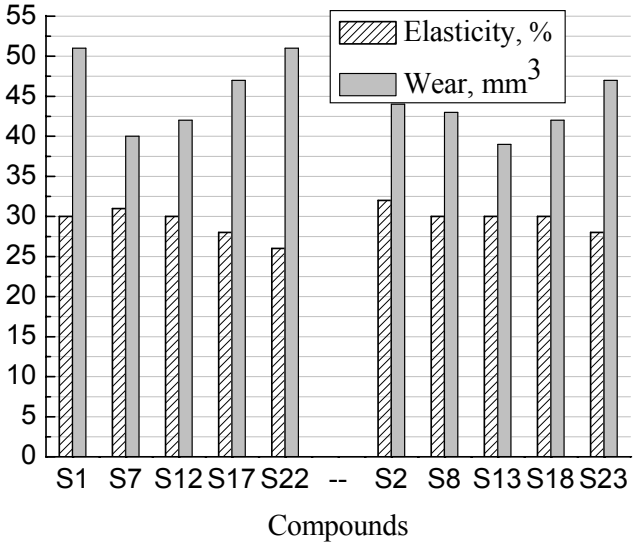

Fig. 6 – Elasticity, % and wear, mm^3 .

Elasticity and wear. As it is seen in Figure 6, in the almost all the cases a higher value of the elasticity is associated with a lower wear. These results were predictable taking into account that a low elasticity could be a result of the regularity of the polymer chains and vice versa.

The effect of accelerated aging. Generally, the effect of accelerated aging lies in an increase of modulus 300% and stress at break and a decrease of strain at break. This behavior is confirmed by the results in Tables 2 and 3 and consists in the improvement of some physico-mechanical properties of the obtained thermoplastic vulcanizates at high temperature. The effect of accelerated aging should be explained as follows: at high temperature, a physical interaction between many vulcanized elastomer particles takes place; this results in a network of vulcanized elastomer.[16] The substantial change of most of tensile properties may also be an indication of a post-curing process. The effect of accelerated aging shows that the prepared thermoplastic vulcanizates are good candidates for industrial applications at high temperatures.

Table 2

The effect of aging on the physico-mechanical properties of some thermoplastic vulcanizates containing as cure agents S, TH, M, DM obtained by using conventional cure systems

Physico-mechanical parameter	Symbol of polymer blends											
	S1		S2		S7		S8		S12		S13	
	a	b	a	b	a	b	a	b	a	b	a	b
°Shore A Hardness	96	96	95	95	96	96	95	96	96	96	95	94
Elasticity, %	30	32	32	30	31	26	30	28	30	28	30	29
Modulus 300%, N/mm^2	8.4	11.8	8.5	10.7	9.1	10.6	9	10.8	9.3	11.2	8.6	11.8
Stress at break, N/mm^2	13	19.8	13	19.3	12.6	21.1	9.7	18.7	13.1	19.5	14	19
Strain at break, %	640	560	620	553	600	600	647	567	667	567	587	520
Tear strength, N/mm	103.5	96.5	98	96	98.5	102.5	101	92.5	98.5	93	104	98.5

a) – Normal conditions: b) – After accelerated aging

Table 3

The effect of aging on the physico-mechanical properties of some thermoplastic vulcanizates containing as cure agents S, TH, M, DM obtained by using semi-EV and EV cure systems

Physico-mechanical parameter	Symbol of polymer blends							
	Semi-EV systems				EV systems			
	S17		S18		S22		S23	
	a	b	a	b	a	b	a	b
°Shore A hardness	96	96	96	95	96	96	96	96
Elasticity, %	28	26	30	30	26	28	28	34
Modulus 300%, N/mm^2	10.2	10.3	9.5	10.4	9	10.6	9.7	10.4
Stress at break, N/mm^2	16.2	18.7	15	18.7	12.2	19	16	19
Strain at break, %	767	580	580	560	610	560	600	580
Tear strength, N/mm	93	96	106	96.5	101.5	98.5	106.5	105

a) – Normal conditions: b) – After accelerated aging

The ATR technique has given fresh hope for IR spectrometry of polymer materials that do not allow the usual methods of sample preparation. Moreover, the literature data reports ATR-FTIR spectrometry being useful for characterization of the surface of complex polymer blends, taking into account that the IR radiation penetrates into the sample a few nanometers depth. As a matter of fact, in the case of polymer blends characterized by a good incorporation of additives, the presence of the IR characteristic peaks of additives in the surface spectra cannot be detected.[17]

On the basis of this well-documented assumption, the ATR-FTIR spectra recorded for the studied polymer blends gave us the following information:

No absorption bands were detected in the range 4000-3200 cm^{-1} for the samples S18 and S23 (see

Fig. 7b). The vibrations responsible for bands in this region are O-H and N-H stretchings and are characteristic IR spectral bands of primary and secondary amines (*i.e.* the antioxidant TMQ), organic acids (*i.e.* the activator stearic acid) and phenols (*i.e.* the antioxidant Irganox 1010).

Many spectral bands occur in the spectra of the other polymer blends (Figure 7ab). They could be attributed to the polymer additives. For example, in Figure 7a, spectra of S7 and S22 present a large band at 3420 cm^{-1} characteristic for tertiary amines (characteristic for the cure accelerator DM). In Figure 7b (spectra of samples S2, S8, S13) a weak N-H stretching band may be seen at 3300-3500 cm^{-1}, assigned to secondary aromatic amines and diamines. This band is characteristic for the additives M, DM, TMQ, TH.

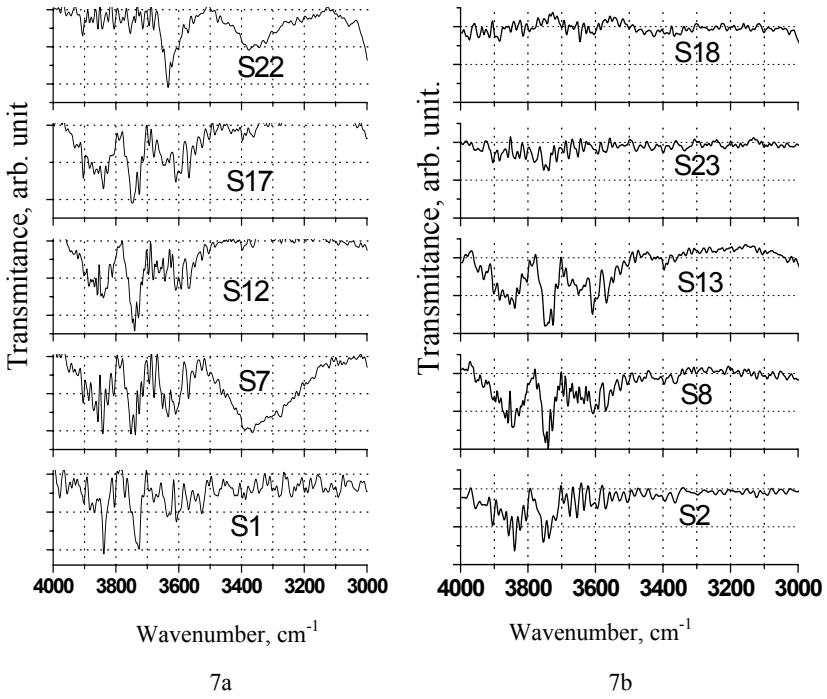

Fig. 7a,b – FTIR spectra of some polymer composites.

On the basis of these spectral information we assume that the activator (stearic acid), the antioxidant (Irganox 1010) and the cure accelerators are completely incorporated in the polymer blends S18 and S23, because in the spectra of these samples do not occur the bands characteristic for these additives. This confirms the compatibility of the ingredients (polymers and additives).

The assignment of the IR bands was carried out according to literature data.[18]

EXPERIMENTAL

Materials. All composites contain the same polymers: the EPDM elastomer (Nordell IP 3745P) and the high density polyethilene (HDPE B084, Petro-Midia), in the ratio 1:1.

In addition to the polymers, other additives were used, as follows: cure accelerators: 2-mercaptobenzothiazole (M); 2,2'–dithiobenzothiazole (DM); tetramethylthiuram disulfide (TH); crosslinking agent: sulfur (S); activators: zinc oxide and stearic acid; antioxidants: di-lauril-orto-dipropionate (Irganox 1010) and 2,2,4–trimethyl-1,2-dihydroquinoline (TMQ).

Preparation of thermoplastic elastomers. All the ingredients were mechanically melt-mixed in a Brabender Plasti-Corder PLE-60 at 180°C for 7-8 minutes. A constant rotor (cam type) speed of 80 rpm was applied. Then, the polymer blend was recovered from the mixer and transferred to a two-roll mill at 155 ± 5°C and 24 rpm. The compound was then compression-molded (using an electrically heated hydraulic press at 190°C under 20 MPa pressure) to achieve a sheet of about 2 mm thick. The sheet was then cooled down to room temperature under the same pressure. The specimens were cut from the compression molded sheet and used for testing after 24 hours of storage at room temperature.

Aging experiments. In order to investigate the effect of lab aging conditions on the physico-mechanical properties of the prepared thermoplastic vulcanizates, the test specimens were placed in an air-circulating oven at 100°C for 168 h.

Apparatus for physico-mechanical tests. Tensile tests were carried out according to ASTM D412-98 using a Zwick Tensile Testing machine 1445, at a constant crosshead speed of 500 ± 5 mm/min.

Hardness was measured using Shore "A" durometer according to ASTM D412-98.

Apparatus for FTIR measurements. The attenuated total reflection Fourier Transform IR (ATR-FTIR) method was chosen for spectral characterization of the prepared polymer blends. The plate samples (6 x 6 mm) were simply posed on the sampling stage, in intimate contact with the optical element, a hemi-cylindrical prism of SeZn (colled Internal Reflection Element (IRE)). ATR-FTIR measurements were run with a Bruker instrument (model Tensor 27), in the following conditions: wavenumber range: 600-4000 cm^{-1}; apperture setting: 6 mm; scanner velocity: 2.2 KHz; background scan time: 32 sec; sample scan time: 32 sec; resolution: 6 cm^{-1}; beamspliter: KBr; angle of incident radiation: 45^{o}.

CONCLUSIONS

The optimum values of the main physico-mechanical parameters, characteristic for thermoplastic vulcanizates (high values of ^{o}Shore A hardness, 300% modulus, stress at break, tear strength and low values of strain at break or elasticity) were obtained in the case of semi-EV and EV systems S18 and S23 respectively. Thus, by using as cure agents sulfur and the two accelerators M and TH (in the ratio cure accelerators/S = 1.9, in the case of sample S18 and 6.34 in the case of sample S23), we have obtained the best thermoplastic vulcanizates. The compatibility of the polymer phases in the case of S18 semi-EV system and S23 EV system was confirmed by their physico-mechanical properties and correlated with IR spectra. Both physico-mechanical and ATR-FTIR techniques allowed understanding the structure of the prepared chemical microstructured systems.

Acknowledgements: This work was performed within the framework of the National Program CEEX-Matnantech, Project no. 88/2006.

REFERENCES

1. A. Jha and K. Bhowmick, *Rubber Chem. Technol.*, **1997**, *70*, 798-814.
2. ASTM D 5593-99: Standard Classification for Thermoplastic Elastomers-Olefinic (TEO).
3. ASTM D 5046-98: Standard specification for Fully Crosslinked Elastomeric Alloys.
4. Y. P. Pankaj and W. J. van Ooij, *Rubber Chem. Technol.*, **2005**, *78*, 155-173.
5. J. D. Patel, M.Maiti, K.Naskar and A.K.Browmick, *Rubber Chem. Technol.*, **2005**, *78*, 893-909.
6. A.M. Gessler and W.H. Haslett (Esso Research and Engineering Co.), *U.S. Pat*. 3037954, June 5, 1962.
7. W. K. Fisher (Uniroyal Inc.), *U.S. Pat*. 3758643, Sept. 11, 1973.
8. A. Y. Coran, B. Das and R. P. Patel (Monsanto Co.), *U.S. Pat*. 3130535, Dec. 19, 1978.
9. A. Y. Coran and R. P. Patel, *Rubber Chem. Technol.,* **1980**, *53*, 141-150.
10. S. Abdou-Sabet and M. A. Fath (Monsanto Co.), *U.S. Pat*. 4311628, June 19, 1982.
11. G. R. Hamed and N. Rattansom, *Rubber Chem. Technol.*, **2002**, *75*, 323-332.
12. A. N. Gent and H. J. Kim, *Rubber Chem. Technol.*, **1978**, *51*, 35-41.
13. A. N. Gent and L. Q. Zhang, *Rubber Chem. Technol.*, **2002**, *75*, 333-343.
14. D. De and A. N. Gent, *Rubber Chem. Technol.*, **1996**, *69*, 834-850.
15. A. Ahagon, *Rubber Chem. Technol.*, **1986**, *59*, 187-203.
16. A. Y. Coran and R. P. Patel, in "Thermoplastic Elastomers", Hanser/Gardner, Munich-Vienna-New-York, 1996, 2nd ed., Chapter 7, p. 153-190.
17. T. Jawhari, L. Quintanilla and J. M. Pastor, *J. Appl. Polymer Sci*., **1994**, *51*, 463-471.
18. G. Socrates, "Infrared and Raman Characteristics Group Frequencies, Tables and Charts", Wiley, New York, 2001, p. 12; 108-110.

Revue Roumaine de Chimie, **2008**, *53*(11), 1059–1064

SOFTWOOD CHEMICAL MODIFICATION BY REACTION WITH ORGANIC ANHYDRIDES

Ruxanda BODÎRLĂU* and Carmen-Alice TEACĂ

"Petru Poni" Institute of Macromolecular Chemistry 41 A Grigore Ghica-Voda Alley, Iaşi 700487, Roumania

Received January 23, 2008

The fir (*Abies alba* Mill.) wood flour (30 mesh particle size) and discs 6.5 x 0.4 cm (diameter x length) were successfully chemically modified by treatment with succinic anhydride (SA) solution in xylene of different concentration values. The time of the reaction was changed between 180s and 1800s in several steps. The progress of modification was followed by the measurement of weight change and infrared spectroscopy investigation (FTIR). Further increase in reaction time influenced the weight change of fir wood. The reduction of surface tension led to significant changes in all interactions between the wood and other substances resulting in a considerable decrease of water absorption, which is the major benefit of modification. Water absorption of fir wood samples measured at 25°C and atmospheric pressure was investigated.

INTRODUCTION

The use of vegetable fibers and/or particles as reinforcement fillers for polymeric matrices has been enjoying a continuous growing interest in the past decade from the scientific and application points of view. Applications go beyond the widely used particleboard and efforts are being made to produce matrices for the construction, packaging and automotive industries among others. Because of the shortage of high-quality wood, reconstituted wood materials, such as particleboards, plywood, and fiberboards are important products of wood-based industries.[1] Moreover, natural fibers are very cheap, easily available, and renewable. Recently the interest in composite materials reinforced with wood flour and natural fibers increased considerably. [2, 3]

Wood is a complex composite material, which consists mainly of cellulose (40–45%), hemicelluloses (20–30%) and lignin (20–30%). Cellulose represents the crystalline part of wood, while the structures of hemicelluloses and lignin are amorphous.

Hardwood and softwood differ in several aspects, like fiber dimensions, chemical components composition, mainly the lignin and cellulose content. Hardwood contains a cell called a vessel element and has lignin containing guaiacyl and syringyl units, while softwood does not contain vessel elements and the lignin is composed of essentially only guaiacyl units.[4]

In recent years, a number of studies and method development work have been directed to apply chemical modification technology to solid wood in order to improve the durability and behavior of wood in adverse environments. The chemical modification of wood can be directed to improve the dimensional stability properties, hardness properties and/or durability properties of wood against decay.[5-7]

The dimensional modification, as well as biological degradation of wood has been attributed to the presence of numerous hydroxyl groups in various wood components. A blockade of such sites by larger groups swells the wood permanently and not only eliminates the moisture adsorption sites but prevents the highly specific enzymatic reactions. Environmental factors regulations about the use of biocides have renewed interest in chemical modification techniques, and efforts are being made to upgrade these techniques.

Besides acetic anhydride, other organic anhydrides, although to less extent, have been used as modifying agents for wood. For instance, modifications of wood with phthalic, succinic or maleic anhydrides have been reported to result in

* Corresponding author: rbodirlau@yahoo.com

reduced tensile strength of the wood.[8] Organic anhydrides groups react chemically with the –OH groups of the wood and improve interfacial adhesion considerably. However, such a modification usually does not solve drawbacks like aggregation, appearance of the product, and water adsorption. Esterification or etherification of the hydroxyl groups is the most often applied approach for modification [9, 10] but attempts are made also for the impregnation of the wood with various monomers and their subsequent polymerization.[11-13]

The purpose of this paper is to investigate structural modification of fir wood as following succinic anhydride treatments. Chemical modification was followed by the measurement of weight change and infrared spectroscopy investigation (FTIR). Influence of dipping time and succinic anhydride concentration on weight change for un-extracted and extracted fir wood samples was investigated.

RESULTS AND DISCUSSION

Effect of chemical treatment on weight change of wood flour

The weight change of wood flour samples was significant as obtained for treatment with succinic anhydride 10% (w/w) in xylene (data not presented here). [14]

Characterization of wood flour by FTIR spectroscopy

The softwood chemical structure was investigated by FT-IR spectroscopy.[15] The FT-IR spectra of fir wood flour (previously extracted in solvents) treated with organic anhydrides confirmed the occurrence of wood-anhydride reaction (Figure 1). The strong vibration obtained in the region 1728-1730 cm^{-1} (C=O) was a distinct pattern present in modified samples which indicates the presence of new formed ester bond. As expected, such absorption band was not present in unmodified wood. An increase in the intensity of OH in plane bending vibration at 1219 cm^{-1} and 1214 cm^{-1} bands specific to wood components, cellulose and hemicelluloses, was also evidenced.

Effect of dipping time on weight change for wood discs

The effect of dipping time on weight change (%) during wood discs chemical modification in the presence of xylene was investigated in order to evaluate the extent of reaction. Experimental data are presented in Table 1. The increasing of dipping time increase weight change both for UW and EW samples, this effect being more significant for EW samples treated with SA solution 30 g/L in xylene.

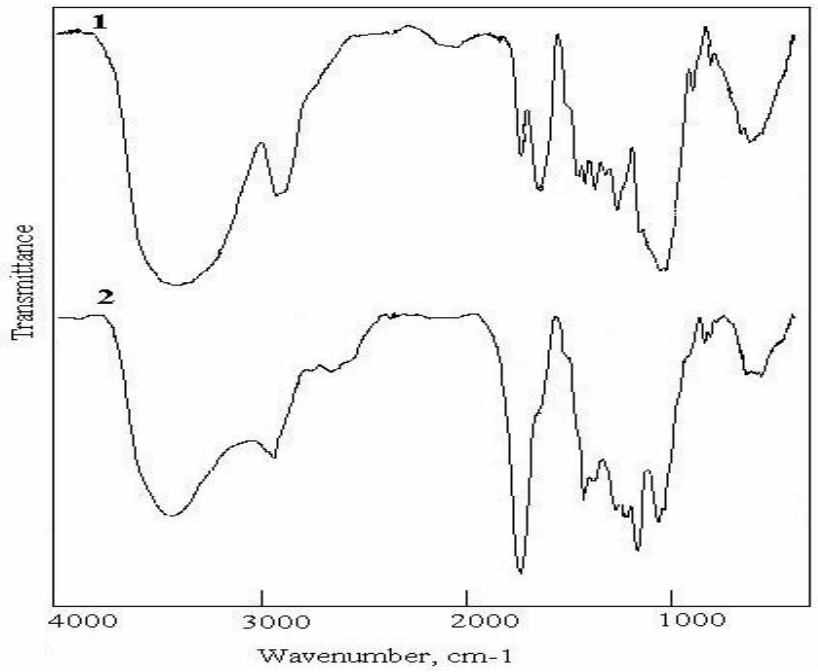

Fig. 1 – FTIR spectra for fir wood flour: 1.EWF; 2. EWF-SA.

Table 1

Weight change (%) for fir wood discs immersed in SA solution 30 g/L in xylene

Sample*	Dipping time, s			
	180	420	900	1800
UW	0.117	0.322	0.594	2.077
EW	0.499	1.066	4.288	7.343

*reported to oven-dried weight wood discs samples

Adsorption of SA on wood discs

Relationship between SA concentration and retention for UW and EW wood discs is presented (Figure 2 a). The retention of SA on wood samples was related to physical adsorption and grafting rate. A large number of succinic anhydride groups provided more opportunities for graft reaction. In general, the grafting rate increased with concentration and retention. For UW samples a higher grafting rate is noticed at most concentration levels (Figure 2 b). Although more hydroxyl groups were exposed on wood surfaces after Soxhlet extraction, the electrostatic blocking effect [16] significantly resisted the graft reaction for SA.

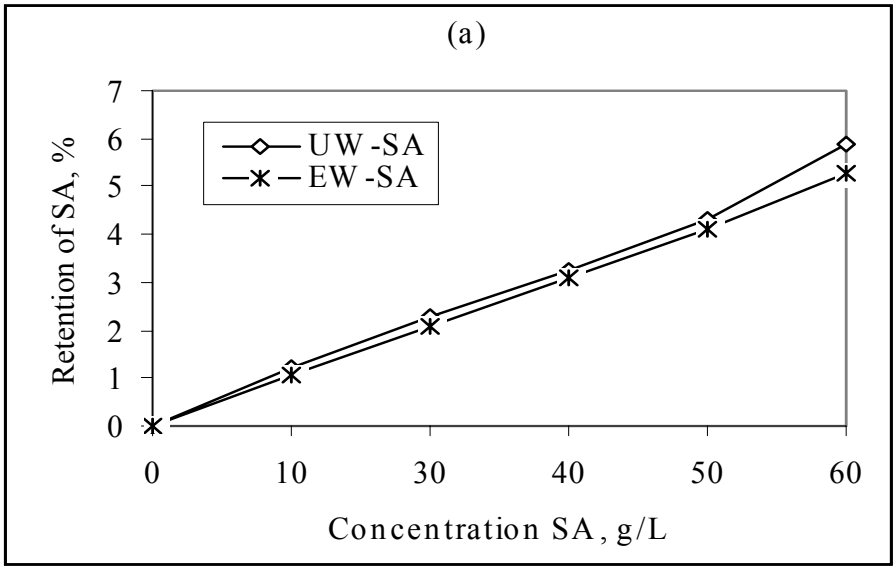

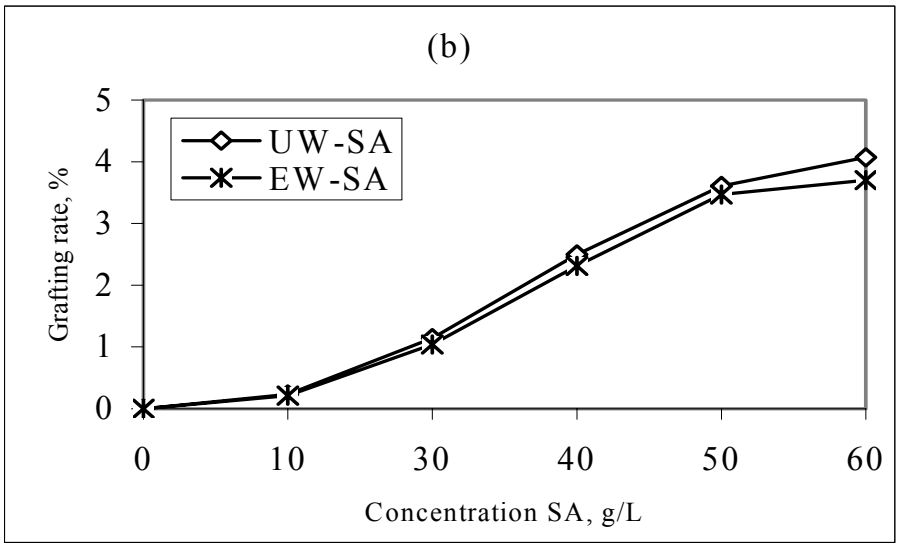

Fig. 2 – Variation of retention (a) and grafting rate (b) with SA concentration value (dipping time: 7 min).

Water absorption investigation for wood discs

In a series of water absorption studies with varying time period, the wood samples treated with succinic anhydride absorbed less water than the untreated ones. Water absorption after five hours decreases with increasing SA concentration value (Figures 3-4).

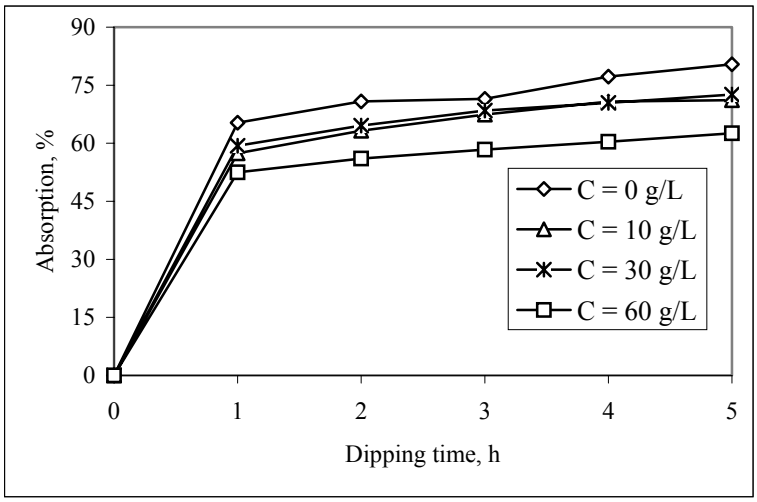

Fig. 3 – Water absorbtion of UW-SA samples for different SA concentration levels.

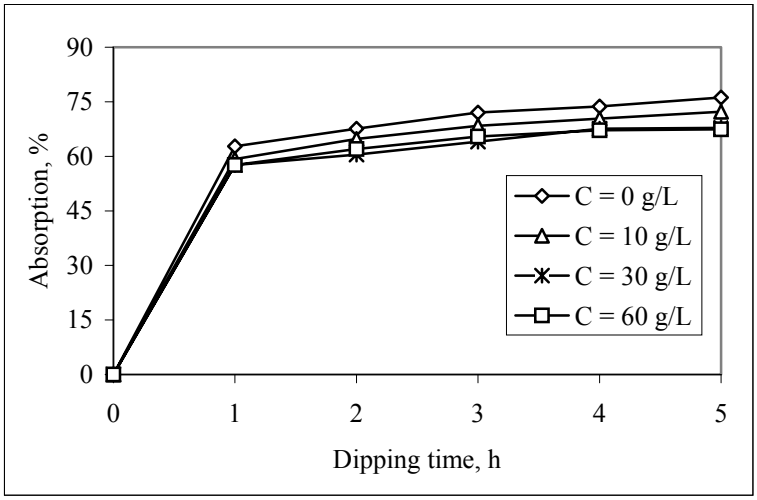

Fig. 4 – Water absorbtion of EW-SA samples for different SA concentration levels.

EXPERIMENTAL

Materials

Wood flour (30 mesh particle size) from a native fir wood species (*Abies alba* Mill.), provided from local sources, namely Forestry Agency, Iasi and discs 6.5 x 0.4 mm (diameter x length) were subjected to succinic anhydride chemical treatments. Moisture content of wood samples was 5-6%. The major chemical components of softwood samples were determined in accordance with TAPPI standards, their values being presented in Table 2.

Succinic anhydride (SA) was obtained from Aldrich (97 %) being used as received. Organic solvents were analytical grade.

Table 2

The main components of fir wood flour

Ash, %	Extractable substances (%) in :			Celullose, %	Lignin, %	Holocelullose, %
	Hot water	NaOH 1%	Ethanol/toluene			
0.25	1.65	9.57	1.53	54.21	30.17	81.12

Chemical modification of wood samples

Fir (*Abies alba* Mill.) wood flour and discs were prepared from dried logs (maintained at ambient temperature for one year). Wood samples (flour and discs) were placed individually in a Soxhlet extractor for solvent extraction using toluene/ethyl alcohol mixture (2:1 by volume) for eight hours. Samples were dried in an oven at 103ºC±2ºC until constant weight. Prior to weighing, samples were transferred to a desiccator and allowed to cool at ambient temperature.

Weighed wood flour samples were further transferred to a flask containing succinic anhydride 10% solution in xylene. The reaction time of wood flour samples was three hours at 120ºC.

Weighed wood discs samples were placed in the succinic anhydride solution under continuous stirring with a magnetic stirrer. The dipping time in succinic anhydride solution in xylene for softwood discs samples were 180, 420, 900, respectively 1800 seconds. Three succinic anhydride concentration levels (*i.e*. 0-control, 10, 30, and 60 g/L) at the same dipping time (7 min) were used to treat unextracted and extracted softwood discs samples. The SA solution was heated on a hot plate with a magnetic stirrer and was kept at 85-100°C. After complete dissolving of SA in xylene, the softwood discs samples were placed in the solution (at each concentration level) for 7 minutes under continuous stirring with a magnetic stirrer. All treated wood discs samples were cooled down to room temperature and finally oven-dried at 70ºC in a vacuum oven until constant weight was achieved. The oven-dry weight of each sample was re-weighted. For determination of the grafting rate, 25 treated wood discs samples underwent the secondary Soxhlet extraction for 24 hours in xylene, then oven-dried at 70ºC to reach a constant weight and weighted.

Sample identification codes are presented in Table 3.

Table 3

Sample identification codes

Code	Samples
EWF	extracted wood flour in toluene-ethyl alcohol
EWF-SA	extracted wood flour in toluene-ethyl alcohol and treated with succinic anhydride
UW	unextracted wood discs (control)
EW	extracted wood discs in toluene/ethyl alcohol
UW-SA	unextracted wood discs subjected to dipping in succinic anhydride solution in xylene
EW-SA	extracted wood discs subjected to dipping in succinic anhydride solution in xylene

Retention of succinic anhydride (Rt) and grafting rate (Gr) for treated wood discs samples were calculated as follows:

$$Rt, \% = [(W_1-W_0)/W_0] \times 100$$
$$Gr, \% = [(W_2-W_0)/W_0] \times 100$$

where: Rt - retention of succinic anhydride in a wood disc sample (%); Gr - grafting rate of succinic anhydride in a wood disc sample (%); W_0 - oven-dry wood disc sample weight after extraction and before chemical treatment (g); W_1 - oven-dry wood disc sample weight after chemical treatment (g); W_2 - oven-dry sample weight after chemical treatment and extraction with xylene (g).

Fourier transform infrared spectroscopy analysis

FT-IR spectroscopy is uniquely suited for studies of chemical reaction because absorbance peaks are characteristic of chemical bonds rather than of atoms.[17] FT-IR analysis was performed by using the KBr (potassium bromide) disk method with a Digilab Fourier Transform Infrared (FTIR) spectrometer, Model Excalibur FTS-2000. The samples were mixed with KBr to form the pellets that contained 1% powdered sample. These KBr disks were employed for FTIR analysis.

Water absorption

Five wood discs samples (6.2–7.2 g) were used to determine the degree of water absorption. The samples were first placed in an oven set at 60 °C, under reduced pressure, for 8 h. The oven-dried weight (W_D) was determined and used to calculate the water absorption as following[18]:

$$WA (\%) = [(W-W_D) / W_D] \times 100$$

where: W is the weight of the sample after water uptake in deionized water at 30 ºC dipping times 1-5 h and atmospheric pressure.

CONCLUSIONS

Wood chemical modification with succinic anhydride is influenced by many factors such as chemical treatment, reaction time, concentration, wood extraction in solvents.

The FT-IR spectra of fir wood flour, previously extracted in organic solvents and further reacted with SA, confirmed the occurrence of wood-succinic anhydride reaction, a strong vibration being observed in the region 1728-1730 cm^{-1} (C=O).

The increase of SA concentration determined increasing weight change, especially at 60 g/L for both UW and EW wood discs samples at dipping time 7 minutes. The increase of dipping time at 30 g/L SA concentration determines an increase of weight change both for UW and EW discs, this effect being pronounced for EW samples.

Retention of SA on fir wood discs increased with increasing SA solution concentration. At low concentration levels and low retention, SA molecules were mainly fixed on wood by

esterification. At high concentration levels, however, most SA molecules were deposited on wood by physical adsorption (such as capillary adsorption).

Water absorption after five hours decreases for both UW and EW discs treated with SA for the same dipping time. The wood discs treated at higher concentrations of SA solution in xylene present reduced water absorption.

REFERENCES

1. D.S. Hon and W.Y. Chao, *J. Appl. Polym. Sci.* **1993**, *50*, 7–11.
2. A. K. Bledzki and J. Gassan, *Prog. Polym. Sci*. **1999**, *24*, 221–274.
3. A. K. Bledzki, V, E. Sperber and O. Faruk, *Rapra Rev. Rep.*, **2002**, *13*, 1-144.
4. R. M. Rowell, J. A. Youngquist, and H. M. Montrey, *Forest Prod. J*., **1988**, *38*, 67-70.
5. M. Nuopponen, H. Wikberg, T. Vuorinen, S. L. Maunu, S. Jämsä and P. Viitaniemi, *J. Appl. Polym. Sci.*, **2004**, *91*, 2128–2134.
6. J. A. Santos, *Wood Sci. Technol.*, **2000**, *34*, 39–43.
7. H. Sivonen, M. Nuopponen, S. L. Maunu, F. Sundholm, and T. Vuorinen, *Applied Spectroscopy*, **2003**,*57*, 266–273.
8. G. Pritchard, *Plast. Addit. Compd.* **2004**, *6*, 18–21.
9. P. Jandura, B. Riedl and B.V. Kokta, *Polym. Degrad. Stability*, **2000**, *70*, 387–394.
10. P. Jandura, B.V. Kokta and B. Riedl, *J. Appl. Polym. Sci.,* **2000**, *78*, 1354–1365.
11. W.D. Ellis and J.L. O' Dell, *J. Appl. Polym. Sci*., **1999**, *73*, 2493–2505.
12. A.K. Bledzki, S. Reihmane and J. Gassan, *J. Appl. Polym. Sci*., **1998**, *59*, 1329–1336.
13. R.M. Rowell, in "Enclyclopedia of Forest Sciences", J. Burley, J. Evans and J.A. Youngquist (Eds.), Elsevier Academic Press, Oxford, 2004, vol. 3, p. 1269–1274.
14. R. Bodîrlău and C.A. Teacă, PRIOCHEM, ICECHIM Bucureşti, October 29-30, **2007**.
15. K. Pandey, *J. Appl. Polym. Sci.* **1999,** *71*, 1969-1975.
16. H. Tanaka, A. Swerin, L. Odberg and S. B. Park, *J. Pulp Paper Sci*., **1999**, *25*, 283-288.
17. L. M. Matuana, J. J. Balatinecz, R. N. S. Sodhi, and C. B. Park, *Wood Sci. Technol.,* **2001**, *35*, 191-201.
18. S. M. B. Nachtigall, G. S. Cerveira, and S.M.L. Rosa, *Polymer Testing*, **2007**, *26*, 619–628.

Revue Roumaine de Chimie, **2008**, *53*(11), 1065–1068

RADIATION-INDUCED PREPARATION OF GYPSUM/ POLY(METHYL ACRYLATE) COMPOSITES

Zaki AJJI*

Polymer Technology Division, Department of Radiation Technology, Atomic Energy Commission of Syria, P. O. Box 6091, Damascus, Syria

Received February 5, 2008

Gypsum/ poly(methyl acrylate) composites have been prepared based on natural gypsum and the monomer methyl acrylate by means of gamma irradiation. The conversion of polymerization was followed up with respect to the irradiation dose using thermogravimetric analyzer. The data show that the yield of polymerization increases with increasing the irradiation dose, and levels off at a dose around 3-4 kGy where a yield of 87-88% was achieved. A thermomechanical analyzer was used to determine the glass transition temperatures (*T*g) of the pure polymers and composites prepared at the same irradiation dose using two modes with alternative variable force and constant force. The *Tg* of the pure poly(methyl acrylate) and the polymer composite are around 18.5 ^{o} and 19.6 ^{o}C, respectively.

INTRODUCTION

Composite materials are used in building construction, in the automotive industry and in aerospace technology. Polymeric materials are virtually able to compete with conventional materials in most industrial fields. Polymers have contributed substantially to the development of better, cheaper and more functional products in the factory or the appliances, and in the recreation and leisure industries.

By incorporation of special fillers into a polymer matrix, desired composite properties could be achieved to suit various applications.[1] In the rubber industry, finely divided fillers have already been utilized to modify the polymer properties. Carbon black has been used for a long time.[2-3] Silicas are also used to modify polymeric materials.[4-6] Gypsum and alumina were also used as filler for preparing polymer composites.[7-9]

The present work reports the preparation of composites consisting of methyl acrylate and commercially available gypsum using gamma radiation.

RESULTS AND DISCUSSION

1. Thermogravimetry

Natural gypsum powder was used as it is, without drying, because it has been previously showed that there is no significant influence of drying of the powder on the polymerization conversion by preparing polymer/ gypsum/ composites. Furthermore, the polymerization yield using chemically pure calcium sulfate powder and natural gypsum powder seems to be very similar.[8]

Various mixtures of methyl acrylate and gypsum powder were exposed to different Gamma doses. Figure 1 shows the TGA thermograms of methyl acrylate/ gypsum/ composites, which are irradiated at different doses: 1, 1.5, and 2 kGy; the first step in the thermogram corresponds to the evaporation of the monomer and the humidity in the samples; the second step corresponds to the decomposition of the polymer. It can be seen that the first step decreases with increasing the irradiation dose due to the increase of the polymerization conversion. The yields of polymerization are represented in Figure (2) with respect to the irradiation dose. The polymerization conversion increases with increasing the irradiation dose, and levels off up a dose of ≈ 3-4 kGy, achieving a conversion of 87-88%. This can be explained by the fact that the radical concentration, which acts as initiator, increases with increasing the irradiation dose and thus the reaction conversion.

* Corresponding author: zajji@aec.org.sy

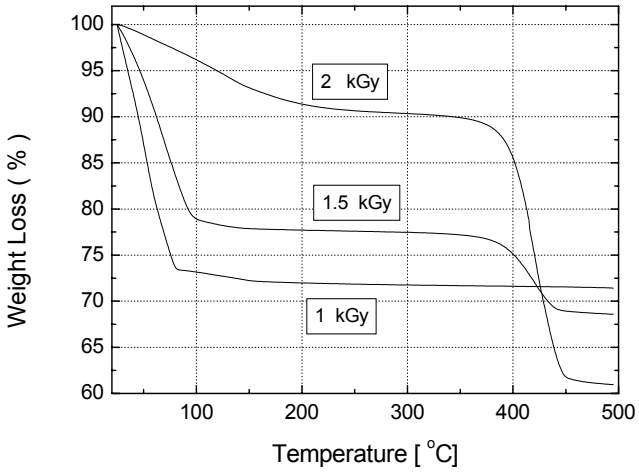

Fig. 1 – TGA thermograms of methyl acrylate/ gypsum/ composites for different preparation doses.

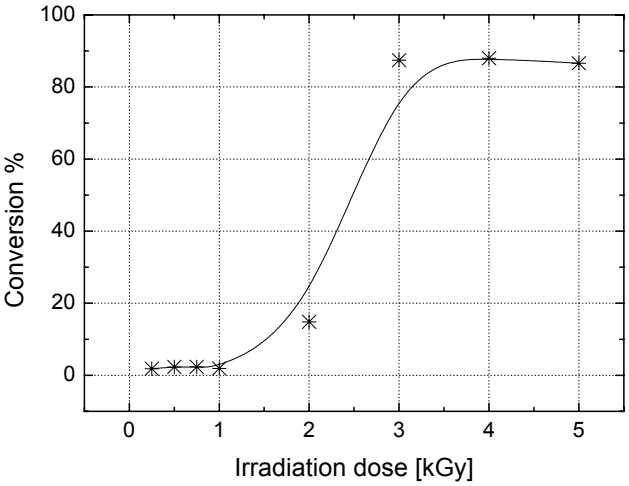

Fig. 2 – The yield of polymerization of methyl acrylate versus the irradiation dose for the methyl acrylate/ gypsum composites.

2. Glass Transition Temperature (T_g)

TMA spectrum has been recorded using an alternated force of 0.2 N in order to ensure that there is a real glass transition and to locate the T_g region as represented in Figure 3; it can be seen that the elongation increases significantly at the T_g region. TMA spectra with alternated force of 0.2 N were recorded for pure poly(methyl acrylate) and the polymer/ gypsum/ composite in order to compare their elasticity. The spectra showed that the elongation of poly (methyl acrylate)/ gypsum/ composite is significantly lower than that of pure polymer. This decrease is maybe due to reduced segmental mobility in the vicinity of the filler particulates.

TMA spectrum was recorded afterwards with constant force in order to determine the T_g; the T_g was then determined from this thermogram using the on-set method. The T_g of gypsum/ poly (methyl acrylate)/ composite is ≈ 19.6 °C. The T_g of the pure poly (methyl acrylate) was about 1 degree lower than that of the polymer composite. Differential scanning calorimetry (DSC) was also used to locate the glass transition temperature (T*g*) of the samples as represented in Figure 4. It can also be seen that the glass transition temperature of the poly (methyl acrylate)/ gypsum/ composites is slightly higher than the glass transition temperature of poly(methyl acrylate); $T_{on\text{-}set}$ and T_{mid} of pure poly (methyl acrylate) are 9.77 and 14.56 °C, respectively. $T_{on\text{-}set}$ and T_{mid} of poly(methyl acrylate)/ gypsum/ composites are 11.07 and 15.76 °C, respectively. This difference is most probably due to the interaction between the polymer matrix and filler particulates. Since the segmental mobility of the chains near the filler particles is reduced, the T_g of the composites

increases. In other composite systems, the increase of T_g has also been observed and documented; this behavior has been explained on the basis of reduced mobility of molecular segments in the vicinity of the filler particulates.[7]

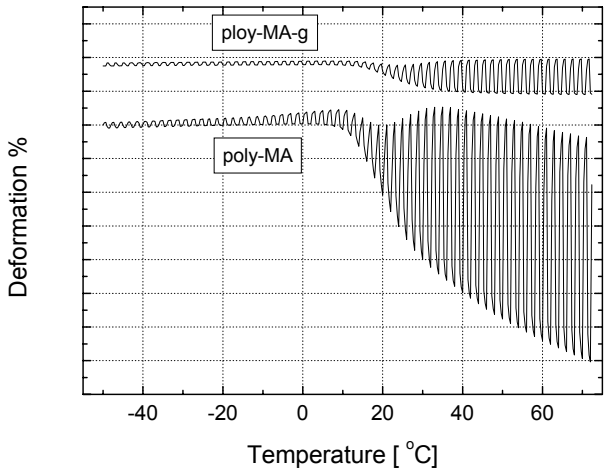

Fig. 3 – TMA spectrum with alternated force of 0.2 N for poly (methyl acrylate)/ gypsum/ composite irradiated at 5 kGy.

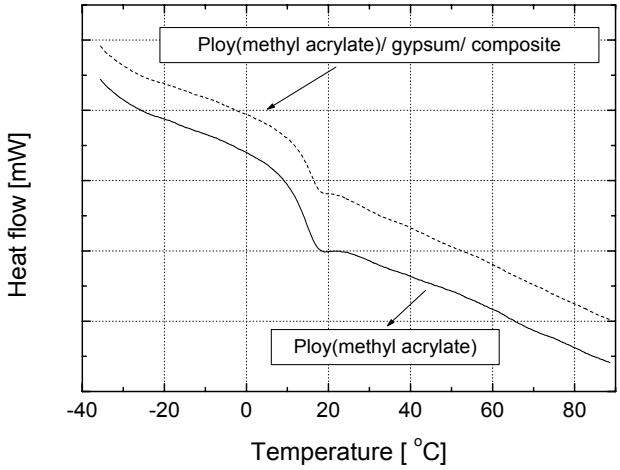

Fig. 4 – DSC spectra for pure poly (methyl acrylate) and poly (methyl acrylate)/ gypsum/ composite irradiated at 15 kGy.

EXPERIMENTAL

Natural gypsum powder was used, which is produced domestically from natural rocks in a mine near the city of Latakia in Syria. The sieved gypsum powder (0.3 meshes) was added to the liquid monomer step by step during stirring at room temperature that a weight ratio of 1:1 was achieved. The monomer/ gypsum/ mixtures were filled up in polyethylene ampoules, and then subjected to a ^{60}Co γ irradiator (Russian Gamma Cell, Type: Issledovatel); the irradiation was carried out at ambient temperature and a dose rate of around 3.5 kGy/h to different doses.

1. Thermogravimetric Measurements (TGA)

The dynamic weight loss tests were conducted using a Mettler instrument (TG50). The tests were carried out in a nitrogen atmosphere, purged (30 ml/ min) using sample weights of 10 - 15 mg at a heating rate of 10 °C / min. The resolution of the balance is given, as 1 microgram for weights less than 100 milligram, and the temperature precision of the instrument is ± 2 °C.

2. Thermomechanical Analysis (TMA)

TMA was used to locate the glass transition temperatures of the prepared samples. A Mettler equipment (TMA 40) was utilized in order to record the TMA spectra. The used instrument has a precision of ± 2 °C, and the total experimental errors in the measurements were estimated to be about ± 3 °C.

The PE container, used for the preparation of the samples, was removed and then sheets of ≈ 1 mm were cut, polished, and cleaned. TMA spectra were recorded in two modes. The first mode was using an alternated force in order to ensure that there is a real glass transition; alternated force between 0.1 and 0.2 N was applied in the most cases. The second mode was using a constant force of 0.1- 0.4 N, and the T_g was determined from these TMA thermograms using the on-set method.

3. Differential Scanning Calorimetry (DSC)

DSC was used to determine the glass transition temperatures of the prepared samples. A Mettler instrument (DSC20) was utilized to record the DSC spectra. All samples were tested in aluminum pans at a heating rate of 10 ^{o}C/ min over a temperature range from room temperature to 400 ^{o}C. The precision of the used instrument is ± 0.2 ^{o}C, and the experimental errors in the measurements were estimated to be about ± 0.5 ^{o}C.

CONCLUSION

Polymer/ Gypsum/ composites have been prepared based on natural gypsum powder and methyl acrylate by means of gamma irradiation. The conversion of polymerization was followed up with respect to the irradiation dose using a thermogravimetric analyzer. The data show that yield of polymerization increases with increasing the irradiation dose, and the highest yield obtained was around 87-88% by exposure of doses 3-4 kGy. Also the glass transition temperatures have been determined for the pure polymer and composites prepared at the same irradiation dose and have been found, to be 18.5 ^{o}C and 19.6 ^{o}C, respectively.

Acknowledgements: The author would like to thank Prof. I. Othman for his encouragement. He is also grateful to Mr's. M.K. Aljoumaa and M.A. Mougrabeya for their efforts during the experiments.

REFERENCES

1. H. Katz and J. V. Milewski (eds.), "Handbook of Fillers and Reinforcement for Plastics", Van Nostrand, New York, 1978.
2. Y. Huali, T. Hao, P. Jianhui, C. Xnfang, *Radiat. Phys. Chem.*, **1993**, *42*, 135-137.
3. N. A. Shaltout, M. M.Abou-Zeid, M. H: Moustafa and A. A.El-Miligy, *Arab-J. Nucl. Sci. Appl.*, **2002**, *35* (1), 25-35.
4. T.Çaykara and Güven O., *J. Appl. Polym. Sci.*, **1998**, *70* (5), 891-895.
5. T. Çaykara, M. S. Eroglu and O.Güven, *Polym. Degrad. Stabil.* , **1999**, *63*, 65-70.
6. T. Çaykara and O.Güven, *Europ. Polym. J.*, **1999**, *35*, 113-119.
7. T. Çaykara and O.Güven, *Polym. Comp.*, **1998**, *19*, 193-197.
8. Z.Ajji and H.Alkassiri, *Proceedings of the Symposium on Radiation Technology in Emerging Industrial Applications*, (IAEA TecDoc), **2003**, 41-45.
9. Z.Ajji, *Radiat. Phys. Chem.*, **2005**, *73*, 183-187.

Revue Roumaine de Chimie, **2008**, *53*(11), 1069–1076

ECO-FRIENDLY BINDERS BASED ON FLY ASH

Annemarie PURI, Alina BĂDĂNOIU* and Georgeta VOICU

University POLITEHNICA from Bucharest
Faculty of Applied Chemistry and Materials Science
PO-Box 12-134, Bucharest, Romania

Received March 18, 2008

The paper presents data on the synthesis, interaction processes and properties of alkaline cements based on fly ash. This type of binders consists in a solid compound - a mixture of fly ash and lime and an activator solution - sodium silicate with/without sodium hydroxide or sulfates (Na_2SO_4 and $CaSO_4$).
The fly ash-sodium silicate-lime system has binding properties at room temperature. The presence in the system of sodium silicate determines the dissolution of the aluminosilicate structures form the fly ash, and facilitate the binding of $Ca(OH)_2$ in calcium silicate hydrates (C-S-H) phases, with positive influence on the developed compressive strength. The increase of the binding system's basicity when using NaOH addition, increases furthermore the hardening processes rate and consequently the compressive strength values.
The use of small amounts of sodium or calcium sulfate has a positive effect on the mechanical strength development most probably due to the formation of ettringite ($3CaO.Al_2O_3.3CaSO_4.31H_2O$).

INTRODUCTION

An important reduction of the CO_2 emissions generated during the portland cement manufacture process can be achieved by the replacement of the portland clinker with supplementary cementitious materials (SCM). One of the most used SCM material is fly ash and in the last century, countless research works regarding the fly ash blended cement were published. In this type of cement the hardening process at early ages consists mainly in the hydration of the portland cement, therefore the fly ash cements have lower early strengths compared with the portland cement.[1-4]

The fly ash reactivity vs. $Ca(OH)_2$, released during the cement or lime hydration process, is influenced by its oxide, mineralogical and phase composition as well as its grain size distribution.[1-5]

Several studies provide information regarding the chemical activation of the fly ash – $Ca(OH)_2$ reaction, also called "pozzolanic reaction", in order to permit the increase of the fly ash content in the blended portland cements without a major negative impact on the early strength or even more in the attempt to produce clinker free binders.[6-11]

The use of Na_2SO_4, $CaCl_2.2H_2O$ or $CaSO_4.0.5H_2O$ admixtures to fly ash-lime (80-20) systems, associated with the hydrothermal curing at 50°C, lead to important increases of the mechanical strengths. Still the mechanical strengths of these binders after 28 days of hardening were small – 13-15 MPa.[6,7]

The chemical activation of class F fly ashes (with less than 10% CaO content) with sodium or potassium silicates with/without hydroxides (NaOH or KOH) admixtures, can lead to the hardening of this system even at the normal temperature.[9-11] The increase of the fly ash specific surface area as well as the reduction of the silicate module "n" ($M_2O.nSiO_2$, M=Na or K) or the increase of the curing medium temperature have a positive effect on the mechanical properties.

In this paper the hydration and hardening processes of fly ash-lime-admixtures (sodium silicate, NaOH, Na_2SO_4, $CaSO_4$) – water systems are studied. The influence of the NaOH content (present in the system as admixture or formed "in situ" by the sodium silicate hydrolysis) on the pozzolanic reaction speed and hardening process was also assessed.

* Corresponding author: a.badanoiu@oxy.pub.ro

EXPERIMENTAL

Materials

The experiments performed in this study were conducted on the following materials: i) class F fly ash with the chemical composition and some properties listed in table 1. The XRD analysis of the fly ash shows the presence of a high amount of vitreous phase as well as small amounts of crystalline compounds – quartz and mullite; ii) lime with 81% CaO and small amounts of $CaCO_3$ as main impurity; iii) 48.5% sodium silicate (water glass) aqueous solution with n=5.2; iv) reagent grade NaOH, dosed as solid material and solved in the mix water; v) reagent grade calcium sulfate - $CaSO_4.2H_2O$ and sodium sulfate - $Na_2SO_4.10H_2O$.

Table 1

Chemical composition and physic properties of the fly ash

Characteristics	Values
L.O.I. (%)	0.49
SiO_2 (%)	55.39
Al_2O_3 (%)	26.55
Fe_2O_3 (%)	8.89
CaO (%)	2.24
MgO (%)	1.79
SO_3 (%)	0.21
Na_2O (%)	0.71
K_2O (%)	2.20
TiO_2 (%)	0.88
Density (g/cm³)	2.16
Specific surface area (cm²/g)	5530

Methods

The solid compounds (fly ash, lime and calcium sulfate) were mixed in a planetary mill for 15 minutes. The activator admixtures (sodium silicate, NaOH, $Na_2SO_4.10H_2O$) were solved in the mixing water.

The hydration processes were assessed by chemical analysis of Ca^{2+} content in suspensions with solid/liquid ratio of 1/100 vs. time. The XRD and themogravimetry (TG, DTG) analysis were performed on pastes (liquid/solid=0.4) after 3, 7 and 28 days of hydration with a SHIMADZU XRD 6000 diffractometer, using Ni-filtered CuKα radiation (λ=1.5418 Å) and SHIMADZU DTG-TA 51H with a heating speed of 10°C/min.

Mechanical strengths were assessed on mortar specimens (15x15x60 mm^3) with binder/aggregate ratio=1/3 and variable water/binder ratios values. The aggregate was sand prepared according to the EN 196-1 standard. The mortar samples were hardened at normal temperature in humid atmosphere (R.H.85%) the first 3 days and in water up to the testing time. The compressive strength tests were performed on a TONINDUSTRIE testing machine, after 3, 7, 28 and 60 days of hardening.

RESULTS AND DISCUSSION

1. Interaction processes in fly ash-lime-sodium silicate (NaOH, sulfates) – water systems

The presence in the fly ash-lime-water system of the sodium silicate (which in aqueous solution hydrolyse and forms NaOH and $Si(OH)_4$)[12] or of the sodium hydroxide, leads to the attack of Si-O-Si and Si-O-Al bonds from the fly ash network and alkaline aluminate and silicate hydrates are formed.[8-11] According to Xie and Xi,[9] these hydrates can subsequently hydrolyse forming reactive silicic acid and releasing NaOH. The process continues and the silicic acid polycondensate and forms an amorphous binding matrix which, together with sodium silicate includes the non reacted fly ash grains. The main disadvantage of this type of binder consists in its reduced stability vs. water, due to the presence of sodium silicate in the hardened matrix.[9]

According to Palomo *et. al.*[10] in ordinary portland cement –fly ash systems activated with NaOH-water glass solutions, the hardening products formed are N-A-S-H gel and C-S-H gel from portland cement hydration process or even from the reaction between the calcium in the cement and soluble silica from the alkaline solution. Coexistence of both gels was also observed in other systems such as metakaolin-slag-alkaline activator,[13] metakaolin-$Ca(OH)_2$-alkaline activator[14,15] and fly ash-$Ca(OH)_2$- alkaline activator.[16] The formation of C-S-H gel and geopolymers depends on many factors such as the crystalinity and thermal history of calcium silicate sources, the ratio between the aluminosilicate and calcium source and the alkalinity of alkali activators.[8,17] At low alkalinity (corresponding to the experimental conditions in this

work) the calcium dissolved from the calcium source forms C-S-H gel in conjunction with geopolymeric gel.[10] Therefore the reduction of the CaO content in the fly ash-lime–water system can provide direct information regarding the pozzolanic reaction kinetic.

The Ca^{2+} consumption due to the pozzolanic reaction with the fly ash (figure 1), is influenced by the nature of the Na^{+} source: i) the rate of Ca^{2+} consumption is quasi-similar in the sample E5N (with 5% NaOH) and E5S (with 5% $Na_2O.nSiO_2$ – corresponding to aprox. 1.1% NaOH); ii) the Ca^{2+} consumption is higher in E10S sample (with 10%$Na_2O.nSiO_2$ – corresponding to aprox. 2.2% NaOH).

These data suggests a higher speed of the reaction of calcium ions with silicic acid (resulted from the water glass hydrolysis) as compared with the dissolution of aluminosilicates, from the fly ash, in the alkaline solution. The data also are in good agreement with Palomo model[8, 10] according to which at the activation of aluminosilicate materials with a mild alkaline solution the main reaction product is C-S-H, opposite to the case of Al_2O_3 and SiO_2 containing materials, activated with high alkaline solutions in which the final product is a geopolymer (chains or networks of mineral molecules linked with covalent bonds).

An interesting aspect was noticed when 4.2% Na_2SO_4 (corresponding to 2.36% NaOH) was added in the system with 5% sodium silicate (E5SNs) - after the first 24 h the rate of the consumption process of Ca ions increases. A quasi-similar behaviour was noticed also for the sample E5NCs with 5% NaOH and 5% $CaSO_4$.

The data obtained by TG and DTG analysis (figure 2) confirms the consumption of $Ca(OH)_2$ in pastes (figure 3), process assesed also by chemical dosage of Ca^{2+} ions in suspensions.

The high speed of the Ca ions consumption process in the compositions with $CaSO_4$ or Na_2SO_4 ($Ca(OH)_2 + Na_2SO_4 \rightarrow$ **$CaSO_4$** + NaOH) is explained by the ettringite - $3CaO{\cdot}Al_2O_3{\cdot}3CaSO_4.32H_2O$ formation trough the reaction of $CaSO_4$ and aluminates from the fly ash (figure 4). The ettringite formation - compound with a high amount of water molecules in it's network, may contribute to the reduction of the free water in the binder matrix – see the good correlation between the ettringite quantity in samples and the amount of bound water in hydrates (assessed by TG) - figure 5.

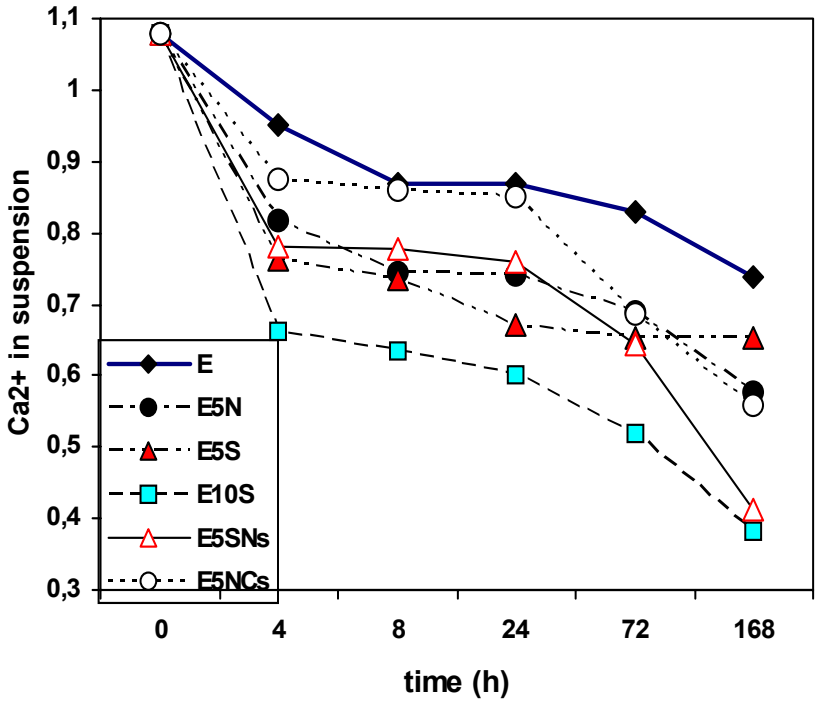

Fig. 1 – Ca^{2+} concentration in suspensions vs. time for: **E** – fly ash+ 20% lime; **E5S** - fly ash+ 20% lime + 5% sodium silicate; **E10S** - fly ash+ 20% lime + 10% sodium silicate; **E5N** - fly ash+ 20% lime + 5%NaOH; **E5SNs** - fly ash+ 20% lime + 5% sodium silicate + 4.2% Na_2SO_4; **E5NCs** - fly ash+ 20% lime + 5% NaOH and 5% $CaSO_4$.

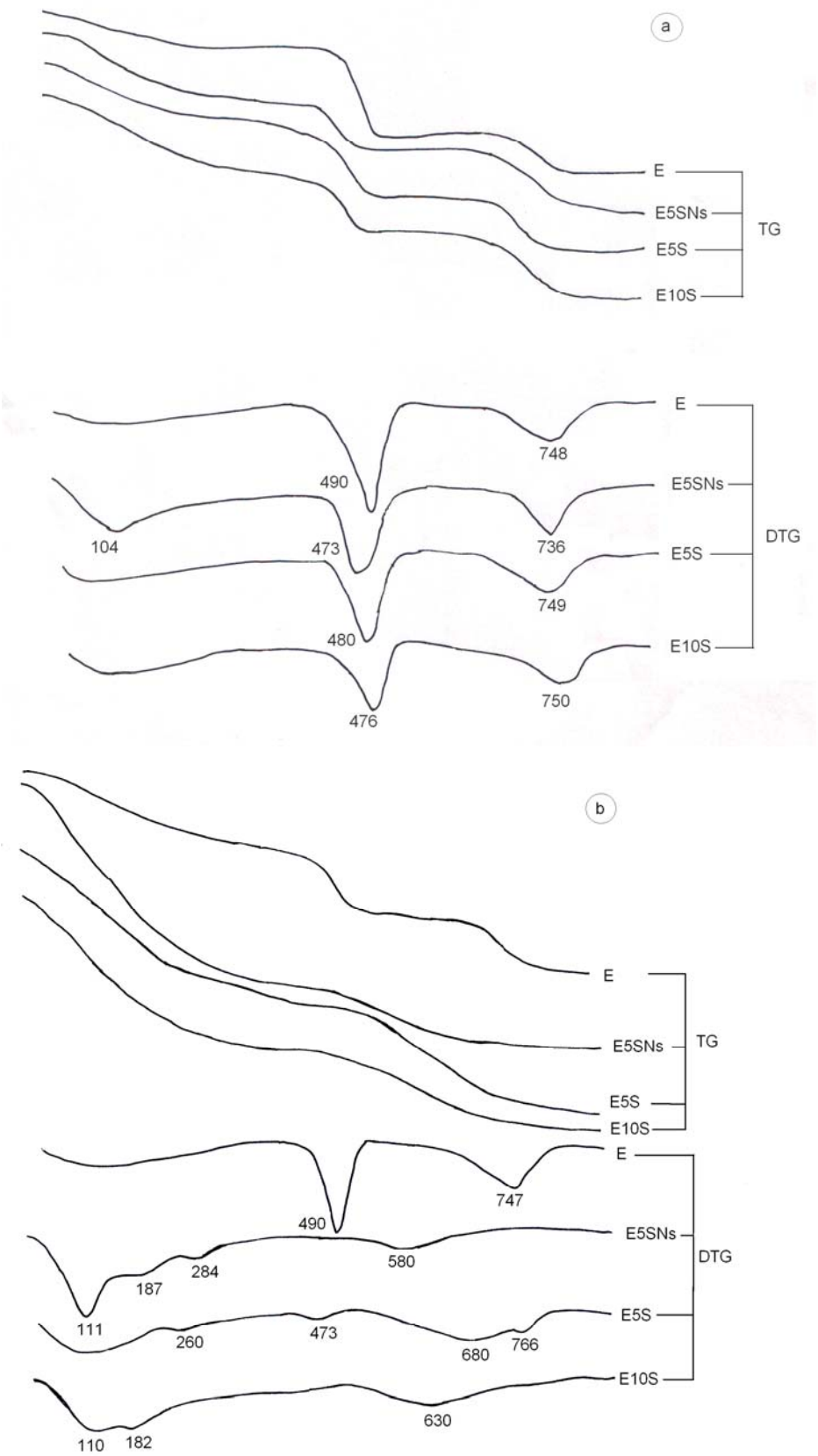

Fig. 2 – TG and DTG curves of the pastes cured for 3 days (a) and 28 days (b). **E** – fly ash+ 20% lime; **E5S** - fly ash+ 20% lime + 5% sodium silicate; **E10S** - fly ash+ 20% lime + 10% sodium silicate; **E5SNs** - fly ash+ 20% lime + 5% sodium silicate + 4.2% Na_2SO_4.

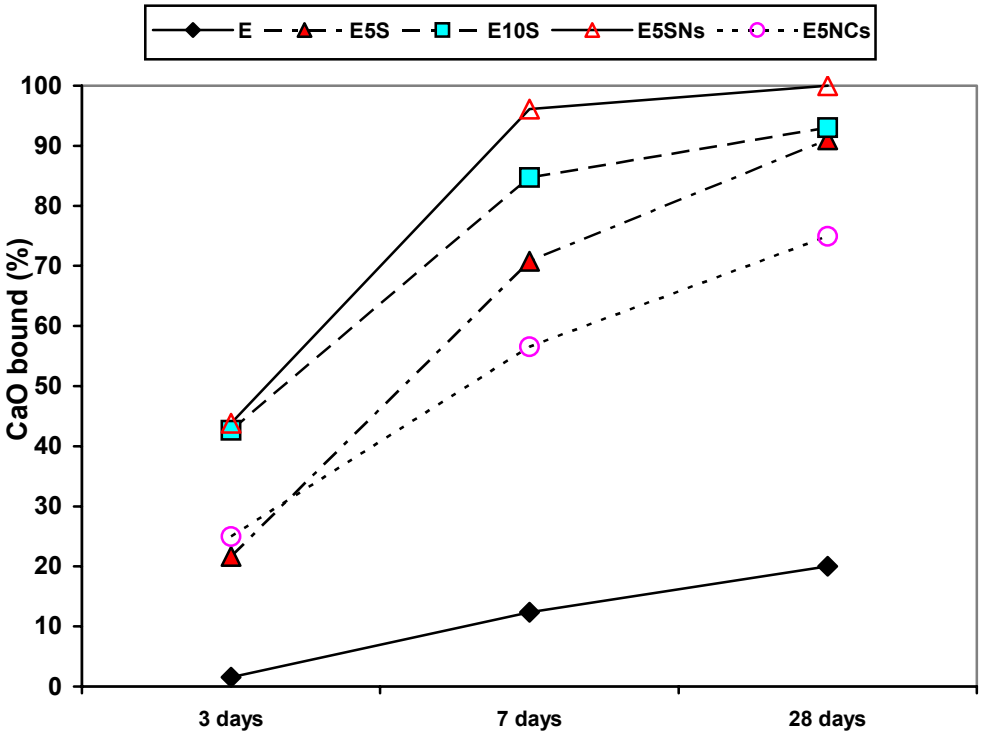

Fig. 3 – CaO bound vs. time.
E – fly ash+ 20% lime; **E5N** - fly ash+ 20% lime + 5%NaOH; **E5S** - fly ash+ 20% lime + 5% sodium silicate; **E10S** - fly ash+ 20% lime + 10% sodium silicate; **E5SNs** - fly ash+ 20% lime + 5% sodium silicate + 4.2% Na_2SO_4.

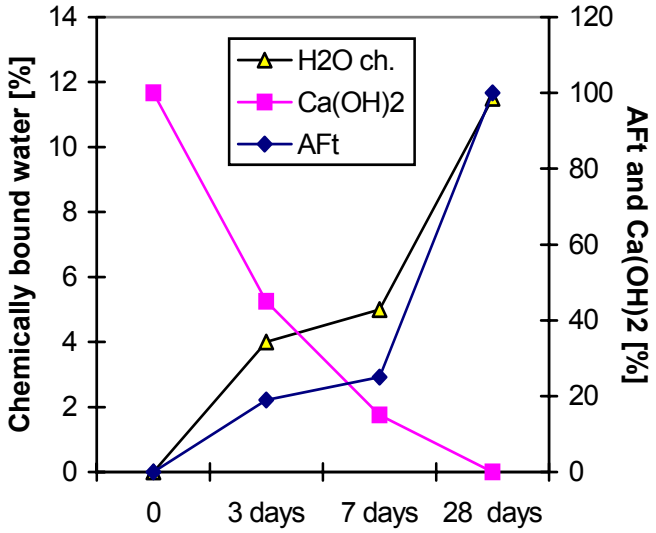

Fig. 4 – Hydrates vs. time for mixture **E5SNs.** Chemically bound water and $Ca(OH)_2$ content was assessed by TG and ettringite (AE_t) content by XRD.

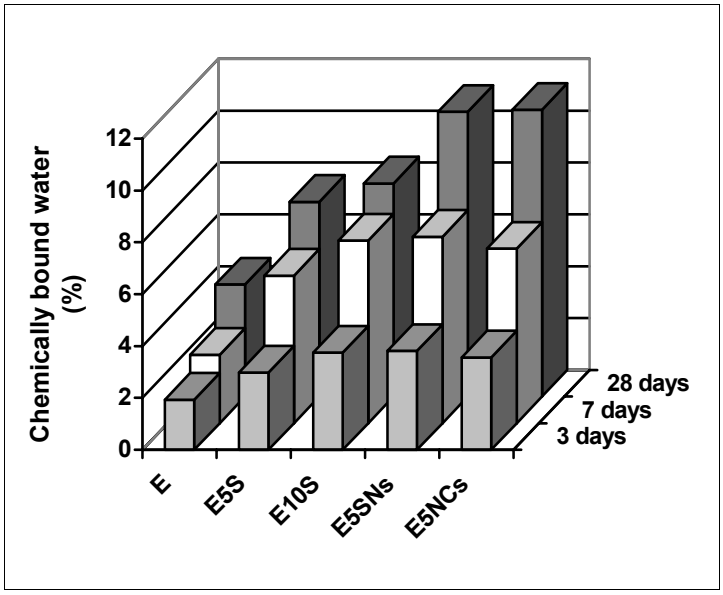

Fig. 5 – Chemically bound water in hydrates for the binders: **E** – fly ash+ 20% lime; **E5S** - fly ash+ 20% lime + 5% sodium silicate; **E10S** - fly ash+ 20% lime + 10% sodium silicate; **E5SNs** - fly ash+ 20% lime + 5% silicat de sodiu + 4.2% Na_2SO_4; **E5NCs** - fly ash+ 20% lime + 5% NaOH and 5% $CaSO_4$.

2. Hardening processes in fly ash-lime-sodium silicates (NaOH, sulfates) – water systems

The compressive strength of the mortar specimens vs. time are presented in figures 6-8.

The binders with sodium silicate (NaOH and sulfate) content develops even after 3 days of hardening measurable compressive strengths opposite to the one containing only fly ash and lime (E), regardless the lime content – figures 6 and 7.

At longer hardening times (28 and 60 days), the binders with sodium silicate content have an important strength increase (up to 100%) as compared with the compressive strength developed by the fly ash – lime binder. The increase of the sodium silicate content (from 5% to 10%) has a positive influence on the early age strength. The increase of the basicity of the system, due to the supplementary NaOH addition, has also a positive effect on the compressive strengths, especially on those developed at longer hardening times (28 and 60 days). The higher compressive strengths were developed by the binders with sodium sulfate (E5SNs) and calcium sulfate (E5NCs) content, probably due to the formation of ettringite as reaction product in these systems. The positive effect of the needle like ettringite crystals upon the mechanical strength of the hardened matrix is well documented.[1,2] The formation of ettringite was also reported by Shi *et.al.*[18] to be decisive for the development of good mechanical strengths in systems containing fly ash and lime activated with Na_2SO_4.

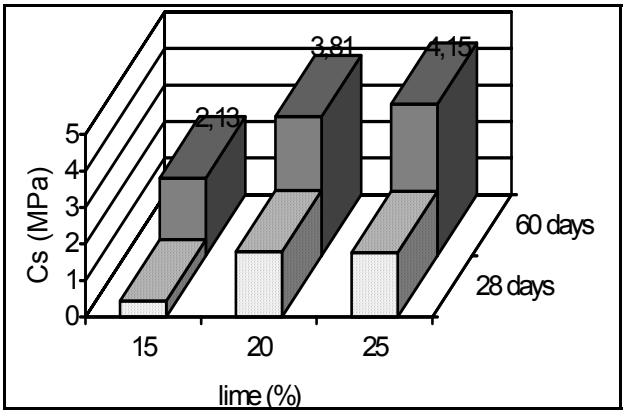

Fig. 6 – The influence of lime content on the compressive strength developed by the binders based on fly ash (water/binder=0.64).

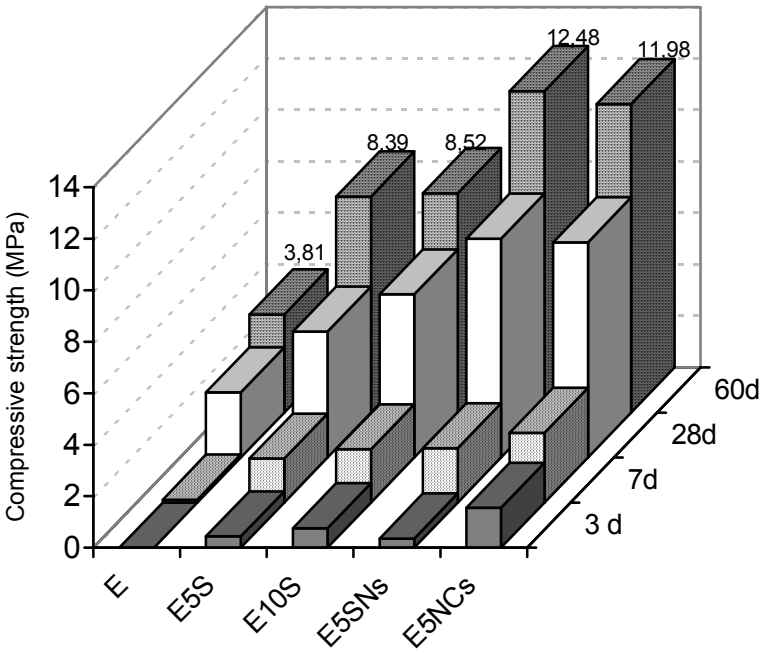

Fig. 7 – Compressive strength for the binders: **E** – fly ash+ 20% lime (w/b=0.64); **E5S** - fly ash+ 20% lime + 5% sodium silicate (w/b=0.77); **E10S** - fly ash+ 20% lime + 10% sodium silicate (w/b=0.84); **E5SNs** - fly ash+ 20% lime + 5% sodium silicate + 4.2% Na_2SO_4 (w/b=0.77); **E5NCs** - fly ash+ 20% lime + 5% NaOH and 5% $CaSO_4$ (w/b=0.5).

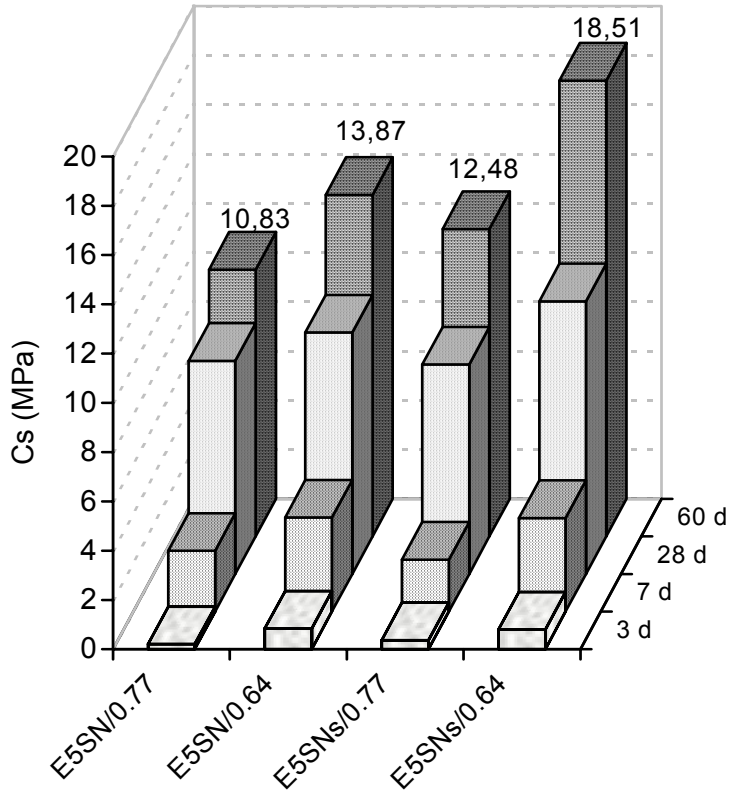

Fig. 8 – Compressive strength for the binders: **E5SN** - fly ash+ 20% lime + 5% sodium silicate +5% NaOH with w/b=0.77 and 0.64 and **E5SNs** - fly ash+ 20% lime + 5% sodium silicate + 4.2% Na_2SO_4 with w/b=0.77 and 0.64.

The increase of the mortars fluidity, noticed for the systems with 5% sodium silicate and NaOH or Na_2SO_4 additions, allowed the reduction of the water to binder ratio for E5S mortar specimens' preparation. The reduction of the water content leads, as expected, to an increase of the compressive strength values - figure 8.

CONCLUSIONS

Sodium silicate act as a catalyst for the dissolution of aluminate and silicate phases present in the fly ash vitreous phase and increases the $Ca(OH)_2$ bounding, through pozzolanic reaction, in calcium silicates hydrates

The increase of the basicity of the system, when 5% NaOH is used as admixture together with sodium silicate, increases the speed of the hardening processes. The increase of the compressive strength when Na_2SO_4 or $CaSO_4$ is added in the system is mainly due to the ettringite formation; the presence of needle like ettringite crystals can reinforce the binding matrix and consequently increases the strength.

Eco-friendly binders based on waste (fly ash) with alkaline activation may be produced at normal curing temperature with positive environmental and economic effects.

REFERENCES

1. I.Teoreanu, ″Bazele tehnologiei lianților anorganici″, Ed. Didactică şi Pedagogică, Bucureşti, 1993.
2. M. Georgescu and A. Puri, ″Chimia lianților anorganici″, Ed. Politehica Press, Bucureşti, 2004.
3. A.Bădănoiu, M.Georgescu, A.Puri, G.Voicu, D.Voinițchi and S.Stoleriu, ″Lianți ecologici complecşi″, Ed. Politehnica Press, 2007.
4. F. Massazza, *Cem. Concr. Compos*., **1993**, *15*,185-214.
5. A. Puri and J. Paceagiu, Proceedings of IBAUSIL 14, Weimar 2000, vol. I, 327-336.
6. C. Shi and R. L. Day, *Cem. Concr. Res.,***2001***, 31*, 813-818.
7. J. Fan, S. Jin, Z. Wen and J. Zhang, *Cem. Concr. Res*.,**1999**, *29*, 467-472.
8. A. Palomo, M. W. Grutzeck and M. T. Blanko, *Cem. Concr. Res.,* **1999**, *29*, 1323-1329.
9. Zh. Xie and Ju. Xi, *Cem. Concr. Res.,* 2001, **31**, 1245-1249.
10. A.Palomo, A.Fernandez-Jimenez, G.Kovalchuk, L.M.Ordonez and M.C.Naranjo, *J.Mater Sci.,* **2007**, 42:2958-2966, DOI 10.1007/s10853-006-0585-7.
11. F. Puertas and A. Fernandez-Jimenez, *Cem. Concr. Compos.,* **2003**, *25*, 287-293.
12. C.D. Nenitescu, ″Chimie generală″, Ed. Didactică şi Pedagogică, Bucureşti 1972.
13. C.K.Yip, G.C.Lukey and J.S.J van Deventer, *Cem.Concr.Res.* **2005**, *35*, 1688-1697.
14. S.Alonso and A.Palomo, *Materials Letters* , **2001**, *47*, 55-62.
15. S.Alonso and A.Palomo, *Cem. Concr. Res*. , **2001**, *31,* 25-30.
16. K.Dombrowski, A.Buchwald and M.Weil, *J. Mater. Sci*, *2007*, 42:333-3043, DOI 10.107/s10853-006-0532-7.
17. C.K.Yip, G.C.Lukey, J.L.Provis and J.S.J.Deventer, *Cem.Concr. Res*., **2007**, doi: 10.1016/j.cemconres.2007.11.001.
18. C.Shi and R. Day, *Cem. Concr. Res.,* **1995**, *25*, 15-21.